UNIVERSITÉ DU QUÉBEC À MONTRÉAL

ÉTUDES BIOPHYSIQUES DE L'AGRÉGATION ET DE L'AUTO-ASSEMBLAGE DES HORMONES PEPTIDIQUES : DES AMYLOÏDES FONCTIONNELLES AUX SYSTÈMES MODÈLES PHYSIOLOGIQUEMENT PERTINENTS

THÈSE
PRÉSENTÉE
COMME EXIGENCE PARTIELLE
DU DOCTORAT EN BIOCHIMIE

PAR
MATHEW SEBASTIAO

MAI 2023

UNIVERSITÉ DU QUÉBEC À MONTRÉAL

BIOPHYSICAL STUDIES OF PEPTIDE HORMONE AGGREGATION AND SELF-ASSEMBLY: FROM FUNCTIONAL AMYLOIDS TO PHYSIOLOGICALLY RELEVANT MODEL SYSTEMS

THESIS
PRESENTED
AS A PARTIAL REQUIREMENT
OF THE DOCTORATE IN BIOCHEMISTRY

BY
MATHEW SEBASTIAO

MAY 2023

ACKNOWLEDGEMENTS

Steve and Isabelle, I consider myself incredibly fortunate to have had both of you supervising me. The advice you each have provided, inside and outside of the lab, has not gone unappreciated. Steve, your passion for science and your impeccable work ethic have been a constant source of motivation. Isabelle, you have consistently offered me room to grow and provided insightful questions and approaches to help me reflect and look at things in a different light. Thank you both for your inspiration, your support, and your patience.

Alexandre, Dror, both of you have guided me and provided much appreciated feedback on my experimental designs, interpretation of the results, and reviewing what was written. I cannot express my gratitude to both of you for your seemingly endless patience to explain in detail (several times) the intricacies of my NMR experiments.

Trang, Margo, Alex, Noé, I hold very dear the years we spent together and the conversations we had. The jokes, the stress, the snacks, and the coffee. To all the members of both labs, I am fortunate to have been surrounded by not only such wonderful minds, but also such kind hearts.

Alexe, thank you for that conversation we had so many years ago. It seemed insignificant at the time, but your gentle encouragement was what I needed to take those first steps towards this thesis. Thank you for being there for me through all of it, the ups and downs and everything in between. Louis and Abby, thank you for your smiles, your hugs, and ensuring I never got bored or overslept.

Finally, I would like to thank my mother and father for everything they have provided me over the years. Thank you both for your never-ending encouragement, support, and love.

"It is impossible to begin to learn that which one thinks one already knows."

"Demand not that things happen as you wish, but wish them to happen as they do, and you will go on well."

Epictetus

TABLE OF CONTENTS_Toc125379240

LIST OF FIGURES

LIST OF TABLES

LIST OF ABBREVIATIONS, SYMBOLS, AND ACRONYMS

ACTH	Adrenocorticotropic hormone
AD	Alzheimer's disease
AFM	Atomic force microscopy
ANF	Atrial natriuretic factor
ANS	8-anilinonapthalenesulfonic acid
Aβ	Amyloid beta
CD	Circular dichroism
CR	Congo red
CS	Chondroitin sulfate
CSA	Chemical shift anisotropy
DLS	Dynamic light scattering
dp	Degree of polymerization
DS	Dermatan sulfate
ECM	Extracellular matrix
FITC	Fluorescein isothiocyanate
FlAsH	Fluorescent biarsenical hairpin
FRAP	Fluorescence recovery after photobleaching
FRET	Förster resonance energy transfer
GAGs	Glycosaminoglycans
GalNAc	N-Acetyl galactosamine
GlcNAc	N-acetyl glucosamine
GPCR	G protein coupled receptor
GPMVs	Giant plasma membrane vesicles
HA	Hyaluronic acid
Hb	Hemoglobin
HEP	Heparin
HFIP	1,1,1,3,3,3-hexafluoroisopropanol
hIAPP	Human IAPP

HS	Heparan sulfate
HSPGs	Heparan sulfate proteoglycans
IAA	Isolated atrial amyloid
IAPP	Islet amyloid polypeptide
IDP	Intrinsically disordered polypeptide
KS	Keratan sulfate
LMWH	Low molecular weight heparin
LUVs	Large unilamellar vesicles
MAS	Magic angle spinning
MLVs	Multilamellar vesicles
mRNA	Messenger RNA
MTC	Medullary thyroid carcinoma
ncRNA	Non-coding RNA
NMR	Nuclear magnetic resonance
PACAP	Pituitary adenylate cyclase activating polypeptide
PC	Phosphatidylcholine
PCC	Pearson correlation coefficient
PE	Phosphatidylethanolamine
PG	Phosphatidylglycerol
Pmel17	Premelanosome protein
PS	Phosphatidylserine
RAGE	Receptor for advanced glycation end products
RAMP	Receptor activity modifying protein
RBCs	Red blood cells
rIAPP	Rat IAPP
RNA	Ribonucleic acid
sCT	Salmon calcitonin
SEM	Standard error of the mean
SM	Sphingomyelin

ssNMR	Solid state NMR
T2D	Type 2 diabetes
TEM	Transmission electron microscopy
TFE	1,1,1-Trifluoroethanol
ThT	Thioflavin T
UV	Ultraviolet
VIP	Vasoactive intestinal peptide
WT	Wild type

RÉSUMÉ

Les fibres amyloïdes sont des arrangements supramoléculaires linéaires non ramifiés résultant de l'autoassemblage organisé de protéines dans des structures quaternaires en feuillets-β-croisés. Les fibres amyloïdes ont été initialement associées à différentes pathologies, bien que des assemblages amyloïdes présentant des fonctions essentielles aux processus physiologiques aient été identifiés chez la majorité des organismes vivants. Parmi les polypeptides associés aux amyloïdes, il a été démontré que les hormones peptidiques forment des amyloïdes à la fois pathologiques et fonctionnels. En plus de ces deux amyloïdes biologiques, les formulations peptidiques sont également sujettes à l'autoassemblage et à l'agrégation, ce qui réduit la stabilité, l'efficacité et la biosécurité du médicament. La formation d'amyloïde par les hormones peptidiques est donc un domaine d'intérêt particulier, mais il demeure difficile de décrire avec précision en raison de la nature dynamique du processus et de sa complexité. Actuellement, il existe un besoin urgent non seulement d'améliorer notre compréhension de la progression par laquelle les amyloïdes se forment, mais également de développer de nouvelles approches et de nouveaux outils pour étudier le processus de formation d'amyloïde dans des conditions biologiques incorporant d'autres biomolécules connues pour co-agréger, tels les glycosaminoglycanes (GAG) et les phospholipides. L'objectif principal de cette thèse est de développer des stratégies innovantes pour étudier les processus et les facteurs affectant l'agrégation des hormones peptidiques en fibres amyloïdes. Deux hormones peptidiques ont été utilisés dans cette étude. Tout d'abord, le *pituitary adenylate activating polypeptide* (PACAP), un peptide cationique hautement soluble qui a été postulé pour exister sous forme d'amyloïdes réversibles à l'intérieur de granules sécrétoires, a été utilisé pour représenter les amyloïdes fonctionnels. Deuxièmement, l'*islet amyloid polypeptide* (IAPP) dont l'agrégation et le dépôt pancréatique sont associés au diabète de type 2 a été utilisé comme modèle d'amyloïdes pathologiques. Trois objectifs spécifiques ont été ciblés : 1) décrire le mécanisme par lequel les GAG stimulent l'autoassemblage du PACAP, 2) établir des modèles de bicouche lipidique biologiquement pertinents pour évaluer les perturbations de la membrane plasmique induites par l'autoassemblage de IAPP, et 3) expliquer les sources de variation expérimentale au cours de la cinétique de l'assemblage amyloïde *in vitro*. Contrairement aux mécanismes classiques de formation principalement déduits d'amyloïdes pathologiques, le PACAP a formé des gouttelettes denses et séparées en phases où l'autoassemblage a été initié. Ni les gouttelettes, ni les fibres de PACAP ne se sont révélées cytotoxiques, ce qui appuie l'hypothèse d'amyloïde fonctionnel. Ensuite, un nouvel essai à base de FRET a été développé pour détecter les perturbations membranaires induites par l'IAPP à l'aide de vésicules de membrane plasmique de cellules eucaryotes, surmontant les limites des modèles synthétiques traditionnels. Enfin, le test standard sur microplaque souvent utilisé pour décrire la cinétique de la formation d'amyloïde s'est avéré hautement sensible aux conditions expérimentales - la fréquence et le nombre de mesures étaient des sources

d'agitation confondantes modulant la cinétique. Ces résultats donnent non seulement un aperçu des mécanismes sous-jacents des amyloïdes physiologiques, mais fournissent également des outils innovants pour étudier l'amyloïdogenèse, comblant l'écart entre les processus biologiques *in vivo* et l'étude biophysique de l'amyloïde *in vitro*. Ces approches et les informations tirées de ces travaux s'avérent des contributions précieuses à l'étude de l'amyloïde dans des conditions biologiquement pertinentes.

Mots clés: *Islet amyloid polypeptide*, *pituitary adenylate cyclase activating polypeptide*, érythrocytes, vésicules de membranes plasmiques géantes, glycosaminoglycanes

ABSTRACT

Amyloid fibrils are linear and unbranched supramolecular arrangements resulting from the organized self-assembly of proteins into cross-β-sheet quaternary structures. Historically, amyloid fibrils have been associated with numerous pathological states, though amyloid assemblies displaying functional properties essential to physiological processes have been described in most living organisms. Among polypeptides associated with amyloid fibrils, peptide hormones have been shown to form both pathological and functional amyloids. In addition to these two biological amyloids, therapeutic formulations of peptide hormones are also subject to aggregation and/or amyloid self-assembly, resulting in reduced storage stability, efficacy, and potential side effects of the drug. Amyloid formation by peptide hormones in these contexts is an area of particular interest, yet it is challenging to accurately depict due to the complex and dynamic nature of the process. Currently, there is a dire need to not only improve the collective understanding of the progression by which amyloid-like materials form, but also to develop new approaches and tools to study the process of amyloid formation under biologically relevant conditions incorporating other biomolecules known to co-aggregate with amyloid – namely, glycosaminoglycans (GAGs) and phospholipids. Therefore, the overarching objective of this research thesis is to develop innovative strategies to study the processes and factors affecting the aggregation of peptide hormones into amyloid fibrils. Two peptide hormone models were used in this study. First, the neurohormone pituitary adenylate cyclase activating polypeptide (PACAP), a highly soluble, cationic peptide which has been postulated to exist as reversible amyloid fibrils inside secretory granules, was used to represent functional amyloids. Second, the islet amyloid polypeptide (IAPP) whose aggregation and pancreatic deposition are associated with type 2 diabetes was used as a model of pathological amyloids. Accordingly, three specific research aims were targeted: 1) to describe the mechanism by which GAGs stimulate the self-assembly PACAP under physiologically relevant conditions, 2) to establish biologically relevant lipid bilayer models to assess plasma membrane perturbations induced by the self-assembly of IAPP, and 3) to explain sources of experimental variation during kinetics of amyloid assembly *in vitro*. Unlike classical mechanisms of amyloid formation mainly inferred from pathological amyloids, PACAP formed dense, phase separated droplets where self-assembly was initiated. Neither the droplets, nor the fibrils of PACAP were found to be cytotoxic, supporting the functional amyloid hypothesis. Next, a novel FRET assay was developed to detect membrane perturbations induced by IAPP using eukaryotic cell plasma membrane vesicles, overcoming the limitations of traditional synthetic models. Finally, the standard microplate assay often used to describe the kinetics of amyloid formation was shown to be remarkably sensitive to the experimental conditions – the frequency and number of measurements were confounding sources of agitation, accelerating self-assembly. Together, our results not only offer key insights into the underlying mechanisms of physiological amyloids, but

also provide innovative tools to study amyloidogenesis, bridging the gap between biological processes *in vivo* and the biophysical study of amyloid *in vitro*. These approaches and the information gained from this work will prove to be valuable contributions to the study of amyloid under biologically relevant conditions.

Keywords: Islet amyloid polypeptide, Pituitary adenylate cyclase activating polypeptide, erythrocyte, giant plasma membrane vesicles, glycosaminoglycans

CHAPTER I:

INTRODUCTION

1.1 Peptide hormones

1.1.1 Roles and physiological functions

Peptide hormones are important signalling molecules in mammals, involved in a wide variety of regulatory processes such as energetics (Morton *et al.*, 2006), regulation of body temperature, and circadian rhythm (Jekely *et al.*, 2018). These peptides are translated from mRNA as (pre)prohormones, which are then cleaved and undergo post-translational modifications before storage/secretion under their mature biologically active isoform. The mature peptide molecules are variable in length, and it is possible for a single prohormone to produce multiple signalling peptides ranging from several amino acids to long peptide chains. These peptides are eventually secreted through secretory vesicles and exert various effects through a signalling cascade after binding to their cognate receptors at the surface of target cells. As a result, peptide hormones and their receptors are important targets for pharmacological research and understanding the pathophysiology behind a multitude of conditions and diseases. Moreover, an important yet overlooked characteristic of peptide hormones is their ability to aggregate, or self-assemble, into large, often insoluble, quaternary structures

(Akter *et al.*, 2016; Jacob *et al.*, 2016; Malmos *et al.*, 2016; Nespovitaya *et al.*, 2016; Nespovitaya *et al.*, 2017; Otzen and Riek, 2019). This may occur under normal physiological conditions, under pathological states, and/or under their pharmacological formulations. .

1.1.2 Aggregation and self-assembly

The aggregation process of peptide hormones needs to be investigated, since it is associated with fundamental biological processes, occurring both under normal and pathological states, as well as limiting the formulation of peptide drugs. Numerous polypeptide aggregates occur *in vivo* and are closely linked with diseases such as Alzheimer's disease, Parkinson's disease, and type 2 diabetes (Chiti and Dobson, 2017). Alternatively, comparable aggregates appear to be harmless or even necessary for normal biological functions such as the storage of peptide hormones within secretory granules (Jacob *et al.*, 2016) and Pmel17 fibrils formed during the biosynthesis of melanin (Fowler *et al.*, 2006). Other peptides with therapeutic applications, such as calcitonin or insulin, are prone to aggregation due to the high concentrations present in pharmacological formulations (Zapadka *et al.*, 2017). Consequently, alternative strategies have been developed to overcome or mediate these undesirable aggregates. Calcitonin has therapeutic applications when treating osteoporosis, yet due to the high concentrations injected, it is prone to aggregation (Itoh-Watanabe *et al.*, 2013). The salmon analog of calcitonin, which displays dramatically reduced aggregation propensity, is therefore used instead. Similarly, pramlintide, an artificial peptide analog of the glucomodulatory hormone islet amyloid polypeptide (IAPP), is used in the treatment of diabetes due to its reduced ability to aggregate compared to the wildtype sequence (Wang *et al.*, 2014). Another important example is insulin, a critical drug for individuals afflicted with type 1 diabetes. It may also aggregate in solution, which commonly occurs in the reservoirs of infusion pumps

that deliver insulin to an individual, and current research is attempting to provide solutions to overcome this issue (Li and Leblanc, 2014).

The self-assembly of peptide hormones can lead to a diversity of aggregates, i.e., amorphous, or highly ordered, but often the type of aggregates formed are long, linear, and unbranched fibrillar structures, termed amyloid fibrils. These fibrils are the primary aggregates of interest in the context of this project, and a variety of peptide hormones where self-assembly is associated with different processes are summarized in table 1.1.

Table 1.1 Aggregation and self-assembly of peptide hormones into amyloid fibrils .

Peptide hormones	**Residues**	**Associated disease or process**	**Native structure**	**Reference**
Islet amyloid polypeptide	37	Type II diabetes Aggregates in formulations	Unstructured	Cao et al., 2021
Insulin	30 + 21	Injection-localized amyloidosis Aggregates in formulations	α-helix	Li and Leblanc, 2014
Calcitonin	32	Medullary carcinoma of thyroid Aggregates in formulations	Unstructured	Itoh-Watanabe et al., 2014
Atrial natriuretic factor	28	Atrial amyloidosis	Unstructured	Vergaro et al., 2022
Medin	50	Aortic medial amyloidosis	Unknown	(Davies *et al.*, 2016)
Prolactin	199	Pituitary prolactinoma	α-helix	(Levine *et al.*, 2013)
Enfurvitide	36	Injection-localized amyloidosis	Unstructured	(Chiti and Dobson, 2017)
Glucagon	29	*In vitro*	α-helix/ unstructured	(Yamane *et al.*, 2019)
Pituitary adenylate cyclase activating polypeptide	38/27	Storage in secretory granules	Unstructured	(Maji *et al.*, 2009)
Growth hormone	191	Storage in secretory granules	α-helix	(Jacob *et al.*, 2016)
β-endorphin	31	Storage in secretory granules	Unstructured	(Nespovitaya *et al.*, 2016)

1.2 Amyloid fibrils

For over a century, amyloid deposits have been detected in individuals afflicted by various pathological conditions, with one description of clay-like deposits in the liver

dating back to 1722 (Doyle, 1988). The initial use of the term amyloid (e.g., pertaining to starches) dates back to the late 1850's, as it was noticed by Rudolph Virchow that the deposits in liver reacted to an iodine stain for starch (Doyle, 1988). Since then, the tissue deposition of amyloids has been found in a variety of different diseases, such as light-chain amyloidosis , Parkinson's disease, and type 2 diabetes. Furthermore, in relatively recent years, various types of non-pathological, "functional", amyloids have been described in bacteria, yeast, and mammals (Fowler *et al.*, 2007). Studying amyloid formation, however, is a challenging endeavor; fibrils are structurally heterogeneous, pre-fibrillar structures are transient and difficult if not impossible to isolate, and the entire process is remarkably sensitive to experimental factors (Chiti and Dobson, 2017).

1.2.1 Organization and structure of amyloid fibrils

A tremendous amount of work has been performed studying and describing the structure of amyloid fibrils (Chiti and Dobson, 2017; Iadanza *et al.*, 2018; Otzen and Riek, 2019; Sciacca *et al.*, 2018; Terakawa *et al.*, 2018). Amyloid fibrils are thread-like aggregates, ranging from 7 to 13 nm in thickness and able to reach several microns in length (figure 1.1). The fibrils themselves are typically composed of 2 to 8 protofilaments, often intertwined in a helical bundle, although there have been some cases where fibrils consisted of a single protofilament (Eisenberg and Sawaya, 2017). Monomeric units within the fibrils adopt β-strand motifs in the protofilaments, which results in long parallel or antiparallel β-sheets. Due to these sheets orienting themselves perpendicular to the long fibril axis, this quaternary structure is known as the cross-β-sheet and is the hallmark of amyloid fibrils. In most cases, X-ray diffraction experiments measure the distances between β-sheets as 10 Å and the distances between β-strands as 4.8 Å (Chiti and Dobson, 2017; Eisenberg and Sawaya, 2017).

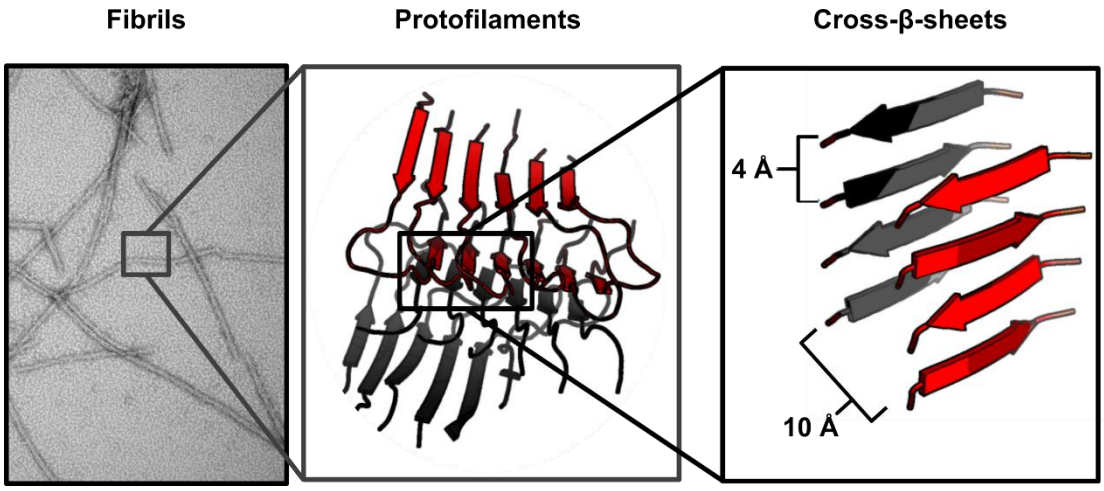

Figure 1.1 Hierarchical organization of amyloid fibrils. On the left, a transmission electron micrograph of amyloid fibrils prepared *in vitro* showing the mesoscopic structure. Middle, three-dimensional organisation of two associated protofilaments. Right, inter-strand and inter-sheet distances of a single protofilament.

Amyloid fibrils are highly resistant to most forms of degradation, or disassembly, as this quaternary structure is more thermodynamically stable than the native state of the monomer and often constitutes a thermodynamic endpoint (Chiti and Dobson, 2009). This is the case for transthyretin, a tetrameric protein associated with several forms of familial amyloidosis (Bourgault *et al.*, 2011c). Although it must pass through several energetically unfavourable intermediates or transition states, the resulting fibrils have a lower free energy than the monomeric structure (Geneste *et al.*, 2015). Frequent polymorphism is also displayed by *in vitro* amyloid preparations (Tycko, 2014), which is described as multiple fibril structures and organizations arising from the same peptide sequence. This suggests that the amyloid structure is an inherent consequence of the physicochemical properties of polypeptide chains and does not necessitate precise residue sequences. For example, due to the nature of the peptide amide bond, there is a significant possibility to engage in hydrogen bonding laterally between amino acid residues in sufficient proximity, which is the primary driving force behind the unique quasi one-dimensional structure of amyloids. (Fitzpatrick *et al.*, 2015). Although certain morphologies of fibrils can be favoured in laboratory conditions, this

can be overcome by using small amounts of pre-formed fibrils as seeds to promote the formation of the desired morphology (Tycko, 2011). It is important to note that fibrils prepared *in vitro* do not match the morphologies of fibrils isolated from patient amyloid extracts, though synthetic peptides may be seeded with fibrils extracted from patients to produce comparable structures (Qiang *et al.*, 2017).

1.2.2 Mechanisms of amyloid self-assembly

The mechanisms by which amyloidogenic precursors self-assemble have been a subject of great interest for several decades. Regardless of the underlying mechanism, amyloid growth is generally considered to be an exponential process and follows a sigmoidal growth curve (Kumar *et al.*, 2017). This results in three distinct phases of amyloid growth, as depicted in figure 1.2A: 1) the nucleation (or lag) phase, where monomers are in a dynamic state until eventually generating nuclei, 2) the elongation (or exponential) phase, where the nuclei grow in length and fibrils begin forming, and 3) the saturation (or equilibrium) phase, where fibril growth eventually depletes sufficient soluble monomers/oligomers to the point that no more can be incorporated into the fibrils (Kumar *et al.*, 2017).

Although a variety of mechanisms have been proposed for the known amyloidogenic polypeptides, they largely fall into three main categories. Nucleated polymerization is arguably the simplest process by which amyloid may form (Arosio *et al.*, 2015; Knowles *et al.*, 2009). In this case, monomers are primarily disordered, or have some exposed disordered region. The rate-limiting step in this model is the formation of nuclei by monomers during the lag phase, with some β-strand character. These nuclei are considered the smallest structures capable of initiating amyloid growth, which then recruit additional disordered, or partially disordered, monomers and fibril growth continues onwards. An alternative mechanism is the process of conformational conversion (Fu *et al.*, 2015). In this model, during the lag phase, soluble monomers are

in a dynamic equilibrium with soluble oligomers that largely retain the same secondary structure as the monomers. At some point, the oligomers undergo a thermodynamically unfavorable change in conformation to generate nuclei, which then are able to incorporate other oligomers, or monomers, through a templating effect. Here, the process is rate-limited not by the formation of oligomers, but rather by the structural conversion of oligomers into nuclei (Meisl *et al.*, 2016). Both of these processes are most often proposed for smaller polypeptides, but for large globular proteins, these pathways are not accessible unless there is a significant degree of unfolding to expose the disordered regions to the solvent. Large globular proteins likely undergo a process of native-like aggregation, where aggregation prone segments are revealed due to local unfolding or the release of a ligand. These proteins then form aggregates and proceed to form fibrils, similar to the process of conformational conversion (Chiti and Dobson, 2017). These processes are represented schematically in figure 1.2B (reproduced from Chiti and Dobson, 2017), which also depicts secondary nucleation. While each of these models can potentially exist in isolation, alternative pathways are possible, and the reality is that there is likely a coexistence of more than one process at any given time (Kumar and Udgaonkar, 2009).

Furthermore, there are secondary processes that may dramatically influence amyloid formation. Two secondary processes of particular importance are fragmentation and secondary nucleation. Fragmentation, as the name implies, involves the fracturing of pre-formed fibrils into smaller segments, whereas secondary nucleation is the process by which monomers associate to pre-formed fibrils to bypass the rate-limiting steps of nucleation. While these processes (primary nucleation, secondary nucleation, fibril elongation, and fragmentation) are difficult to discuss separately in any given system, a generalized equation can be formulated to describe the overall process. This mathematical analysis allows for the determination of rate constants, which permits the mathematical reconstruction of the fibrilization mechanism. This enables the study of

various perturbations on the amyloid system, such as membrane surfaces, chaperones, or small molecules (Arosio *et al.*, 2016).

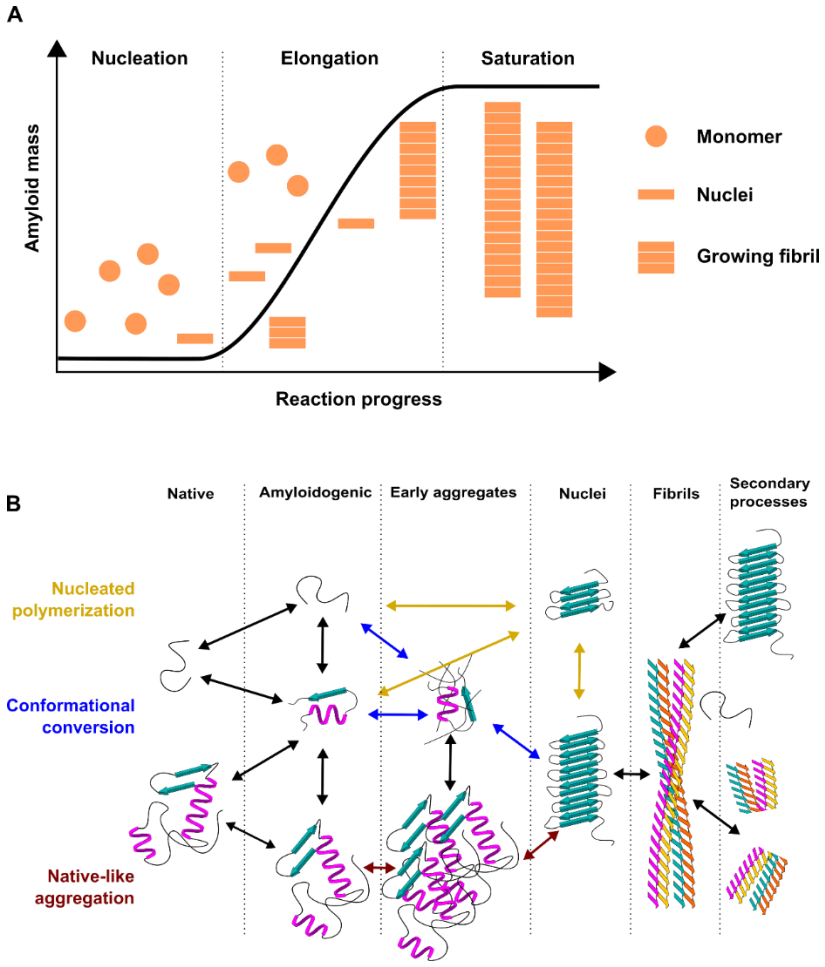

Figure 1.2 Mechanisms of amyloid self-assembly. A) Kinetic profile of amyloid formation, showing the three phases of self-assembly. B) Different aggregation pathways, illustrating the transitions between native, nucleated, and fibril forms. Secondary processes are included which depict fragmentation and secondary nucleation. Reproduced in part from Chiti and Dobson, 2017.

1.2.3 Functional amyloids

The stable and highly unique amyloid superstructure does play a functional role in numerous organisms (Fowler *et al.*, 2007). While most cases of functional amyloid

were characterized in yeast and bacteria, several interesting forms of functional amyloid were also discovered in mammals, including humans. Selected examples are displayed in table 1.2 (Fowler *et al.*, 2006; Otzen and Riek, 2019). Functional amyloids are grouped by their activities, such as chemical storage, structural roles, information, loss-of-function, and gain-of-function/signalling (Otzen and Riek, 2019). For example, Pmel17 forms a structural amyloid scaffold for the biosynthesis of melanin in melanocytes (Fowler *et al.*, 2006). Additionally, amyloid bodies, or A-bodies, form within the nucleus as a response to various cell stressors as an adaptive mechanism (Audas *et al.*, 2016). These functional, protective amyloids are dynamically formed and reversible, using RNA as a linear polyanion to initiate the phase change from soluble proteins to insoluble amyloids (Lyons and Anderson, 2016).

Table 1.2 Functional amyloids in mammals.

Classification	**Example**	**Reference**
Structure	Pmel17 – Templates biosynthesis of melanin Amyloid converting motif – sequence which stores proteins as A-bodies in nucleus	Fowler et al., 2006, Audas et al., 2016
Storage	Peptide hormones – storage and release of various hormones	Maji et al, 2009
Loss of function	MBP – inert storage of toxic MSP	Soragni et al., 2015
Gain of function	RIP1/RIP3 – signalling and cell death	Li et al 2012

A particularly interesting example of functional amyloids in humans is the storage of peptide hormones as amyloid-like deposits within secretory granules. After secretion, due to changes in pH between granular and extracellular environments, the amyloid-like aggregates dissociate and release biologically active monomeric peptides (Badtke *et al.*, 2009; Maji *et al.*, 2009). A further potential utility of this phenomenon is the sorting of peptide hormones in the Golgi, which may occur due to the nature of the aggregation process being self-selective. This would imply that newly processed peptide hormones group together and form granule cores consisting of specific hormones rather than a mixture. However, due to the observed ability of amyloids to

cross-seed, it may even be possible for co-aggregates of hormones to occur, resulting in granules with defined hormone release ratios (Otzen and Riek, 2019). This was observed under experimental conditions for adrenocorticotropic hormone (ACTH) and β-endorphin, such that despite not forming amyloid on its own, ACTH did co-aggregate with β-endorphin to form amyloid-like fibrils (Maji *et al.*, 2009). Both ACTH and β-endorphin are processed from the same prohormone and secreted together, further corroborating this hypothesis. Similarly, the pituitary adenylate cyclase activating polypeptide (PACAP) is another peptide hormone presumed to be stored as amyloid inside secretory granules (Maji *et al.*, 2009), and the specifics of PACAP regarding its physiological roles and aggregation will be addressed below.

1.2.4 Pathological amyloids

While functional amyloids are important, they are nonetheless a more recent area of research and consequently, the vast majority of work conducted to date concerns the pathological nature of amyloid. Alzheimer's disease (Atwood *et al.*, 2002), Parkinson's disease (Mehra *et al.*, 2019), and various forms of systemic amyloidosis (Wechalekar *et al.*, 2016) are all active areas of interest, studying the behaviour of the monomeric proteins, the corresponding aggregation, and the ensuing pathophysiology.

Table 1. 3 A non-exhaustive list of pathological amyloids in humans.

Peptide or protein	Residues	Associated disease	Reference
Amyloid-β	40/42	Alzheimer's	Yasumoto et al., 2019
α-synuclein	140	Parkinson's	Mehra et al., 2019
Prion protein	208	Creutzfeldt-Jakob	Rouvinski et al., 2014
Transthyretin	127 x 4	Familial amyloidotic neuropathy	Geneste et al., 2015
Serum amyloid A	45 – 104	AA amyloidosis	Aguilera et al., 2014

In the context of peptide hormones, there are also numerous important cases to study. One such example is the peptide atrial natriuretic factor (ANF) (figure 1.3A). ANF is

densely stored in secretory granules inside cardiomyocytes as shown in figure 1.3B (Inagami, 1989) and upon release, enters the bloodstream. Several physiological responses can be elicited by ANF, primarily directed towards lowering blood pressure. This is achieved through the regulation of renin secretion, and both uresis and natriuresis – *i.e*., the excretion of excess sodium (Inagami, 1989). ANF has been shown to aggregate, however, and amyloid-rich deposits known as isolated atrial amyloid (IAA) can be found in the atria of the heart, with the majority of amyloid deposits found in the extracellular space along the outside of cardiomyocytes (figure 1.3C) (Johansson and Westermark, 1990). Although heterogenous in composition, the major peptide constituent within IAA deposits is the peptide hormone ANF. The presence of IAA is a common form of amyloid associated with increased age, appearing in over 80% of individuals aged 80 years or older, (Louros *et al.*, 2014). IAA deposits are detrimental to heart function and can increase the risk of congestive heart failure, atrial fibrillation, and atrial thromboembolism (Louros *et al.*, 2014).

Another important example is the peptide hormone calcitonin (figure 1.3D). Human calcitonin is secreted by para-follicular cells in the thyroid. Calcitonin primarily acts on bones, inhibiting resorption and osteoclast activity, though it also decreases the reabsorption of calcium and other minerals in the kidneys (Srinivasan *et al.*, 2020). While there is some interest in improving the therapeutic aspects of calcitonin as a treatment for bone diseases (osteoporosis, Paget's disease, hypercalcaemia), its important role in medullary thyroid carcinoma (MTC) needs to be considered. In MTC, significant amounts of calcitonin-rich fibrillar amyloid aggregates are localized within the thyroid (Khurana *et al.*, 2004). Fibrils of synthetic calcitonin and amyloid deposits of calcitonin in MTC are shown below in figure 1.3E and F, respectively. Although a rare form of thyroid cancer (2-5% of all thyroid cancer cases) (Erickson *et al.*, 2015), MTC has the ability to spread to surrounding lymph nodes and other organs (Jaber *et al.*, 2021). Treatment options for MTC are primarily surgical, although in recent years immune-based therapies appear promising (Vergaro *et al.*, 2022).

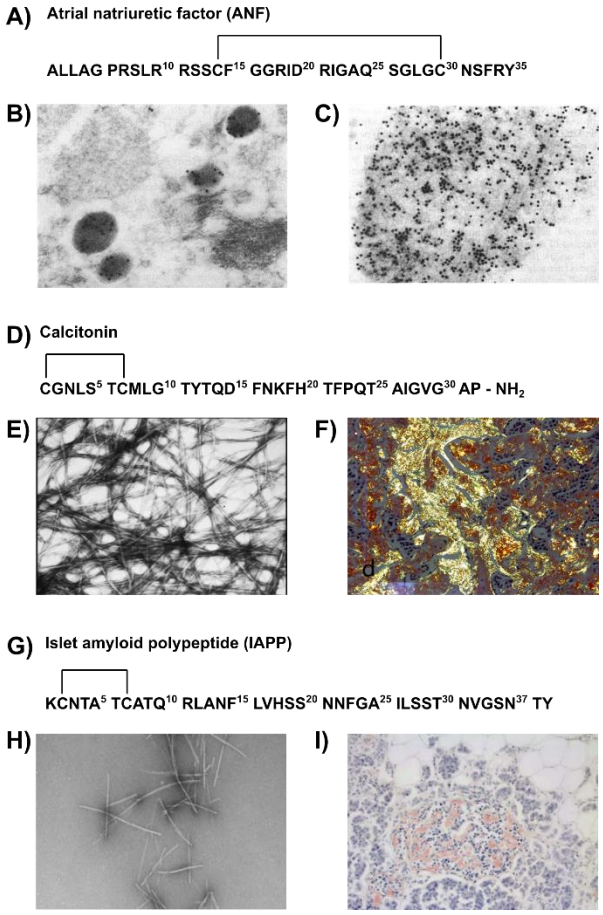

Figure 1.3 Pathological cases of peptide hormone amyloidosis. A) ANF primary sequence, B) immunogold detection of ANF in cardiomyocyte secretory granules, C) immunogold detection of ANF fibrils in atrial tissue after necropsy (Kaye *et al.*, 1986). D) calcitonin primary sequence, E) fibrils formed from calcitonin *in vitro*, F) Congo red birefringence of calcitonin aggregates in medullary thyroid carcinoma (Erickson *et al.*, 2015). G) primary sequence of IAPP, H) fibrils formed from synthetic IAPP *in vitro*, I) Congo Red staining of IAPP amyloid deposits in pancreatic tissue (Westermark *et al.*, 2011).

Arguably, the most well-known case of pathological peptide hormone aggregation is IAPP (figure 1.3G). Co-secreted with insulin by the pancreatic islet cells, IAPP has implications in controlling gastric emptying and satiety (Montane *et al.*, 2012), though the full function of IAPP is not fully understood (Westermark *et al.*, 2011). IAPP rapidly assembles into amyloid fibrils under physiological conditions (figure 1.3H). Aggregates rich in IAPP are found in the vast majority of individuals afflicted with

type II diabetes mellitus (T2D), though can occasionally be found in otherwise healthy individuals (Westermark *et al.*, 2011). This is detected histologically using the birefringence of Congo red (CR) (figure 1.3I). The presence of amyloid in the pancreas is associated with reduced β-cell mass and the disturbance of normal cellular function. It has been observed that the fibrils located inside the amyloid deposits were able to penetrate deep within the surrounding cells. Additionally, *in vitro* experiments clearly demonstrated that IAPP can disrupt the plasma membrane and cause the unregulated influx of calcium ions – a process which would significantly impair cellular function (Kawahara *et al.*, 2000; Sciacca *et al.*, 2020). The specific behaviours and mechanisms by which IAPP aggregates and interacts with plasma membranes will be addressed in detail below in the corresponding sections.

1.3 Islet amyloid polypeptide (IAPP)

1.3.1 Physiological role and function

IAPP was first discovered in 1986 and identified as the main proteinaceous component contributing to the lesions found in pancreatic samples described over a century earlier (Opie, 1901). This 37-residue peptide hormone derives from the cleavage of an 89-residue precursor, preproIAPP, and the further processes of the corresponding 67-residue prohormone, proIAPP, by carboxypeptidase E and prohormone convertase (Westermark *et al.*, 2011) in the Golgi and secretory granules of pancreatic β-cells. IAPP undergoes two post-translational modifications necessary for its full biological activity: C-terminal amidation, and the formation of a disulfide bridge between residues Cys-2 and Cys-7 (Young *et al.*, 1996). IAPP is found in all mammals so far and the primary sequence is generally well conserved, yet several substitutions at key positions may alter the physicochemical and biological properties of the peptide significantly. For example, human IAPP is well-known for its ability to aggregate and form amyloid fibrils whereas IAPP sequence from rodents can not form fibrils under

physiological conditions (figure 1. 4A). Notable substitutions include multiple prolines in the region between residues 20 – 29, a segment of the peptide recognised for its important role in initiating the aggregation (Westermark *et al.*, 1990).

IAPP is a member of the calcitonin family and consequently shares significant homology with calcitonin, calcitonin gene-related polypeptide, and adrenomedullin (Akter *et al.*, 2016). Although a relatively hydrophobic polypeptide, IAPP contains a few cationic residues and typically has an overall charge of +2 to +4, depending on pH. Despite being an intrinsically disordered peptide (IDP), IAPP does possess a slight degree of α-helical conformation in solution and is not a pure random coil *per se* (Williamson *et al.*, 2009; Williamson and Miranker, 2007). In the presence of phospholipid bilayers, however, IAPP adopts a helix-kink-helix structure, with the first α-helix occurring between residues 5 – 17, and the second α-helix between residues 20 – 27 (figure 1. 4A) (Nanga *et al.*, 2011).

IAPP exerts a diverse array of biological effects as a peptide hormone, though it is primarily associated with the regulation of satiation, gastric emptying, and inhibiting glucagon secretion (Lutz, 2010; Montane *et al.*, 2012; Westermark *et al.*, 2011). As with other peptide hormones (*e.g.*, secretin, calcitonin), IAPP activates multiple G-protein coupled receptors (GPCRs) found across a variety of cell types (Hay *et al.*, 2015). Despite exhibiting some minor activity with calcitonin receptors, IAPP binds with significantly higher affinity to the AMY1, AMY2, and AMY3 receptors. These receptors are fundamentally calcitonin receptors with a single additional transmembrane domain termed the “receptor activity-modulating protein” (RAMP) (Christopoulos *et al.*, 1999; Muff *et al.*, 1999) (figure 1. 4B). With these receptors, IAPP exhibits such a high affinity that it can induce signalling even at the low picomolar concentrations found circulating in the plasma (Akter *et al.*, 2016; Hay *et al.*, 2015).

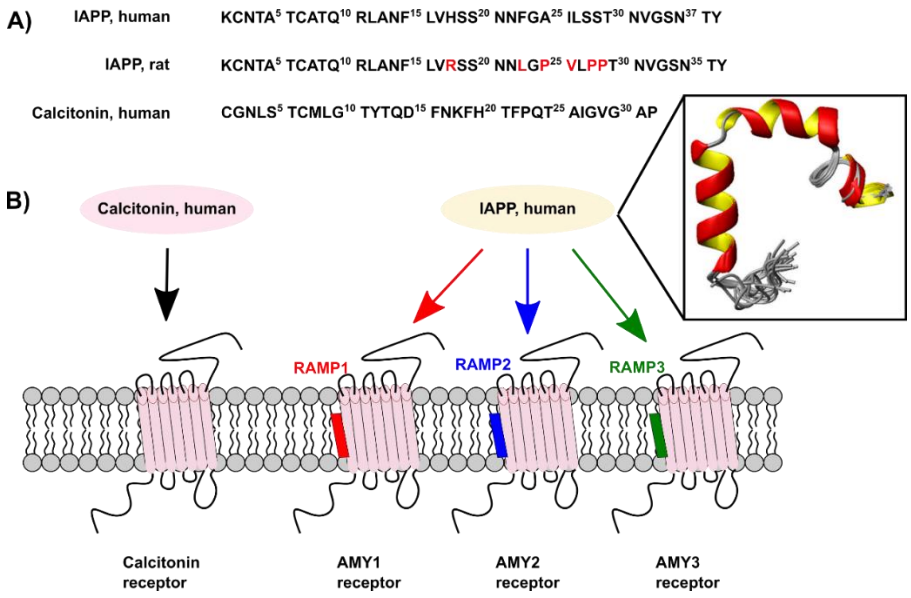

Figure 1. 4 Sequences of IAPP and calcitonin, and their associated receptors. A) Primary sequences of human IAPP, rat IAPP with substituted residues highlighted in red, and human calcitonin. B) Schematic representation of calcitonin and IAPP receptor systems, showing RAMPs and biologically active conformation of IAPP in the inset, obtained from Nanga et al., 2011.

1.3.2 Storage, aggregation, and self-assembly

While the plasma levels of IAPP are in the low picomolar range, inside secretory granules of the pancreatic β-cells the concentrations are up to low millimolar levels (Hay *et al.*, 2015). This results in a dramatic concentration gradient for IAPP, starting from high storage concentrations and decreasing after secretion into the extracellular space, until finally reaching the lowest concentrations in the circulating plasma. IAPP is not the only peptide inside β-cell secretory granules; it is stored in an approximately 1:100 ratio with insulin. Both IAPP and insulin are prone to aggregation and are each sufficiently concentrated that intragranular aggregation could occur yet does not. This is most often explained by several contributing factors such as the acidic pH, the presence of Zn^{2+}, and the competitive aggregation inhibition between the two peptides (Klaips *et al.*, 2018; Wiltzius *et al.*, 2009).

IAPP readily aggregates to form amyloid deposits in the extracellular space, and these deposits are present around islet cells for the vast majority of patients with type 2 diabetes (Milardi *et al.*, 2021; Westermark *et al.*, 2011). The role of these amyloid deposits in type 2 diabetes pathophysiology is not entirely understood, though it is suspected that the aggregation process of IAPP plays an important part. Interestingly, there are also epidemiological links between IAPP and other protein aggregation pathologies such as Alzheimer's and Parkinson's diseases (Hu *et al.*, 2007; Peila *et al.*, 2002). Patients presenting with type 2 diabetes exhibited a roughly two-fold increased risk for developing dementia in the Rotterdam study (Ott *et al.*, 1996). Furthermore, a new type of diabetes has been recently proposed, termed "type 3 diabetes" or "Alzheimer's disease-associated insulin resistance" and "brain phenotype diabetes" (Raimundo *et al.*, 2020; Stanciu *et al.*, 2020). There appears to be an important relationship between IAPP and Alzheimer's disease (AD) since IAPP has been found in AD brain tissue extracts (Bharadwaj *et al.*, 2020; O'Nuallain *et al.*, 2004) and *in vitro* experiments demonstrated the ability of IAPP and the AD-associated peptide, amyloid-β (Aβ), to accelerate aggregation and amyloid formation. Although a clear link between IAPP aggregation and pancreatic cell death has been found, the precise mechanisms by which this occurs remain elusive and various hypotheses are possible.

A number of intermediate structures are occupied by IAPP during its transition from the monomeric to the aggregated state, many of which are short-lived and dynamic. The resulting structures of the amyloid fibrils formed from IAPP are, by definition, cross-β-sheets; consequently, the monomeric peptide – which is natively unstructured – must undergo significant folding to be packed into the cross-β-sheet arrangement. The process of IAPP self-assembly results in multiple fibril morphologies, likely occurring from the competition between thermodynamic stability and reaction kinetics (Luca *et al.*, 2007). The actual supramolecular structures of amyloid fibrils may vary significantly, such as in terms of the number of twists, diameter, or length (vandenAkker *et al.*, 2011). The first structure proposed for fibrillar IAPP was

determined by solid-state nuclear magnetic resonance spectroscopy (ssNMR) (Luca *et al.*, 2007). To obtain this structure, however, fibrils were prepared under unique conditions, favouring a certain morphology described as the striated ribbon. In more recent years, fibril structures for synthetic IAPP (among other polypeptides) have been proposed using cryo-electron microscopy (Cao *et al.*, 2020; Röder *et al.*, 2020). Additionally, in a particularly interesting case, fibrils were prepared from synthetic IAPP, seeded with pancreatic amyloid extracts from patients with diabetes. The cryo-electron microscopy structures obtained from this seeded preparation demonstrated multiple different fibril morphologies arising from the arrangements of the protofilament cores, likely representing the fibrillar structure of pathological IAPP fibrils (Cao *et al.*, 2021).

1.3.3 Mechanisms of cytotoxicity

The cytotoxicity associated with the tissue deposition of amyloid fibrils is likely multifactorial. Reports of various mechanisms are present in the literature, ranging from biophysical models and *in vitro* studies, all the way to *in vivo* observations. Much of the early work studying amyloid-associated cytotoxicity was centered around the fibrils themselves. These large aggregates can be present in significant amounts and directly lead to organ failure or tissue dysfunction. However, for most amyloid peptides and proteins, it is currently suspected that the mechanisms of cytotoxicity occur through multiple overlapping pathways (Abedini and Schmidt, 2013). This is the case for IAPP, where increasing evidence suggests that the fibrils themselves are markedly less damaging to pancreatic β-cells than pre-fibrillar structures (oligomers, protofibrils, etc.) (Abedini *et al.*, 2016b; Akter *et al.*, 2016). Mechanisms involved in IAPP-associated cytotoxicity can be divided into two categories: non-receptor based mechanisms where IAPP aggregation directly disrupts the cellular integrity, and receptor-mediated mechanisms where soluble pre-fibrillar IAPP species binds cell surface receptors and triggers apoptotic pathways (Abedini and Schmidt, 2013).

Receptor-mediated mechanisms of IAPP-induced β-cell toxicity involve generating oxidative stress, the production of cytokines, and the activation of signalling cascades leading to apoptosis. It was demonstrated with cultured islet cells that IAPP activated the pro-apoptotic cJUN N-terminal kinase pathway. In pancreatic islet cells, the cJUN N-terminal kinase pathway has also been observed to be upregulated in response to endogenous IAPP aggregates (Subramanian *et al.*, 2012). Similarly, the interaction of IAPP aggregates with the FAS receptor leads to the activation of caspase-3 signalling. Interestingly, using Fas knockout, β-cells were protected from IAPP toxicity (Park *et al.*, 2012). Additionally, toxic aggregates of IAPP are able to activate the inflammasome – multiprotein caspase-activating complexes, implicated in metabolic diseases. The triggering of such signalling cascades by IAPP leads to the production of cytokines such as interleukin-1β (Masters *et al.*, 2010). IAPP may also play a role in autophagy dysfunction. Autophagy is an important cellular process to destroy and recycle damaged cellular materials. In cases where IAPP is overexpressed, however, before the onset of hyperglycemia, autophagy can be impaired. Consequently, this reduced capacity to handle misfolded or aggregated proteins further facilitates the aggregation of IAPP, leading to many of the other described processes (Morita *et al.*, 2011; Rivera *et al.*, 2011). Somewhat more recently, the interactions of receptors for advanced glycation end-products (RAGE) with IAPP aggregates have been explored and offers another potential cytotoxic pathway (Abedini *et al.*, 2018). Nonetheless, the vast majority of mechanisms explaining IAPP associated cytotoxicity revolve around the direct, physical disruption of cell phospholipid bilayers and consequently, this will be the main process addressed throughout the relevant sections of this research thesis.

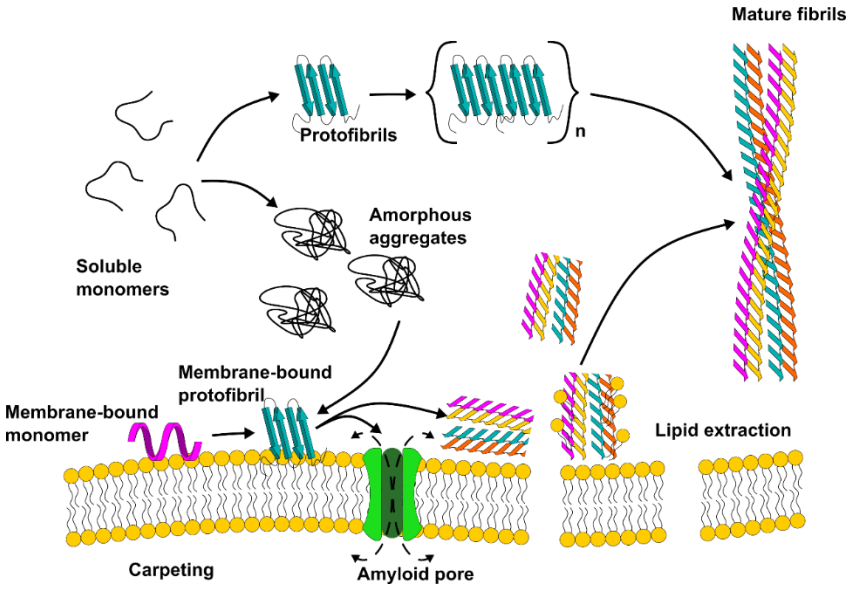

Figure 1.5 Proposed mechanisms of IAPP-induced membrane damage. Multiple processes are suspected to occur which lead to the destabilization of the plasma membrane and consequently cell death. Several mechanisms are illustrated here: carpeting of the peptide on the membrane surface, lipid extraction of the nascent fibrils, and the formation of amyloid pores.

Due to its aggregation, IAPP also exerts non-receptor mediated cytotoxic activity involving the non-specific permeabilization of plasma and mitochondrial membranes. Necessarily, a loss of integrity in these regions results in cellular dysfunction and eventually, cell death. As illustrated in figure 1.5, monomeric IAPP may adhere to the membrane surface and form protofibrillar aggregates that would insert into the bilayer and form a transmembrane pore. Such pores can be formed from soluble IAPP aggregates as well. Finally, membrane bound IAPP may continue to aggregate on the bilayer surface, resulting in the extraction of lipids from the membrane. Membrane permeabilization through mechanisms such as these results in increased Ca^{2+} influx and consequently mitochondrial dysfunction, and the production of reactive oxygen species (Schubert *et al.*, 1995).

One criticism of the membrane permeabilization studies of IAPP is that these are generally conducted using synthetic model membranes, whose composition does not reflect that of biological membranes. In many such cases, excessive amounts of anionic phospholipids are used, and it is uncommon for cholesterol and gangliosides to be incorporated into synthetic models, all of which are present in cell plasma membranes (Abedini and Schmidt, 2013; Sciacca *et al.*, 2018). Additionally, there is a notable lack of literature addressing the other differences between plasma membranes and synthetic bilayers, such as the role of the cytoskeleton and glycocalyx during perturbations.

1.4 Pituitary adenylate cyclase activating polypeptide (PACAP)

1.4.1 Physiological role and function

PACAP is a neuropeptide, which was first isolated from ovine hypothalamus extracts in 1989. It exists in two isoforms: a 38-residue polypeptide, and a C-terminal truncated 27-residue polypeptide (Hirabayashi *et al.*, 2018). PACAP has a high degree of sequence homology with vasoactive intestinal polypeptide (VIP) and glucagon and is a member of the VIP/glucagon/secretin superfamily (figure 1.6A). Both the 38 and 27 residue isoforms are highly conserved sequences among species, with identical forms of PACAP38 and PACAP27 found in all mammals, and only several minor substitutions in non-mammals (e.g., tunicates) (Rudecki and Gray, 2016). PACAP is synthesized from the 176 residue preproPACAP, where the first 25 residues are cleaved by signal proteases to produce a signal peptide (1 – 25) and proPACAP (26 – 176). The proPACAP is further cleaved into a large peptide fragment (26 – 79), a small peptide fragment (82 – 129), and the c-terminal peptides PACAP38 (132 – 170) and PACAP27 (132 – 159) by peptidylglycine and α-amidating monooxygenases, respectively, resulting in C-terminal amidation of PACAP (Hirabayashi *et al.*, 2018). Both isoforms have similar, sub-nanomolar affinity for the GPCR PAC1, and also act on the shared GPCRs VPAC1 and VPAC2 with VIP (figure 1.6B) (Rudecki and Gray, 2016).

PACAP27 and PACAP38 are both intrinsically disordered peptides, though it has been shown that each isoform of PACAP can adopt an α-helical structure to become biologically active (Bourgault *et al.*, 2009; Tchoumi Neree *et al.*, 2014). Interestingly, PAC1 is one of the most highly spliced receptors known to date, and PACAP is involved in a wide range of biological processes such as the response to fear, post-traumatic stress disorder, obesity, migraines, Parkinson's disease, and potentially AD (Tan and Waschek, 2011; Waschek, 2013). Furthermore, PACAP plays a critical role in the adaptation to psychogenic and metabolic stress by means of regulating the hypothalamic-pituitary-adrenal axis and sympathetic nervous system, respectively (Eiden, 2013; Ferguson *et al.*, 2013; Mustafa, 2013; Stroth *et al.*, 2011).

With its role as a sort of master regulator, and its ability to act both on the central and peripheral nervous system, there is a great deal of interest in studying PACAP in a pathophysiological context. Not only has increased PACAP expression been observed in individuals with migraine headaches, but infusions of PACAP were able to induce migraines as well (Markovics *et al.*, 2012; Tuka *et al.*, 2013). Conversely, reduced PACAP expression was observed during autoimmune and neurodegenerative diseases such as Alzheimer's, Parkinson's, multiple sclerosis, schizophrenia, and traumatic brain injury (Han *et al.*, 2014; Rudecki and Gray, 2016). Outside of the brain, however, PACAP has notable roles in the pancreas, as both PAC1 and VPAC1/2 receptors are expressed in pancreatic α/β cells (Portela-Gomes *et al.*, 2003). There is, furthermore, some indication that PACAP is expressed by pancreatic cells themselves, as immunoreactivity demonstrated that PACAP was localized within secretory granules of glucagon and insulin. Sustained insulin secretion during increased demand is also maintained by PACAP, which protects against oxidative stress and regulates β-cell proliferation/apoptosis (Sakurai *et al.*, 2011; Yamada *et al.*, 2004).

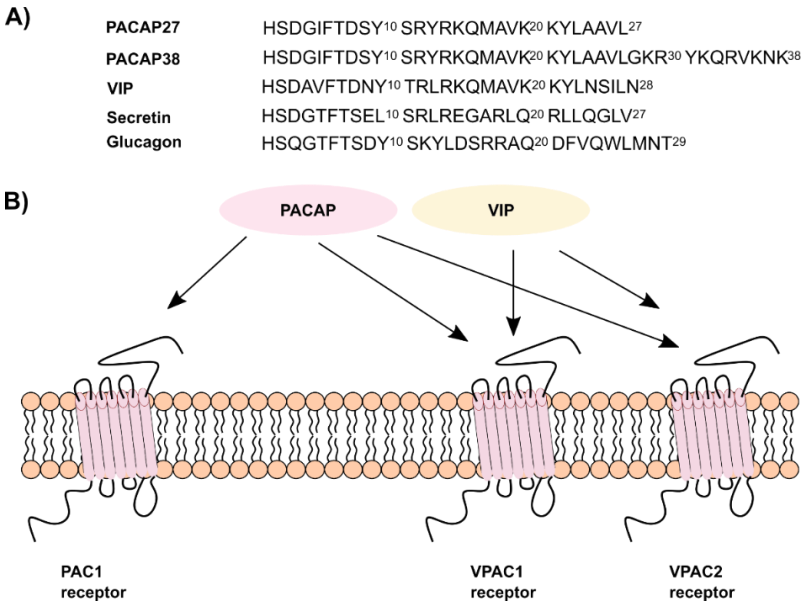

Figure 1.6 PACAP and related peptide sequences and receptor activities. A) Primary sequences of PACAP isoforms and related peptides. B) Schematic representation of PACAP and VIP receptor system.

1.4.2 Storage, aggregation, and self-assembly

In 2009, a study published in *Science* proposed that PACAP, among a large number of other peptide hormones, was stored in secretory granules as insoluble fibrils (Maji *et al.*, 2009). Furthermore, it was demonstrated that such aggregates were reversible and able to release monomeric peptide units. The aggregates were considered to be a new form of functional amyloid fibrils which conferred an energetically favourable storage system inside of secretory granules. Since the high concentrations of peptide hormone were stored in an insoluble state, no osmotic gradient was created and consequently, no energy required to store such large amounts. Upon secretion of the hormones into the extracellular space, the change in pH from acidic (pH 5.5 inside the granules) to slightly alkaline (pH 7.4 in the interstitial fluid) induced the disassembly of the fibrils, releasing the peptide hormones back into solution (Maji *et al.*, 2009; Nespovitaya *et al.*, 2016). Further supporting this hypothesis, several co-factors present in the secretary

granules have been identified to favour amyloid fibril formation in peptide hormones: metal ions, such as zinc (Jacob *et al.*, 2016), peptide-peptide coaggregation (Ranganathan *et al.*, 2012), and glycosaminoglycans (GAGs) (Jha *et al.*, 2013; Malmos *et al.*, 2016; Mehra *et al.*, 2018). PACAP itself is a cationic peptide and contains a sequence of amino acids that follows the heparin binding motif XBBXBX, where B represents a basic residue and X represents any other residue (figure 1.6A). The relationship between polypeptides and GAGs has already been explored to a significant degree in the context of amyloid formation (Aguilera *et al.*, 2014; Bazar and Jelinek, 2010; Corlin *et al.*, 2010; De Carufel *et al.*, 2013; Jha *et al.*, 2013; Madine *et al.*, 2013; Neree *et al.*, 2015; Rullo *et al.*, 2011; Solomon *et al.*, 2011; Tchoumi Neree *et al.*, 2014), though in this work, particular importance is placed on the mechanisms by which GAGs induce the fibrillar aggregation of the otherwise highly soluble and non-aggregating PACAP.

1.5 Biological cofactors in amyloid formation

Although the major constituents of amyloid deposits are of proteinaceous nature, significant amounts of other biological molecules are present, such as metal ions, lipids, and glycosaminoglycans (Nguyen *et al.*, 2015). Each of these cofactors plays an important role in amyloid pathophysiology and the fibrilization process. These cofactors can either facilitate or impede the fibrilization of amyloidogenic peptides. Interestingly, certain co-factors, such as metal ions, display divergent effects on amyloid self-assembly depending on the peptide in question. For example, zinc (II) is able to both prevent and promote the fibrilization of different peptide hormones, such as preventing the formation of IAPP fibrils inside secretory granules (Salamekh *et al.*, 2011), yet favouring the formation of fibrils from the growth hormone inside of secretory granules (Jacob *et al.*, 2016) and with human prolactin (Christensen *et al.*, 2016).

Linear polyanions, such as GAGs and RNAs, have demonstrated a persistent ability to promote and/or to accelerate fibrilization of peptide hormones. For example, a large number of the peptides studied in the original work proposing the storage of peptide hormones as amyloid were only able to form dense fibrils in the presence of low molecular weight fractions of heparin (Maji *et al.*, 2009). Similarly, in the case of a peptide fragment from the phospholamban protein, the addition of GAGs immediately induced the formation of fibrillar aggregates while the peptide remained soluble under control conditions (Madine *et al.*, 2013). This was even described specifically for the hormone β-endorphin, where the structural role of heparin was demonstrated during fibril growth and the reversibility of said fibrils (Nespovitaya *et al.*, 2016; Nespovitaya *et al.*, 2017). Moreover, it is important to note that at certain concentrations, GAGs are actually able to do the reverse and prevent the aggregation of peptides (Bazar and Jelinek, 2010). Arguably the two most studied cofactors, however, are lipids and GAGs. Therefore, most of the ensuing work will be devoted to the roles of these two biomolecules and the importance of each one in the amyloidogenic process.

Table 1.4 Biological cofactors found in amyloid deposits *in vivo*

Cofactor	Example	Reference
Metal ions	Zinc (II)	(Khemtemourian et al., 2021)
	Copper (II)	(Crooks et al., 2020)
Proteins	Heat shock proteins	(Wentink et al., 2019)
	Apolipoprotein E	(Chargé et al., 1996)
Polyanions	RNA	(Audas et al., 2016)
	Glycosaminoglycans	(Young et al., 1992)
Lipids	Cholesterol	(Caillon et al., 2014)
	Anionic phospholipids	(Zhang et al., 2017)

1.5.1 Glycosaminoglycans

GAGs are long, linear anionic polysaccharides, which are found on the outer leaflet of plasma membranes, or as major structural components of the extracellular matrix

(ECM) (Papy-Garcia *et al.*, 2011). Important biopolymers, GAGs play essential roles in cellular differentiation, proliferation, migration, and survival through their interactions with cytokines, growth factors, or other heparin binding proteins (Maiza *et al.*, 2018). The polysaccharide chains of GAGs are composed of up to 200 disaccharide building blocks, able to reach sizes of approximately 100 kDa. Depending on the disaccharide units, GAGs can be classified into four subfamilies, with each having distinct physicochemical properties (charge, degree of sulfation, etc.): heparan sulfate (HS), chondroitin sulfate (CS), keratan sulfate (KS), and hyaluronic acid (HA) (figure 1.7A) (Papy-Garcia *et al.*, 2011). Interestingly, KS are the only GAGs to incorporate galactose in the disaccharide units. GAGs can be found in two forms: free/soluble GAGs or bound to a protein core resulting in the formation of a proteoglycan (Gandhi and Mancera, 2008). HS and CS chains are bound to the proteoglycan core by O-linkages with serine residues, while KS chains can be found with both O- and N-linkages to Ser/Thr or Asn residues, respectively (Maiza *et al.*, 2018; Papy-Garcia *et al.*, 2011).

The biosynthesis of GAGs is complex, and results in a diverse array of final polysaccharide structures. Firstly, in the endoplasmic reticulum, xylosyltransferases join a xylose-containing tetrasaccharide (Xyl-Gal-Gal-GlcA) to a Ser residue on the proteoglycan core (Persson *et al.*, 2018). Secondly, the process is then initiated with either specific transferases for GlcNAc or GalNAc. Thirdly, disaccharide units are added to elongate the growing polysaccharide chains, and sulfate groups are added at acetyl or hydroxyl moieties by sulfotransferases. Fourthly, the proteoglycans are then transported from the Golgi to the cell surface/extracellular matrix (Li and Kusche-Gullberg, 2016). Finally, further processing at this stage is still possible, such that oligosaccharides can be liberated through enzymatic cleavage. It is important to note that in the ECM, growth factors and cytokines can be stored in a bound state with GAGs (Jin *et al.*, 2021). While the types of GAGs in the ECM are varied (HS, CS, KS, HA), those found on the plasma membrane of cells are primarily HS proteoglycans (HSPGs)

(figure 1.7). Another type of GAG, heparin, is expressed in mast cells and is the most highly sulfated form of GAGs. Isolated heparin (approximately 2.7 sulfate groups per disaccharide unit) is often used in *in vitro* experiments to represent the most densely charged segments of HSPGs (averaging 1 sulfate group per disaccharide) (Iannuzzi *et al.*, 2015; Quittot *et al.*, 2017b).

While GAGs have numerous physiological roles that are well defined, they are also important players in the more enigmatic processes of protein aggregation and amyloid formation. Indeed, virtually all intra- and extra-cellular insoluble proteinaceous deposits from patients contained significant amounts of GAGs (Ancsin, 2003). In these extracts, GAGs appeared to be an integral component of the aggregates and consequently initiated a wealth of research on the roles GAGs played in amyloid disorders (table 1.5). Generally, *in vitro* experiments demonstrated that GAGs such as heparin, HS, and CS accelerated the process by which monomeric proteins/peptides form amyloid fibrils (Quittot *et al.*, 2017b). This acceleration is dependent on the chain length, or the degree of polymerization (dp) and smaller chains ($dp \leq 4$) exhibit minimal effects on fibrilization (Jha *et al.*, 2011). At longer chain lengths, however, ($6 \leq dp \leq 18$), fibrilization is markedly accelerated. Beyond this length ($dp >>> 18$) a plateau is reached, and under certain conditions can even discourage fibrilization (Jha *et al.*, 2011). It is thus far suspected that shorter chain lengths of GAGs (i.e., $dp \leq 4$) are incapable of binding multiple peptide monomers and therefore unable to sufficiently increase the local concentration of peptide, thereby accelerating the self-assembly process. Similarly, the relative GAG-to-protein molar ratios have been demonstrated *in vitro* to be an important variable in determining the role that GAGs play during fibrilization. Lower GAGs:peptide molar ratios ($\leq$ 1:1) displayed the ability to accelerate fibrilization, whereas high molar ratios once again impeded fibrilization (Bazar and Jelinek, 2010; Mehra *et al.*, 2018). This was explained as the peptides being too dispersed among GAGs, such that insufficient numbers of peptide monomers were in close enough proximity on the same GAG chain. Research has also described the

importance of sulfation in this process, such that higher degrees of sulfation increase the binding affinity for proteins and accelerate the process of fibrilization, while non-sulfated GAGs such as HA or N-acetylated heparin did not favour fibrilization despite maintaining the same overall anionic charge (Aguilera *et al.*, 2014; Bourgault *et al.*, 2011c).

Several groups have analyzed the mechanisms by which GAGs modulate amyloid fibril formation, and four different mechanisms have been postulated using HS/heparin with a variety of amyloidogenic proteins and peptides (Maiza *et al.*, 2018). Firstly, HS may promote the folding of proteins/peptides into amyloid-competent precursors (Schultz *et al.*, 2017; Xu and Esko, 2014). Secondly, HS may act as a molecular platform for monomer self-assembly, increasing local concentrations and therefore monomer unit density around the polysaccharide chain (McLaurin *et al.*, 1999; Rouvinski *et al.*, 2014). Thirdly, HS may act as a platform for oligomer self-assembly by stabilizing transient pre-fibrillar species (Rodriguez *et al.*, 2017; Snow *et al.*, 1994). Fourthly, HS may act as a platform allowing for post-translational modifications of the protein/peptide, which can favour aggregation (Sepulveda-Diaz *et al.*, 2015). Additionally, the presence of HS/heparin also catalyses the lateral aggregation of assembled fibrils, thereby decreasing the solubility and increasing the resistance to proteolysis (Maiza *et al.*, 2018). These mechanisms have been proposed by studying the aggregation of amyloidogenic peptides – typically associated with diseases. To date, there exists substantially less information regarding the mechanisms by which GAGs induce the formation of amyloid in peptides with comparatively low amyloidogenicity.

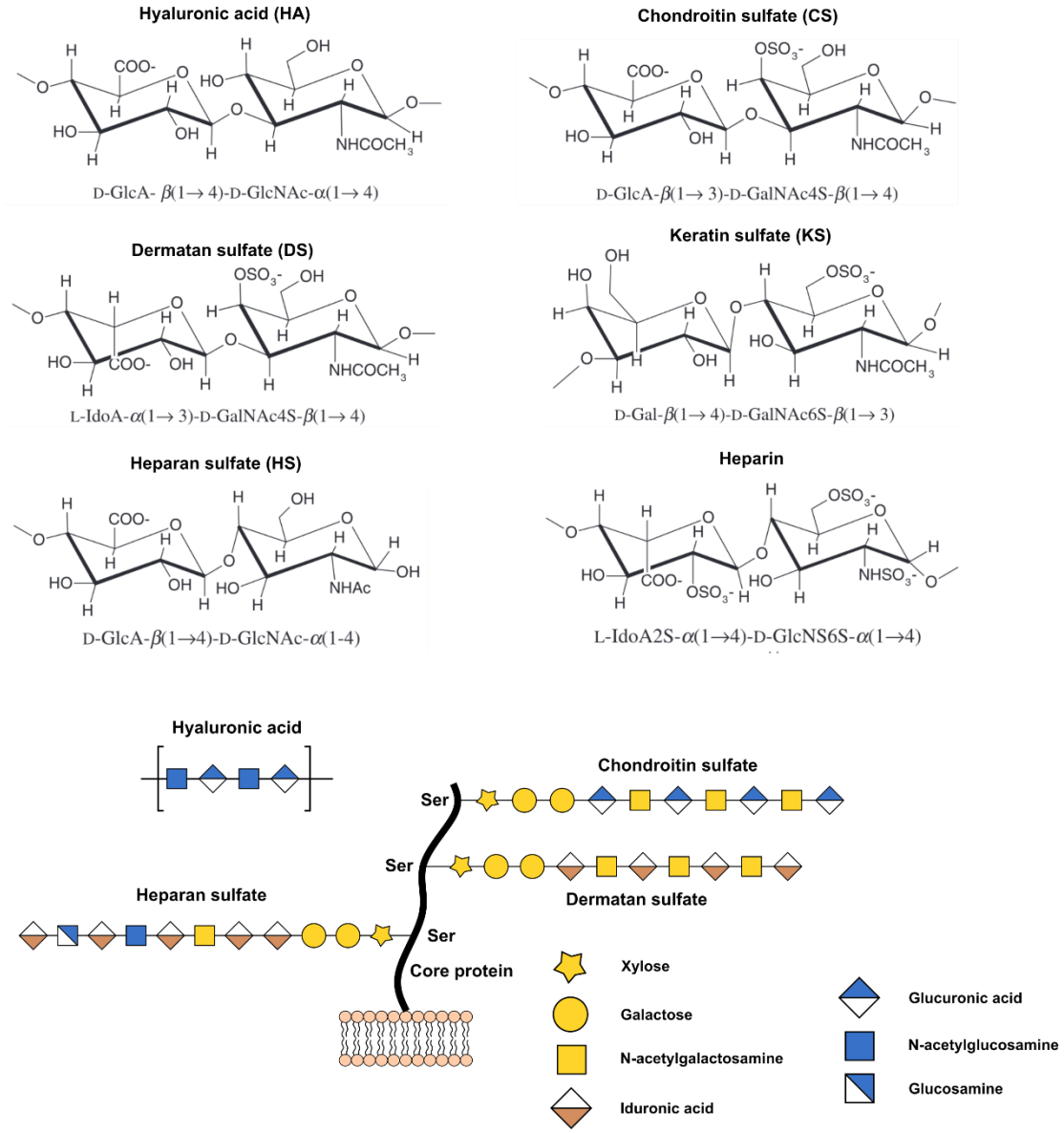

Figure 1.7 Chemical structures of disaccharides and GAGs. Top: Chemical structures of the disaccharide building blocks used in each type of GAGs. Bottom: schematic representation of soluble GAGs (HA) and proteoglycans incorporating CS, HS, and DS. Reproduced in part from Gandhi and Mancera, 2008.

Much research has been done to study the role of GAGs in amyloid-associated pathologies. Consequently, the majority of experiments use proteins such as Aβ (Alzheimer's), IAPP (type 2 diabetes), α-synuclein (Parkinson's), or prion related

protein, PrP (Creutzfeldt-Jakob). There is, however, another potential role of GAGs in the formation of amyloid, which is not associated with pathological states. As first proposed in 2009, there is a high likelihood that GAGs can stimulate the formation of functional amyloids within secretory granules as a form of high-density peptide hormone storage. While certain peptide hormones are capable of aggregating on their own, others are highly soluble and stable species yet, in the presence of GAGs, these too can form amyloid. Essentially all mechanistic studies conducted to date have focused on the role of GAGs in pathological rather than functional amyloid.

Table 1.5 Known peptides and proteins which have been shown to form amyloid in the presence of GAGs. Peptides with intrinsic amyloidogenicity that form amyloid regardless of the presence of GAGs are denoted with (+) while those that require GAGs are denoted with (-). Certain peptides are able to form amyloid under particular conditions on their own, which are labelled (+/-) (Quittot *et al.*, 2017b).

Polypeptide	Amyloidogenecity	Associated pathology	Reference
hIAPP	+	Type II diabetes mellitus	(De Carufel *et al.*, 2013)
Amyloid-β	+	Alzheimer's disease	(Brunden *et al.*, 1993)
α-synuclein	+	Parkinson's disease	(Holmes *et al.*, 2013)
ANF	+	Isolated atrial amyloidosis	(Millucci *et al.*, 2011)
Medin	+	Aortic medial amyloidosis	(Madine and Middleton, 2010)
sCT	+/-	Therapeutic	(Malmos *et al.*, 2016)
hCT	+	Thyroid medullary carcinoma	(Itoh-Watanabe *et al.*, 2013)
VIP	-	None	(Maji *et al.*, 2009)
rIAPP	+/-	None	(Wang and Raleigh, 2014)
PLB(1-23)	-	None	(Madine *et al.*, 2013)
β-endorphin	-	None	(Nespovitaya *et al.*, 2016)
Somatostatin	+/-	None	(Anoop *et al.*, 2014)
PrP (106-126)	+	Fatal familial insomnia	(Bazar and Jelinek, 2010)
Gelsolin	+	Finnish-type familial amyloidosis	(Solomon *et al.*, 2011)
Transthyretin	+/-	Familial amyloidosis	(Bourgault *et al.*, 2011c)
β-2-microglobulin	+	Dialysis-related amyloidosis	(Corlin *et al.*, 2010)
Serum amyloid A	+/-	Rheumatoid arthritis	(Egashira *et al.*, 2011)
Apomyoglobin	+/-	None	(Vilasi *et al.*, 2011)
Tau protein	+	Alzheimer's disease	(Luo *et al.*, 2013)
Acylphosphatase	-	None	(Motamedi-Shad *et al.*, 2009)

1.5.2 Membrane lipids

Lipids have a longstanding association with amyloid formation. In pathological cases, patient extracts commonly contain a variety of lipids localized within the amyloid plaques. Moreover, several of the prevailing hypotheses, which describe the associated cytotoxicity of amyloids, are directly linked to the disruption of cell membranes. It is important to note that the plasma membrane is the nearest source of lipids for extracellular amyloid formation, and therefore it is not surprising that within a variety of amyloid deposits, both cholesterol and sphingomyelin are detectable (Gellermann *et al.*, 2005). The role of lipids, and correspondingly lipid bilayers, in amyloid formation is complex, however, and is therefore an important area to understand in the context of amyloids.

Lipids are composed of a long hydrophobic chain with a hydrophilic headgroup, allowing them to form bilayers, which act as a barrier between cellular compartments (Kusumi *et al.*, 2011). Membrane lipids are divided into three classes: 1) glycerophospholipids (figure 1.8A), composed of two hydrophobic fatty acyl chains (sn-1 and sn-2), a glycerol backbone, and a phosphatidyl head group with a variable moiety. The sn-1 chain is typically a saturated fatty acid while the sn-2 chain contains most of the unsaturations. 2) Sphingolipids (figure 1.8B), composed of a sphingoid base which may vary in the hydroxylation/unsaturation, an N-acyl chain and a phosphatidyl head group. The N-acyl chain in sphingolipids is normally saturated and longer than the acyl chains in glycerophospholipids. 3) Sterols (figure 1.8C) represent the third class of lipid, primarily cholesterol in mammalian cells (Harayama and Riezman, 2018).

Structural differences in cell membranes arise from the chemical and compositional diversity of lipids (Harayama and Riezman, 2018). For example, at the subcellular level the endoplasmic reticulum contains less cholesterol and more unsaturated fatty acyl

chains than the plasma membrane. Similarly, other organelles may contain specific lipids, such as cardiolipin in the mitochondria, or lysobisphosphatidic acid found in late endosomes. Even further differences can be found at the sub-organellar level, such as a pronounced asymmetry between the outer and inner leaflets of the plasma membrane, where phosphatidylserine lipids are localized almost exclusively in the inner leaflet under normal conditions (Bretscher and Raff, 1975). Another example in the plasma membrane comes from the complex formation of rafts, where certain lipids and membrane proteins form phase-separated segments within the bilayer (Kalappurakkal *et al.*, 2020).

Models such as liposomes, micelles, and monolayers have been essential tools to study the behaviour of amyloidogenic peptides in the presence of lipids (figure 1.8D). Due to the amphiphilic nature of lipids, they rapidly self-assemble in aqueous solution, and depending on the length of the acyl chains and the nature of the polar headgroups, adopt different three-dimensional structures. Shorter lipids, fatty acids, and detergents will form micelles spontaneously, which will remain in a dynamic equilibrium strongly in favour of the assembled structure; however, a small amount of non-assembled material will remain in solution. Phospholipids generally self-assemble into multilamellar vesicles (MLVs) spontaneously. MLVs are large structures, typically on the order of 1 μm in diameter, composed of multiple hydrated bilayers. Liposomes are prepared by extruding MLVs through a porous membrane, thereby stripping away the larger outer bilayers. Common preparations of liposomes are in the range of 50 – 200 nm in diameter, since for larger diameter liposomes the extrusion process becomes less efficient and some amount of MLVs remains (Lasic, 1988). The preparation of planar monolayers is less robust, however, and highly sensitive to impurities or contaminants (Diociaiuti *et al.*, 2016). Nonetheless, it is routinely achieved in the Langmuir-Blodgett approach. Most of the literature is centered around liposomes, however, since they allow for the analysis of a vast range of experimental conditions, including the role of

lipid chain length, surface charge, vesicle size, lipid composition (Sciacca *et al.*, 2018; Terakawa *et al.*, 2018).

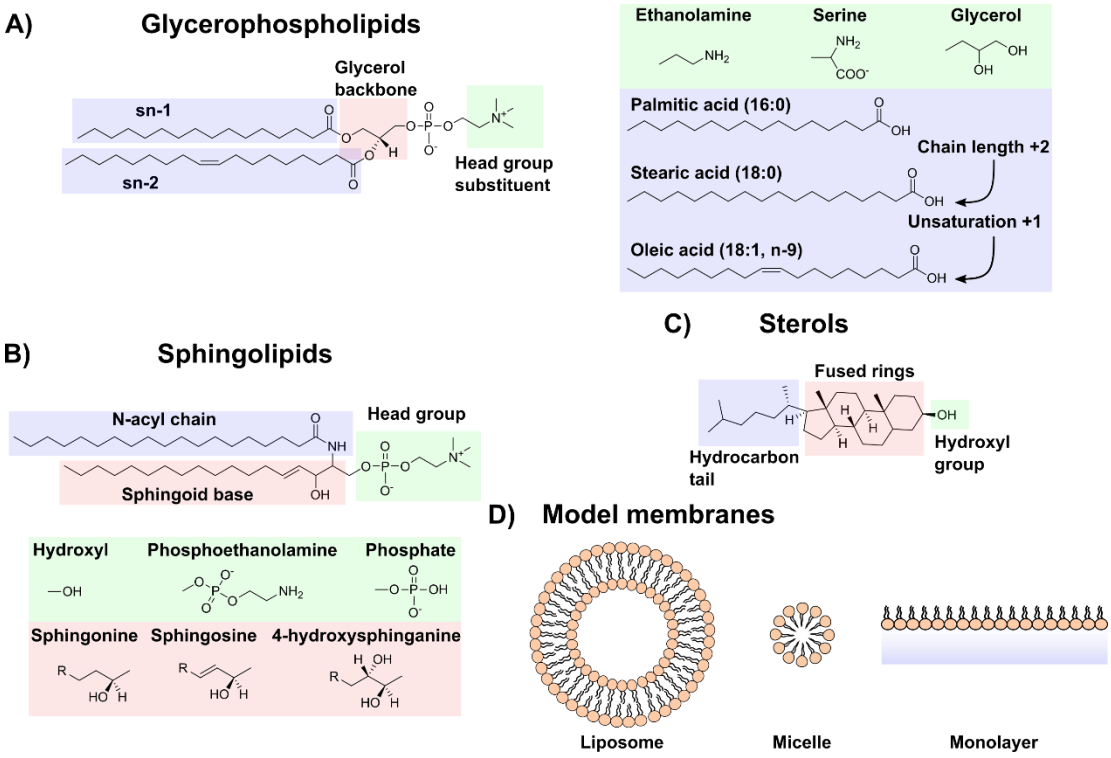

Figure 1.8 Lipid structures, composition, and model membranes. A) Representative structure of glycerophospholipids showing the head group (green), glycerol backbone (red), and acyl chains (blue). Common head groups and acyl chains are illustrated on the right. B) Representative structure of sphingolipids, with the variable head group (green) , N-acyl chain (blue), and variable sphingoid base (red). C) Representative structure of sterols showing hydroxyl head group (green), fused rings section (red), and the hydrocarbon tail (blue). D) Typical sources of model membranes to study amyloid biophysics, showing liposomes, micelles, and monolayers. Reproduced in part from Harayama and Riezman, 2018.

Liposomes are the primary model system employed to study amyloidogenic peptide-lipid interactions, having been used for structural and mechanistic studies of amyloid fibrils, and the corresponding membrane damage (Haya *et al.*, 2020; Naito *et al.*, 2018; Yamane *et al.*, 2019). Dye-leakage experiments, where a fluorescent dye is encapsulated within liposomes and its passage across the bilayer can be detected, are a

high-throughput and valuable method to detect membrane perturbations during amyloid formation (Sciacca *et al.*, 2020).

Significantly smaller than liposomes, micelles are still useful tools to study membrane-mimicking environments and the interplay between lipids and amyloidogenic peptides. Micelles have been used to induce structural changes in peptides and to stabilize pre-fibrillar species (Serra-Batiste *et al.*, 2016). Monolayers (and planar bilayers) are particularly useful when attempting to detect the forces and pressures involved during the insertion of a peptide into the membrane (Thakur *et al.*, 2011). While the versatility and general simplicity of these model membranes has been essential to advance the collective understanding of the complex processes by which amyloid interacts with lipids, there is an increasing interest in developing more accurate models to better reflect the heterogeneous composition of biological membranes.

The organization of the plasma membrane is highly complex and dynamic, with various sub-structures and regions. The first model proposed in the 1970's of the plasma membrane was the fluid mosaic model, where it was postulated that lipids and proteins were free to diffuse laterally throughout the bilayer (Singer and Nicolson, 1972). Since, the model has been refined and while lipids and proteins may diffuse laterally, it was also observed that a second, much slower diffusion was taking place. This led to the patchwork quilt model (Kusumi *et al.*, 2012; Kusumi *et al.*, 2011), where membrane lipids would separate into various patches based on their biophysical properties (Figure 1. 9). Within these patches, diffusion was quick; however, at the junction between two patches, diffusion was far less favourable and considerably slower. Further research described networks of membrane proteins anchoring into the actin filaments, which restricted the motions of transmembrane proteins (*e.g.*, ion channels, GPCRs, *etc.*) (Kusumi *et al.*, 2011). Interestingly, while transmembrane proteins in nucleated cells retain significant lateral mobility within the bilayer, this is not the case in erythrocytes.

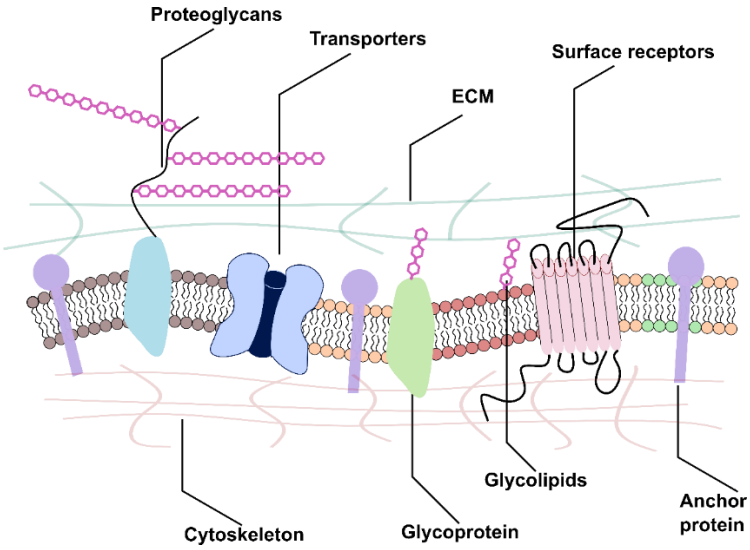

Figure 1. 9 Composition and structure of the plasma membrane. A non-exhaustive illustration depicting the myriad of non-lipid components found in, or associated with, the plasma membrane in typical eukaryotic cells.

Within the context of amyloid formation, a great deal of interest has revolved around the plasma membrane, although other biological membranes, such as the mitochondrial membrane, are also of interest (Ludtmann *et al.*, 2018). In fact, a significant number of current hypotheses regarding amyloid-associated cytotoxicity revolve around the disruption of phospholipid bilayers, with most of the supporting biophysical work being carried out using artificial bilayers (Sciacca *et al.*, 2018). Currently, it is hypothesized that amyloid fibril formation occurring around phospholipid bilayers is in close contact with the bilayer surface. As the monomeric protein/peptide subunits assemble into pre-fibrillar species such as oligomers and/or protofibrils, several possible interactions with the bilayer may occur. Oligomers/protofibrils may insert themselves into the membrane, creating transmembrane pores, or channels, which result in the uncontrolled passage of solutes across the membrane. Additionally, further aggregation and carpeting of the oligomers/protofibrils at the membrane surface may lead to the removal of lipids by the increasingly hydrophobic aggregates, which would then result in lipid-containing amyloid fibrils (Caillon *et al.*, 2013; Cao *et al.*, 2013a;

Sasahara, 2018; Sciacca *et al.*, 2016; Sciacca *et al.*, 2020). Of course, lipid bilayers also exert an effect on the process of amyloid fibril growth. In virtually all known cases, the presence of anionic phospholipid head groups such as phosphatidylserine (PS) or phosphatidylglycerol (PG) in synthetic bilayers accelerates fibrillogenesis compared to neutrally charged head groups such as phosphatidylcholine (PC), phosphatidylethanolamine (PE), and sphingomyelin (SM). (Christensen and Schiott, 2019; Terakawa *et al.*, 2018; Walsh *et al.*, 2014).

1.6 Research problems and objectives

Despite the progress made in the last two decades to better understand the molecular basis of amyloidogenic processes, several important questions remain. These gaps in the collective understanding notably stem from the complex and dynamic nature of amyloid formation, a lack of tools to study amyloid in biological environments, and often irreproducible or highly variable results when investigating the kinetics and thermodynamics of amyloid formation.

It is hypothesized, therefore, that since the amyloidogenic process is highly sensitive to a wide variety of factors and implicated in normal biological processes as well as pathological states, new tools and models will be beneficial to improve the quality of data obtained from *in vitro* biophysical characterizations.

The overarching objective of this research thesis is to uncover innovative biophysical strategies and approaches to study the process and factors affecting the aggregation of peptide hormones into amyloid fibrils. Toward this goal, three specific objectives will be addressed using PACAP and IAPP as models of peptide hormones:

1. Elucidate the mechanism by which glycosaminoglycans stimulate the self-assembly of the soluble peptide hormone PACAP under physiologically relevant conditions.
2. Develop and establish biologically relevant lipid bilayer model systems to study plasma membrane perturbation induce by the pathological amyloid self-assembly of IAPP.
3. Investigate causes of experimental variation during kinetics of amyloid formation *in vitro* and improve assay reproducibility.

CHAPTER II:

ARTICLE 1

GLYCOSAMINOGLYCANS INDUCE AMYLOID SELF-ASSEMBLY OF A PEPTIDE HORMONE BY CONCERTED SECONDARY AND QUATERNARY CONFORMATIONAL TRANSITIONS

Mathew Sebastiao, Noe Quittot, Isabelle Marcotte and Steve Bourgault

Manuscript published in the journal ACS Biochemistry 58 (2019) 1214 – 1225

Author contributions:

Mathew Sebastiao helped in the conceptualization of the project, experimental design and conceptualization of the project, data collection (microscopy, kinetics, circular dichroism, chromatography), data processing and interpretation, wrote the manuscript, and revised the manuscript. Noé Quittot carried out experimental work (DLS, chromatography, kinetics) and revised the manuscript. Isabelle Marcotte was responsible for the experimental design, conceptualization of the project, and revised the manuscript. Steve Bourgault was responsible for the conceptualization and supervision of the project, experimental design, and revised the manuscript.

2.1 Abstract

Amyloids are polypeptide supramolecular assemblies that have been historically associated with numerous pathologies. Nonetheless, recent studies have identified many amyloid structures that accomplish vital physiological functions. Interestingly, amyloid fibrils, either pathological or functional, have been reported to be consistently associated with other biomolecules such as RNA and glycosaminoglycans (GAGs). These linear polyanions, RNA and GAGs, have also demonstrated an inherent ability to accelerate and/or to promote amyloid formation. GAGs, including heparan sulfate, are highly charged polysaccharides that may have essential roles in the storage of peptide hormones in the form of amyloids. In this study, we evaluated the ability of sulfated GAGs to promote the self-assembly of the peptide (neuro)hormone PACAP27 and investigated the secondary and quaternary conformational transitions associated with the amyloidogenic process. PACAP27 readily self-assembled into insoluble, α-helix-rich globular particulates in the presence of sulfated GAGs, which gradually condensed and disappeared as non-toxic β-sheet-rich amyloid fibrils are formed. By designing a PACAP27 derivative for which helical folding was hindered, we observed that the α-helix-to-β-sheet conformational transition within the amorphous particulates constitutes the rate-limiting step to primary nucleation events. The proposed mechanism of GAG-induced self-assembly within insoluble particulates appears to be fundamentally different from usual amyloidogenic systems, which commonly implicates the formation of soluble pre-fibrillar proteospecies. Overall, this study provides new insights into the mechanistic details involved in the formation of functional amyloids catalyzed by polyanions, such as the assembly of nuclear amyloid bodies and the storage of peptide hormones.

2.2 Introduction

Amyloid fibrils are well-ordered protein assemblies characterized by a cross-β-sheet quaternary structure organisation (Eisenberg and Sawaya, 2017; Tycko, 2014). The aggregation and tissue deposition of numerous endogenous proteins as insoluble amyloid fibrils have been originally associated with a variety of human diseases, such as Alzheimer's disease, Parkinson's disease, type II diabetes *mellitus* and systemic familial amyloidosis (Chiti and Dobson, 2017). In these pathological deposits, the fibrillar protein core is ubiquitously associated with different non-fibrillar biomolecules, including proteins (Bellotti and Chiti, 2008; Kisilevsky, 2000; Pepys and Hirschfield, 2003), metals (Alexandrescu, 2005), lipids (Gellermann *et al.*, 2005), and glycosaminoglycans (GAGs) (Ancsin, 2003). GAGs are well known to accelerate the *in vitro* formation of amyloid fibrils from amyloid disease-related polypeptides such as transthyretin (Bourgault *et al.*, 2011c), islet amyloid polypeptide (De Carufel *et al.*, 2013), gelsolin (Solomon *et al.*, 2011), α-synuclein (Cohlberg *et al.*, 2002), and amyloid-β (Castillo *et al.*, 1998). Interestingly, GAGs were also shown to induce the amyloid self-assembly of numerous natively poorly amyloidogenic proteins, including apomyoglobin, β-microglobulin as well as short hydrophilic peptides (Borysik *et al.*, 2007; Madine *et al.*, 2013; Vilasi *et al.*, 2011). One important example of GAGs-induced fibril formation is in the context of peptide hormones, which were revealed to be stored as amyloid-like assemblies in the secretory granules (Maji *et al.*, 2009). In fact, functional amyloids have been documented in various organisms, such as in the formation of bacterial biofilms (Chapman *et al.*, 2002), the adhesion and coat formation in fungi (Mackay *et al.*, 2001), as structural components in egg shells in insects and fish (Iconomidou *et al.*, 2000), and as a scaffolding system during melanin biosynthesis in humans (Fowler *et al.*, 2006). Another form of functional amyloid in humans is as a response to cellular stressors, whereby non-coding RNA (ncRNA) facilitates a reversible aggregation of cytosolic proteins into phase-separated amyloid bodies (Audas *et al.*, 2016). Thus, GAGs and ncRNAs both demonstrate the ability to induce

amyloid formation in otherwise soluble proteins, which has been attributed to the polyanionic nature of these biomolecules. The implications of biological polyanions, such as GAGs, in the formation of amyloid assembly are far-reaching and may lead to a better understanding of the amyloidogenic process.

GAGs are primary constituents of the extracellular matrix and are found on the outer leaflet of the plasma membrane as components of proteoglycans (Theocharis *et al.*, 2016). These linear unbranched polysaccharides composed of repeating disaccharide units have anionic charges in the form of carboxylate and sulfate ions. GAGs play crucial physiological roles as structural components in the extracellular matrix (ECM) and in cell differentiation, morphogenesis, and migration (Theocharis *et al.*, 2016). Whereas it is well-known that GAGs strongly associate with polypeptides harboring a heparin-binding domain, such as cytokines and growth factors (Cardin and Weintraub, 1989; Gandhi and Mancera, 2008), there is growing interest in investigating the nature of peptide-GAGs interaction in the context of amyloid fibril formation (Quittot *et al.*, 2017b). It has been reported that the type of GAGs (heparin, chondroitin sulfate, hyaluronic acid) can exert different effects on amyloid self-assembly (Borysik *et al.*, 2007; Dharmadana *et al.*, 2018; Takase *et al.*, 2016). This has largely been attributed to the degree of sulfation of the polysaccharide, with less sulfated GAGs being generally less effective at promoting fibrillisation (Bourgault *et al.*, 2011c). Clear evidence exists that even *in vitro*, GAGs are incorporated into the mature fibril structure and are not simply acting as catalytic bystanders (Nespovitaya *et al.*, 2017). Structural similarities between different amyloid-GAG complexes, such as GAGs bound longitudinally along the fibril axis for fibril assembled from Aβ or salmon calcitonin, have suggested similar mechanisms of self-assembly (Malmos *et al.*, 2016; Stewart *et al.*, 2016; Stewart *et al.*, 2017). Additionally, there has been progress made on the mechanisms by which GAGs exert their amyloidogenic effect, using proteins whose aggregation is associated with pathologies (Bourgault *et al.*, 2011c; Solomon *et al.*, 2011; Vilasi *et al.*, 2011). Transthyretin and gelsolin have been proposed to aggregate

into oligomeric intermediates, which then bind to GAGs, increasing local concentrations and formation of larger aggregates through quaternary conformational conversion (Bourgault *et al.*, 2011c; Solomon *et al.*, 2011). In contrast, although the distinction between GAGs binding monomeric or oligomeric species was not made in the case of apomyoglobin, it was proposed that GAGs may act as templates for the fibril assembly and increase the local concentration of the protein (Vilasi *et al.*, 2011).

Despite extensive interest in understanding the mechanisms behind GAG-promoted amyloidogenesis of peptides with low intrinsic amyloidogenicity, this process has not yet been characterised in sufficient detail. Consequently, the present study focuses on elucidating the mechanisms by which short non-amyloidogenic disordered proteins, such as peptide hormones, convert from a soluble state into an amyloid-like conformation in the presence of GAGs. The 27-residue pituitary adenylate cyclase-activating polypeptide (PACAP27) was used as a model peptide hormone to investigate this process. It has been previously proposed from biological and biophysical characterization that this peptide neurohormone is stored in the secretory granules as amyloid-like structures (Maji *et al.*, 2009). This study demonstrates that despite having a low aggregation propensity, PACAP27 readily self-assembles into an amyloid structure in the presence of GAGs under physiologically relevant conditions. Our results suggest that the mechanism responsible for the self-assembly of PACAP27 involved concerted secondary and quaternary conformational conversions, in which amyloid nuclei are formed subsequently to the binding of the peptide on the sulfated GAG-scaffold.

2.3 Materials and methods

2.3.1 Material.

Thioflavin T, low molecular-weight heparin (LMWH), un-fractionated heparin (HEP), 8-anilino-1-naphthalenesulfonic acid (ANS) and all other chemicals were purchased from Sigma-Aldrich. 1,1,1-3,3,3 hexafluoroisopropanol (HFIP) was purchased from Oakwood chemicals.

2.3.2 Peptide Synthesis and Purification.

Peptides were synthesized on rink amide resin using a Tribute peptide synthesizer (Protein Technologies) by standard Fmoc chemistry, as previously described (Nguyen *et al.*, 2017). After cleavage from the solid support, crude peptides were precipitated and washed with diethyl ether, recovered by vacuum filtration, and dissolved in distilled water before being lyophilized. Peptides were purified by reverse-phase high performance liquid chromatography (RP-HPLC) on a preparative Luna C18 column (250mm x 21.2 mm, 5 μm, 100 Å, Phenomenex) with a linear gradient of acetonitrile (ACN) in TFA/H_2O (0.06% v/v). Collected fractions were analyzed by analytical RP-HPLC using a Kinatex EVO C18 column (150 mm x 4.6 mm, 3.6 μm, Phenomenex) and mass-verified by electrospray ionization time-of-flight mass spectrometry (ESI-TOF MS). Fractions containing the peptide of interest at 95% purity or greater as measured by RP-HPLC were pooled and lyophilized. To ensure that peptides were monomeric, each peptide was dissolved in HFIP at 1 mg/mL and sonicated for 30 minutes. The HFIP solution was then filtered through a 0.22 μm PVDF filter and lyophilized. Peptides were stored dry at -20 °C.

2.3.3 Amyloid Fibril Formation.

Stock solutions were prepared by dissolving peptides at 4 mg/mL (1.27 mM) and LMWH at 4 mg/mL (0.8 mM) in mannitol buffer (D-mannitol 5% w/v, NaN_3 0.01% w/v, pH 6.0) and diluted to the required experimental concentrations, based on a previously reported protocol (Maji *et al.*, 2009). A total of 600 μL of solution was used in 1.5 mL microcentrifuge tubes, which were incubated at 37°C with longitudinal rotation (50 rpm). At various time of incubation, aliquots were taken and diluted with 19 volumes of nanopure water. These solutions were subsequently analyzed by fluorescence spectroscopy, circular dichroism spectroscopy, atomic force microscopy, and transmission electron microscopy.

2.3.4 Kinetics of Amyloid Self-Assembly.

Lyophilized and monomerized peptides were dissolved at 2.54 mM in mannitol buffer containing 20 μM thioflavin-T (ThT). GAGs were dissolved to 1.6 mM (8 mg/mL LMWH; 27.2 mg/mL heparin) stock in the same mannitol buffer containing ThT. These solutions were diluted to relevant experimental concentrations with mannitol buffer containing 20 μM ThT, and the stock GAG solution was added to the peptide solution immediately before the initiation of the experiment. Assays were conducted in corning polystyrene microplates (96 wells, 100 μL/well, non-treated surface, black walls with clear bottom) sealed with silicone lids. Measurements were performed at 37 °C using an M1000 Pro plate reader (Tecan) taken at 10-minute intervals (10 seconds of linear agitation between each read; 2 mm amplitude, 168 rpm). Amyloid formation was monitored by ThT fluorescence ($\lambda_{excitation}$ = 440 nm, $\lambda_{emission}$ = 485 nm), and data were fitted with a Boltzmann sigmoidal function where t_{50} is the time to half-maximum intensity, k is the apparent first-order rate constant, and F_0, F_{max} are the minimum and maximum fluorescence intensities, respectively).

$$F = \frac{F_0 + (F_{max} - F_0)}{1 + e^{\frac{-(t - t_{50})}{k}}}$$

The lag phase (t_{lag}) was defined as the time before detectable amyloid formed and was calculated from the sigmoidal model as: $t_{lag} = t_{50} - 2k$.

2.3.5 Fluorescence Spectroscopy.

All spectra were recorded using a Horiba spectrofluorimeter. ANS and ThT were used as fluorogenic probes to follow aggregation and/or the formation of amyloid fibrils. ThT or ANS was added to the sample at a final concentration of 20 μM and 40 μM, respectively. ThT emission was measured with excitation at 440 nm and detected between 450 – 550 nm, while ANS emission was measured between 385 – 585 nm after excitation at 370 nm. All spectra were blank-subtracted with the corresponding peptide-free solution and normalized.

2.3.6 Circular Dichroism Spectroscopy.

Far-ultraviolet circular dichroism (CD) spectra were recorded at room temperature using a J-810 CD spectrometer (Jasco, Easton, MD, USA). Spectra were recorded from 260 to 190 nm and were blank-subtracted. All data was collected in 2 mm path length quartz cuvettes and converted to mean residue ellipticity (MRE):

$$MRE\ (deg \cdot cm^2 \cdot dmol^{-1}) = \frac{MRW(g \cdot mol^{-1}) \times CD\ (deg)}{10 \times \ell\ (cm) \times \mathcal{C}\ (g \cdot mL^{-1})}$$

Where MRW = mean residue weight, CD = circular dichroism signal, ℓ = path length, $\mathcal{C}$ = concentration. For 1,1,1-trifluoroethanol (TFE) titrations, peptides were dissolved in water with increasing amounts of TFE to obtain a final peptide concentration of 50

μM. Peptide/TFE solutions were analyzed by far UV CD spectroscopy (190-260 nm) using a 2 mm quartz cuvette.

2.3.7 Atomic Force Microscopy.

Acetic acid was added to samples at a final concentration of 1% (v/v). Samples were immediately applied to freshly cleaved mica discs and left to stand for 2 minutes. The mica was blotted dry with filter paper and washed twice with nanopure water, blotted dry between washings. The washed mica was allowed to dry completely (24h) before imaging. Mica were analyzed with a Veeco-Bruker Multimode AFM in ScanAsyst mode with a silicon tip (2 – 12 nm tip radius, 0.4 N/m force constant) on a nitride cantilever. Images were taken at a scan rate of 0.488 Hz and 1024 samples/line.

2.3.8 Transmission Electron Microscopy.

Samples were applied to a glow-discharged carbon film on a 400-mesh copper grid and left to stand for 1 minute. The grid was then blotted with filter paper and the sample immediately negatively stained with uranyl-formate (1.5% w/v). The stain was left to stand for 1 minute before being blotted dry and the grid set aside to dry completely (24h) before analysis. Sample grids were analysed on a FEI Tecnai 12 BioTwin system at 120 kV, and images were captured with a AMT XR80C CCD camera system.

2.3.9 Dynamic Light Scattering.

Undiluted samples were analyzed with a Malvern Zetasizer unit (75 μL in plastic Sarstedt cuvettes) for a total of 30 acquisitions per sample (3 x 10 runs) after a 20-second period of equilibration. Representative distributions were selected, and data was extracted from Zetasizer software (average particle size, polydispersity index).

2.3.10 Heparin affinity chromatography.

Lyophilized peptides were dissolved in water at a concentration of 0.5 mg/mL and filtered through 0.22 μm syringe filters. 500 μL of peptide solution was injected on a 1 mL heparin column (GE HiTrap). Peptides were eluted at a flow rate of 0.5 mL/min using a linear gradient of NaCl, from 0 to 2 M, and detected by absorbance at 280 nm.

2.3.11 Monomer quantification by analytical HPLC.

Stock solutions were prepared as described above. After 0 and 24 hours incubation, 100 μL were recovered and centrifuged at room temperature at 16 000g for 30 min to remove insoluble aggregates and fibrils. The supernatants were analyzed by RP-HPLC with a linear gradient (20 – 60%) of acetonitrile in TFA/H_2O (0.06% v/v) on a Kinatex EVO C18 column (150 mm x 4.6 mm, 3.6 μm, Phenomenex) at a flow rate of 1 ml/min.

2.3.12 Cellular Assays.

H9C2 (cardiomyocyte cell line) cells were seeded in black-wall, clear-bottom 96-well plates (tissue culture-treated) at a density of 5 000 cells/well (100 μL/well) in high glucose (4.5 g/L) Dulbecco's Modified Eagle's Medium (DMEM) supplemented with 10% FBS, 4 mM L-glutamine, 100 U/ml penicillin, 100μg/ml streptomycin and 1 mM sodium pyruvate. After 48 h incubation at 37 °C in 5% CO_2, cells were treated by the direct addition of 50 μL of monomeric peptides, aggregates, or amyloids. Monomeric PACAP27, aggregates, amyloid fibrils, and LMWH were prepared as described above in D-mannitol (5% w/v) without NaN_3 and subsequently diluted to the necessary concentrations. For islet amyloid polypeptide (IAPP), solutions were prepared at 3× the final concentrations and solubilized in 20 mM Tris (pH 7.4). Cells were incubated for 24 h and cellular viability was measured using the resazurin reduction assay. Cell viability (in percent) was calculated from the ratio of the fluorescence of the treated

sample to the control cells (vehicle treated). Data (in percentage) for 3 lots of peptides were averaged and were expressed as the mean ± S.E.M. Results were analysed using the Student's t-test and the statistical difference (between buffer and sample) was established at $P < 0.01$. Statistical analysis was performed using Prism 6.0.

2.4 Results and discussion

2.4.1 PACAP27 readily self-assembles into non-toxic amyloid fibrils in the presence of sulfated GAGs.

PACAP27 is a cationic 27-residue peptide hormone, which stimulates adenylyl cyclase activity in various cells and tissues through the activation of specific G protein-coupled receptors (Vaudry *et al.*, 2009). PACAP27 is part of the secretin/VIP/GHRH superfamily and has no known link to protein aggregation pathologies. Computational predictions for the ability of PACAP27 to aggregate were made using AGGRESCAN (Conchillo-Solé *et al.*, 2007), CamSol (Sormanni *et al.*, 2017; Sormanni *et al.*, 2015), and TANGO (Fernandez-Escamilla *et al.*, 2004; Linding *et al.*, 2004; Rousseau *et al.*, 2006) (figure s2.1). For comparison, the same analysis was conducted using two peptides with high intrinsic amyloidogenicity, human islet amyloid polypeptide (hIAPP) and amyloid-$\beta_{1\text{-}40}$ ($A\beta_{40}$), and another peptide hormone resistant to amyloid formation, salmon calcitonin (sCT). These analyses were in agreement with the known tendency of hIAPP and $A\beta_{40}$ to aggregate and correctly identified the putative β-sheet regions in the fibril structures (Luca *et al.*, 2007). sCT was also predicted to have aggregation-prone segments by AGGRESCAN and CamSol, despite being resistance to amyloid formation (Malmos *et al.*, 2016; Tycko, 2016). Predictions for PACAP27 indicated a potential aggregation segment at the C-terminal domain. This is most likely due to the presence of a patch of hydrophobic residues (Tyr-Leu-Ala-Ala-Val-Leu) from position 22 to 27.

The incubation of peptide hormones with sulfated GAGs has been consistently shown to yield amyloid-like materials under physiologically relevant conditions (Madine *et al.*, 2013; Maji *et al.*, 2009; Vilasi *et al.*, 2011). To understand the underlying mechanisms behind this process, PACAP27 and low molecular weight heparin (LMWH) were used as peptide and GAG models, respectively. The structure of heparin and the peptide sequence are given in figure 2.1a and b, respectively. Based on previously established protocols (Madine *et al.*, 2013; Maji *et al.*, 2009; Malmos *et al.*, 2016; Nespovitaya *et al.*, 2016; Nespovitaya *et al.*, 2017), PACAP27 (635 μM in 5% w/v D-mannitol with 0.01% NaN_3, pH 6) was incubated in presence, or in absence, of 400 μM LMWH at 37 °C under constant longitudinal rotation (50 rpm) for 24h. The amyloid-sensitive dye ThT (Naiki *et al.*, 1989; Sebastiao *et al.*, 2017), showed no increase of fluorescence signal when the peptide was incubated in the absence of LMWH (figure 2.1c) and CD spectroscopy revealed that PACAP27 remained in a random coiled conformation (figure 2.1d). PACAP27 is mainly unstructured in aqueous solution, although it exhibits a high propensity to adopt an α-helix in membrane-mimicking environment (Bourgault *et al.*, 2011a). In sharp contrast, incubation of PACAP27 with LMWH for 24 h led to a drastic increase of ThT fluorescence (figure 2.1c), indicative of a cross-β-sheet quaternary structure. The CD spectrum was characterized with a maximum at 195 nm and a minimum at 218 nm (figure 2.1d), typical of amyloid fibrils rich in β-sheets. By AFM imaging, well-defined fibrils were observed for the peptide incubated with LMWH, with fibril lengths ranging between 0.5 to 2 μm and heights in the low nanometer range (figure 2.1e), which correspond well with previously described amyloid (Madine *et al.*, 2013; Maji *et al.*, 2009; Nespovitaya *et al.*, 2016; Nespovitaya *et al.*, 2017). No amyloid was detected by ThT, CD, and AFM in absence of LMWH, even when PACAP27 was incubated for over one week (figure s2.2).

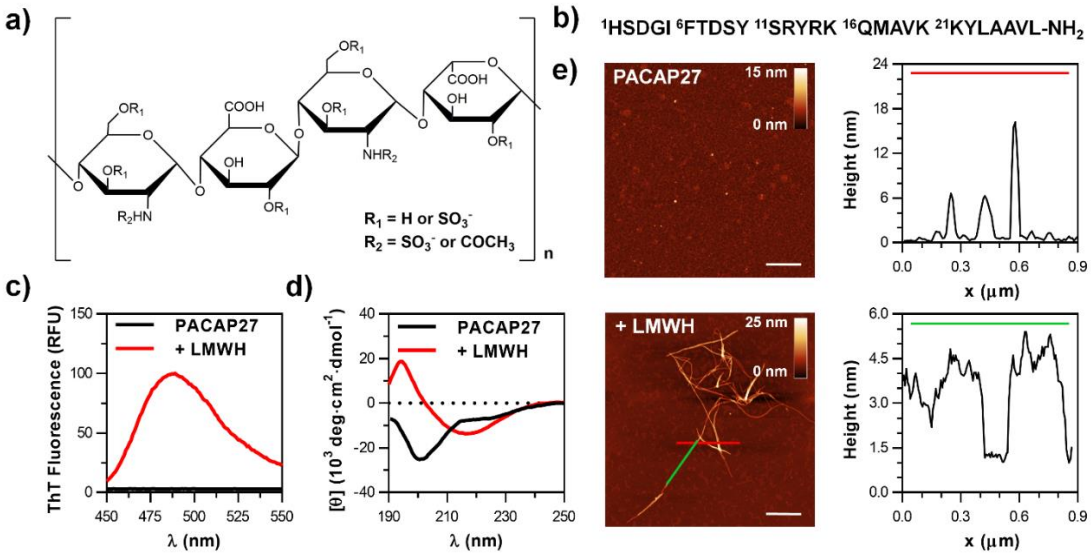

Figure 2.1 PACAP27 assembled into amyloid fibrils in the presence of LMWH. (a) Structure of heparin composed of glucuronic acid linked to glucosamine disaccharide repeating subunit. (b) Sequence of PACAP27 with amidated C-terminal. (c) ThT fluorescence of PACAP27 (635 µM) after 24 h incubation in presence, or in absence, of LMWH (400 µM). (d) CD spectra showing changes to PACAP27 secondary structure after 24 h incubation with, or without, LMWH. (e) AFM images of PACAP27 after 24 h incubation alone (top left) or in presence of LMWH (lower panel), scale bar = 1 µm. Representative height profiles for transverse (red) and longitudinal (green) sections of fibrils.

Since amyloids are historically associated with pathological states, the cytotoxicity of PACAP27 fibrils was evaluated by measuring the metabolic activity of H9C2 cardiomyocytes upon treatments. Cardiomyocytes are commonly used to evaluate the toxicity of amyloidogenic proteins and are known to be sensitive to toxic pre-amyloid aggregates (Bourgault *et al.*, 2011b). PACAP27, either monomeric or assembled in presence of LMWH, was found to be non-toxic to cardiomyocytes (Figure S2. 3). In contrast, amyloid fibrils assembled for 24 h from the highly amyloidogenic peptide IAPP demonstrated noticeable toxicity at 50 µM, while the monomeric IAPP (dead control) was highly toxic. Taken together, these results highlight that the poorly aggregation prone PACAP27 readily forms non-toxic amyloid in the presence of LMWH.

2.4.2 Amyloid self-assembly is sensitive to GAG concentration and ionic strength.

Although the ability of GAGs to promote amyloid formation has been recognized for over two decades (Quittot *et al.*, 2017b), the mechanisms behind this process remain partially elusive. To further characterize GAGs-induced PACAP27 self-assembly, we monitored amyloid formation using ThT fluorescence over time under different conditions in a microplate assay format. PACAP27 (635 μM in 5% w/v D-mannitol with 0.01% NaN_3, pH 6) was incubated in the absence or presence of LMWH (5 kDa average MW), or unfractionated heparin (HEP, 17 kDa average MW). Amyloid assembly is rate-limited by the formation of nuclei, *i.e.*, oligomeric species capable of initiating fibril growth. During the kinetics of amyloid self-assembly, this delay is ascribed as the lag phase (t_{lag}), or nucleation phase. Incubation of PACAP27 with LMWH resulted in a longer lag phase compared to the HEP aggregation mixture (9.1 h *vs* 6.8 h, respectively), and a lower ThT fluorescence intensity at the end point (figure 2.2a, table s2. 1). This is in agreement with the previously described direct correlation between GAG length and rate of fibrillisation (Jha *et al.*, 2011). Despite the apparent enhanced ability of HEP to induce amyloid formation compared to LMWH, the heterogeneous chain length of HEP makes it difficult to accurately describe the intermolecular interactions. Therefore, LMWH was selected as the model to further investigate GAG-promoted PACAP27 amyloid self-assembly.

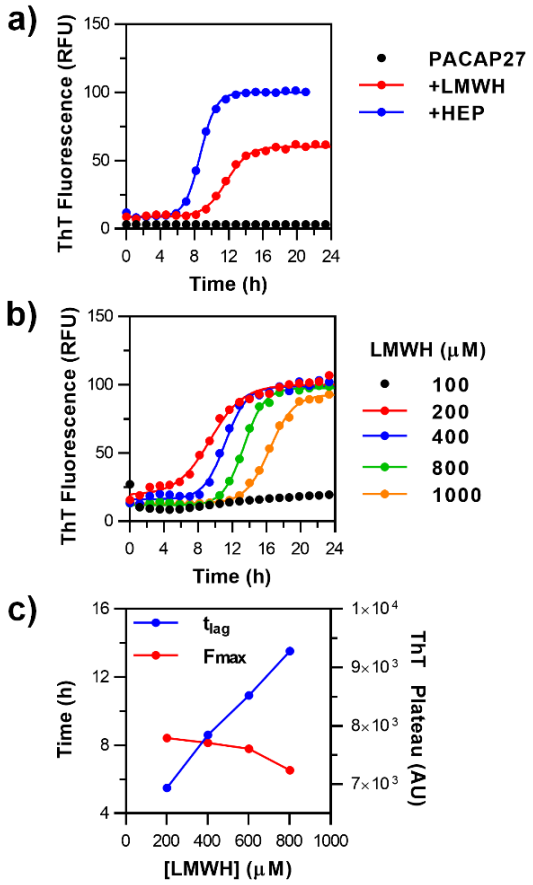

Figure 2.2 Kinetics of PACAP27 amyloid self-assembly are sensitive to GAG chain length and concentration. (a) ThT-fluorescence kinetics of PACAP27 amyloid formation in presence of heparin (HEP; 400 μM) and LMWH (400 μM). (b) ThT-fluorescence kinetics of PACAP27 in the presence of varying LMWH concentrations. (a,b) Data from at least three separate experiments performed in triplicate were averaged and fitted to a sigmoidal curve when possible ($R^2 \geq 0.95$), indicated by a solid line. (c) Lag times (t_{lag}) and maximum fluorescence values (F_{max}) for the fitted curves in (b).

There is a critical interplay between the relative concentration of sulfated GAGs and their ability to promote or accelerate amyloid assembly (Bazar and Jelinek, 2010; Jha *et al.*, 2011) It was found that the GAG:peptide molar ratio drastically modulated the self-assembly kinetics of prion-derived peptides (Bazar and Jelinek, 2010). Here, a similar trend was observed for PACAP27, where no fibrilisation took place below a threshold of 100 μM (molar ratio of 1:6.25 (LMWH:PACAP27)), followed by

increasingly longer lag phases as the concentration of LMWH increased (Figure 2.2b and c, table s2. 1). This could be explained by the peptide requiring a minimum number of intermolecular interactions to initiate primary nucleation. As the relative concentration of LMWH increases, the peptide is likely more distributed among the LMWH molecules, thereby reducing the potential for self-assembly by decreasing the number of peptide-peptide encounters (Bazar and Jelinek, 2010). This is in agreement with the model proposing that GAGs accelerate fibril formation by increasing the local concentration of polypeptides, although this mechanism remains to be confirmed for non-amyloidogenic peptides, such as PACAP27.

Due to the anionic nature of GAGs, it is likely that electrostatic forces drive GAG-induced amyloid formation. This was first evaluated by varying the ionic strength in the self-assembly kinetics assay (figure 2.3a, table s2. 1). It was observed by ThT fluorescence that under low to moderate salt concentrations (50 to 150 mM NaCl), the kinetics of self-assembly were slowed down compared to low ionic strength (0 mM NaCl). Increasing NaCl concentration up to 500 mM further slowed the amyloidogenic process, although it did not completely halt it. To further examine the importance of ionic interactions, the pH was varied from highly acidic (pH 2) to highly alkaline (pH 12) to identify the interactions necessary for nucleation. GAGs-induced self-assembly persisted among a wide range of pH values and only under highly acidic conditions (pH of 2) was the process disturbed (Figure 2.3b). This is likely attributed to the protonation of the carboxylate (pKa between 3.1 and 3.4) and/or partial protonation of the sulfate groups (pKa between 0.5 and 1.9) on LMWH (Remko *et al.*, 2013), which would prevent ionic interactions necessary for fibril formation and/or PACAP27 binding. In contrast, at pH values above the pKa of Lys side chain amines (pKa ≅11), no changes in lag phase relative to milder pH values (pH 6, 7.4, 8.5) were observed. Overall, these data suggest that GAG-promoted amyloid formation is highly favourable and resistant to perturbation across a wide range of conditions.

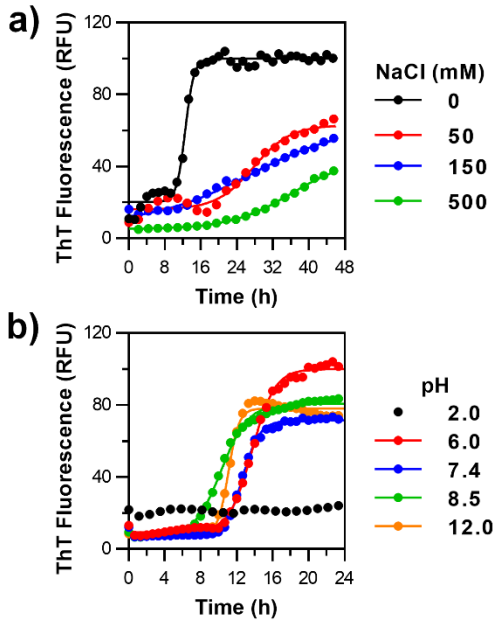

Figure 2.3 Roles of electrostatic interactions in GAG-promoted amyloid assembly. (a) ThT-fluorescence kinetics of PACAP27 with LMWH in the presence of increasing NaCl concentrations. (b) ThT-fluorescence kinetics of PACAP27 with LMWH at different pH and buffers (pH 12 = NaOH; pH 8.5 = 20 mM Tris-HCl; pH 7.4 = 20 mM PO_4, pH 6.0 = 5% w/v D-mannitol; pH 2 = HCl). (a,b) Data from at least three separate experiments performed in triplicate were averaged and fitted to a sigmoidal curve when possible ($R^2 \geq 0.95$), indicated by a solid line.

2.4.3 PACAP27 rapidly forms large spherical aggregates rich in α-helix in presence of GAGs.

The available literature on amyloid self-assembly, which is mainly associated with pathological amyloids, describes the process of fibril formation as initiating from soluble oligomeric species (*i.e.* nuclei). In sharp contrast, mixing PACAP27 with LMWH immediately resulted in highly turbid suspensions of particles that precipitated. This solution remained partially turbid after the 24 h incubation period (figure s2.4a). Previous research studying the formation of amyloid fibrils has described large variations in ThT microplate assay kinetics (Sebastiao *et al.*, 2017). To improve experimental reproducibility, the self-assembly of PACAP27 was studied instead in 1.5

mL centrifuge tubes under constant longitudinal rotation. We therefore sought to characterise the secondary structural transition and the changes in the mesoscopic morphology during self-assembly by periodically sampling the incubation mixture and analysing the aliquots by CD spectroscopy, fluorophore binding (ThT and ANS) and TEM. PACAP27 incubated alone remained soluble and did not aggregate over time as detected by ThT and ANS fluorescence (figure 2.4a and b). Furthermore, no structural changes were observed by CD; the peptide remained disordered regardless of the incubation time (figure 2.4c). Conversely, immediately after mixing the peptide with LMWH (0h; dead time of 3 minutes), the CD spectrum of PACAP27 presented two minima at 208 nm and 222 nm, indicative of the presence of an α-helical secondary structure. The ability of sulfated GAGs to induce secondary conformational conversion upon peptide binding has already been shown for numerous polypeptides, including cell-penetrating peptides (Bechara *et al.*, 2013; Tchoumi Neree *et al.*, 2014), amyloidogenic peptides (De Carufel *et al.*, 2015; Marek *et al.*, 2012), peptide hormones (Maji *et al.*, 2009; Quittot *et al.*, 2017a), as well as the lytic peptide melittin (Klocek and Seelig, 2008). The initial mixture (0 h) induced a small increase of ThT and ANS fluorescence in comparison to the peptide alone (figure 2.4a and b). However, the relative hydrophobicity (ANS binding) and the presence of cross-β-sheet quaternary structure (ThT binding) compared with amyloid fibrils (24 h) remained very low (figure 2.4d). Upon mixing with LMWH, the formation of large spherical aggregates, or particulates could be observed by TEM (figure 2.4e) and DLS revealed heterogeneous size distributions (figure s2.4b).

Considering the key role of ionic interactions for GAGs-induced amyloid formation, it is likely that these aggregates are formed from large clusters of PACAP27 and LMWH that gathered through a dense network of electrostatic interactions. LMWH has an average MW of 5 kDa and a corresponding average chain length of approximately 8 disaccharides. Heparin has an average sulfate content of 2.7 groups per disaccharide (Shriver *et al.*, 2012), representing 21.6 sulfate groups per LMWH molecule. Other

anionic functional groups on GAGs, such as carboxylates, have not demonstrated the same ability to accelerate amyloid fibril formation (Borysik *et al.*, 2007; Bourgault *et al.*, 2011c). It is helpful to consider the equivalent concentration in terms of sulfate groups relative to the number of cationic groups on each peptide (3 Lys, 2 Arg, 1 His, and the terminal primary amine) at pH 6. Therefore, under these experimental conditions (635 μM peptide, 400 μM LMWH) the charge ratio was approximately two sulfate groups per cationic group (8.6 mM SO_3^-, 4.4 mM cation). The excess negative charge may ensure total charge neutralisation of PACAP27, overcoming any potential inter-peptide charge repulsion, allowing aggregation to proceed. The spherical aggregates formed spontaneously were very distinct from pre-fibrillar soluble oligomers, and closely resembled the description of protein particulates (Krebs *et al.*, 2007). We evaluated if these large spherical aggregates were cytotoxic, as previously reported for soluble oligomeric species of IAPP (Abedini *et al.*, 2016b; Quittot *et al.*, 2018). Interestingly, the particulates formed immediately after solubilisation of PACAP27 in presence of LMWH were practically non-toxic to cardiomycocytes, with a slight significant reduction of cell viability at 100 μM. This observation further highlights the differences in the physicochemical and structural properties between GAG-peptide large supramolecular assemblies and oligomeric proteospecies of amyloidogenic polypeptides. After 2 h incubation, no significant changes to either ThT or ANS fluorescence could be detected while an increase in the α-helix signal intensity was observed on the CD spectra. By TEM, the spherical aggregates appeared to be more condensed in comparison to those observed at 0 h. Interestingly after 5 h incubation, fibrillar structures branching out from these spherical aggregates were observed. By CD spectroscopy, this 5 h mixture showed a profile indicative of a mixture of helical and β-sheet structure. This mixture of fibrillar structures and dense spherical aggregates

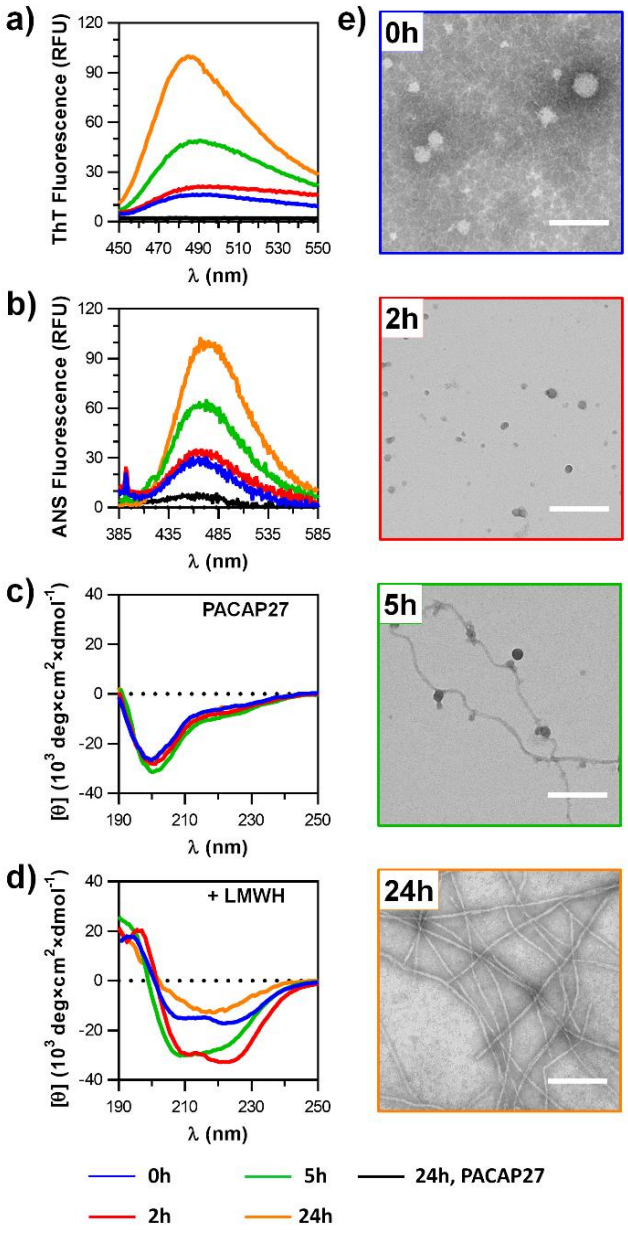

Figure 2.4 PACAP27 rapidly self-assembles into spherical aggregates while adopting a helical conformation before converting into amyloid fibrils. (a) ThT-fluorescence spectra of PACAP27 incubated in absence (black) or in presence of LMWH. (b) ANS-fluorescence spectra of PACAP27 incubated in absence (black) or in presence of LMWH. (c) CD spectra of PACAP27 incubated alone. (d) CD spectra of PACAP27

incubated in presence of LMWH. (e) TEM images of PACAP27 incubated in presence of LMWH. Scale bar = 100 nm.

showed an increased hydrophobicity by ANS binding and a moderate degree of ThT fluorescence, indicative of an amyloid-like morphology. After 24 hours incubation, PACAP27 adopted a secondary structure rich in β-sheets and a network of fibrillar assemblies was observed by TEM. These β-sheet fibrils yielded strong ThT fluorescence and had more hydrophobic sites than the proteospecies assembled after 5 h incubation. Observations by TEM imaging agreed with the size distributions and the calculated average size values from DLS measurements (figure s2.4).

It is likely that the prompt formation of large PACAP27-LMWH aggregates incorporated a certain degree of hydration and over time, the water was slowly excluded from the droplet core resulting in denser, less hydrated particulates (figure 2.4e). We hypothesized that as the aggregates became increasingly hydrophobic, the peptide reached sufficiently elevated local concentrations and was able to self-assemble into amyloid fibrils using LMWH as a scaffold, as previously described (Nespovitaya *et al.*, 2017). Amyloid fibrils appeared to grow outward from these particulates. Consequently, it is unclear whether the increase in hydrophobicity detected by ANS binding arises from the conformational rearrangements within the aggregates, or simply from the appearance of hydrophobic folds in the growing amyloid fibrils. To address this question and the roles of α-helical intermediates, a PACAP27 derivative was designed.

2.4.4 Inhibiting GAG-induced helical folding of PACAP.

The common description of amyloidogenesis involves conformational changes occurring within soluble species. For GAG-induced PACAP27 self-assembly, an intriguing observation was the prompt appearance of an α-helical intermediate within insoluble particulates, prior to the secondary conformational transitions into amyloid

β-sheet-rich structure. The presence of helical intermediates in amyloidogenic pathways has been the subject of previous studies with disease-related intrinsically disordered peptides (Abedini *et al.*, 2016a; Abedini and Raleigh, 2009; De Carufel *et al.*, 2015). Nevertheless, whether these helical structures are on- or off-pathway to amyloid formation remains an important unsolved question. To study the implications of the helical intermediates in amyloid formation promoted by polyanions, we designed a helically-frustrated variant of PACAP27 by substituting a pair of adjacent residues by their corresponding D-enantiomers (dd-PACAP27). This modification is known to disrupt helical conformation without affecting the hydrophobicity and the net charge of the peptide, as the primary sequence remains identical (Quittot *et al.*, 2017a). According to PACAP27 helical secondary structure adopted in presence of DPC micelles, which spans from position 7 to 26 (Bourgault *et al.*, 2009), residues Gln-16 and Met-17 were substituted by their D- enantiomers (figure 2.5a). To initially validate that this modification actually precluded the capacity of PACAP27 to fold into α-helix, we compared the ability of PACAP27 and dd-PACAP27 to adopt α-helix in presence of trifluoroethanol (TFE), a potent helix-inducer (Shiraki *et al.*, 1995). TFE-titration by CD spectroscopy revealed the reduced ability of this analog to switch into a well-defined helix (figure 2.5b). For instance, at 15% TFE (v/v), the native peptide adopted a well-defined helical structure, while dd-PACAP27 remained disordered (figure 2.5c). Moreover, upon the addition of 400 μM LMWH, dd-PACAP27 displayed predominantly a disordered conformation whereas PACAP27 adopted a helical secondary structure (figure 2.5d). To validate that these differences were not simply related to a lower affinity of dd-PACAP27 for LMWH, both peptides were analysed by heparin-affinity chromatography using a NaCl gradient. Although WT PACAP27 eluted with a slightly wider peak, there was no difference in the NaCl concentration (0.6 M) required to elute both peptides from the heparin column (figure s2.5a).

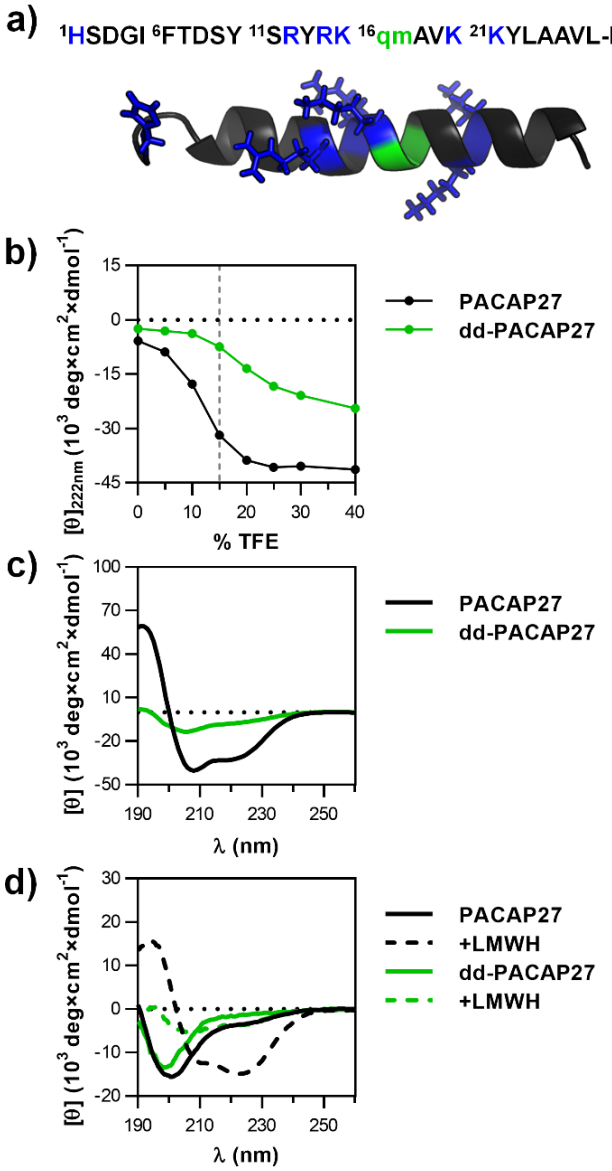

Figure 2.5 Preventing PACAP27 helical folding. (a) Primary sequence and DPC-micelles secondary structure of PACAP27 showing the positions of the D-enantiomer substituted residues in green and the cationic residues in blue. (b) CD signal at 222 nm during TFE titration of WT PACAP27 and dd-PACAP27. (c) Far-UV CD spectra of WT PACAP and dd-PACAP27 in 15% TFE (v/v). (d) CD spectra of WT PACAP and dd-PACAP27 in absence (solid lines) and in presence of 400 μM LMWH (dashed lines).

Broadening of the elution peak of WT PACAP27 was not due to impurities, as both peptides were over 95% pure, as measured by RP-HPLC (figure s2.5b). Furthermore, solutions of native PACAP27 and dd-PACAP27 (635 μM in 5% w/v D-mannitol) were respectively mixed with 2 mg/mL LMWH and either immediately centrifuged at 16 000g for 20 minutes (0 h) or incubated for 24 h and then centrifuged (24 h). Supernatants were collected and analysed by RP-HPLC to verify if any peptide remained in solution. Both supernatants had no detectable amount of peptide, indicating that virtually all monomeric peptides were rapidly incorporated into the particulates, with no detectable peptide being released after amyloid formation (figure s2.5c). These results indicated that despite the reduced ability of dd-PACAP27 to adopt a helical conformation, binding and association to LMWH was not perturbed.

2.4.5 Inhibiting helical folding accelerates GAGs-mediated amyloid assembly.

Next, we evaluated the impact of hindering PACAP27 helical folding on GAGs-mediated amyloid formation. In absence of LMWH and as observed for the WT peptide, dd-PACAP27 remained in a random coil conformation and no indication of self-assembly was reported by ThT and ANS fluorescence (figure 2.6). In presence of LMWH, dd-PACAP27 assembled into well-defined amyloid assemblies. Interestingly, amyloid formation appeared to occur significantly faster for dd-PACAP27 than its WT counterpart, as indicated by the presence of β-sheet-rich CD spectra, fibrillar morphology by TEM as well as ThT and ANS fluorescence (figure 2.6b-e vs figure 2.4b-e). As observed for WT PACAP27, dd-PACAP27 solution instantaneously became turbid upon the addition of LMWH. However, after 24h the solution was significantly less turbid (figure s2.6a). This was particularly interesting because the mature fibrils appeared morphologically identical at the mesoscopic level and displayed similar ThT and ANS binding. One notable difference between dd-PACAP27 and native PACAP27 was that the early aggregates formed at time 0 h responded differently to the hydrophobic probe ANS. Whereas PACAP27 aggregates

responded at 30% of the final intensity (24 h; amyloid fibrils), dd-PACAP27 early aggregates exhibited 60% of the ANS fluorescence intensity of the final assemblies (24 h). These early aggregates also differed in their polydispersity; dd-PACAP27 aggregate sizes being noticeably more homogeneous, as measured by DLS (figure s2.6). Furthermore, the number of hydrophobic regions of dd-PACAP27 aggregates remained constant over the first 5 hours of incubation in presence of LMWH. This contrast with the changes in hydrophobicity measured during WT PACAP27 aggregation, suggesting that the increase in hydrophobicity over time most likely arises from modifications within the amorphous aggregate and not from the growth of amyloid fibrils. In addition, a further distinction was the evolution of the particle sizes, as observed both by TEM imaging and DLS. Whereas native PACAP27 particulates shrank during the first two hours, dd-PACAP27 particulates grew larger immediately from the start (figure s2.6d). The fibrillar morphology observed by TEM after 24h incubation of dd-PACAP27 was similar to native PACAP27 assemblies (figure 2.6e vs figure 2.4e). These observations suggest that α-helix intermediates are off-pathway to amyloid formation or that the same mesoscopic structure could be obtained regardless of the assembly pathways. Interestingly, when either dd-PACAP27 or WT PACAP27 were incubated with LMWH in the presence of 150 mM NaCl, no helical conformation was observed by CD spectroscopy (figure s2.7), most likely related to the less tight binding of the peptide on the sulfated GAGs. Under these conditions, the peptide aggregates remained ThT-negative and in a random coil conformation before conversion into ThT-positive and β-sheet-rich structures (figure s2.7). This observation further demonstrates that the formation of helical intermediates is not a prerequisite for GAG-induced amyloid formation.

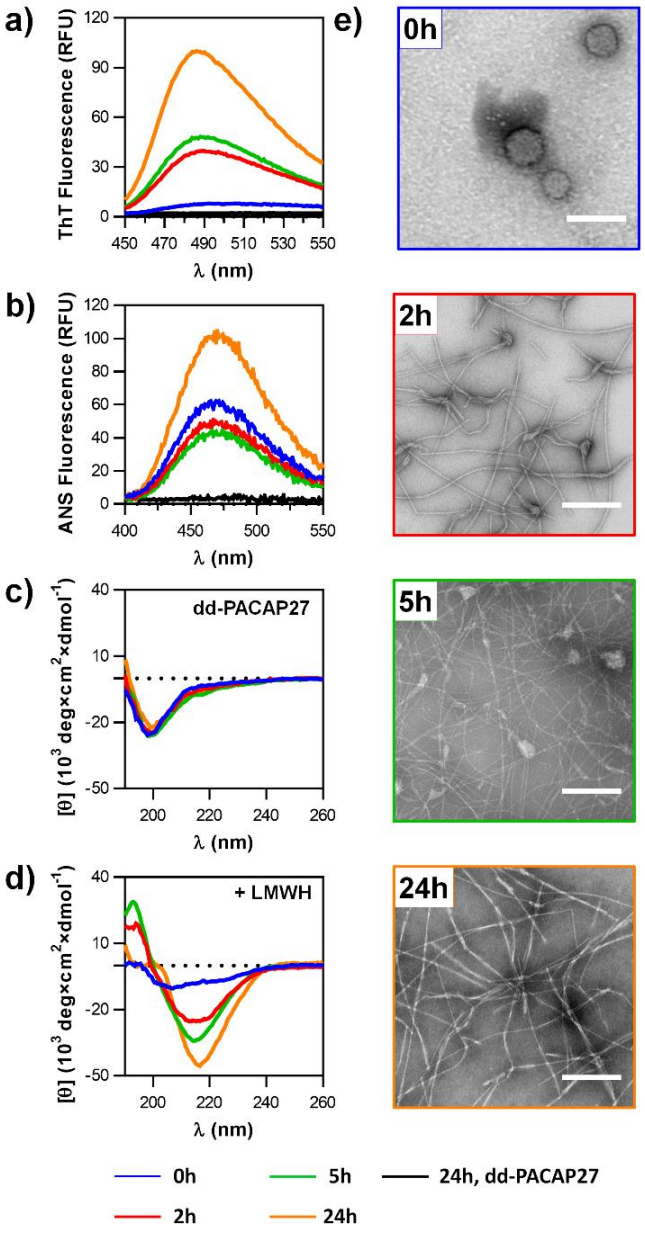

Figure 2.6 Effects of preventing PACAP helical folding on GAG-induced amyloid assembly. (a) ThT-fluorescence spectra of dd-PACAP27 incubated in absence (black) or in presence of LMWH. (b) ANS-fluorescence spectra of dd-PACAP27 incubated in absence (black) or in presence of LMWH. (c) CD spectra of dd-PACAP27 incubated alone. (d) CD spectra of dd-PACAP27 incubated in presence of LMWH. (e) TEM images of dd-PACAP27 incubated in presence of LMWH. Scale bar = 100 nm.

Structural and morphological changes appeared to occur significantly faster when α-helical folding is impeded in the case of dd-PACAP27. Thus, the kinetics of dd-PACAP27 amyloid self-assembly was measured by ThT fluorescence to validate these observations (**Error! Reference source not found.**). As ThT fluorescence increased rapidly (dead time of 60 seconds), the lag-phase was too short for the fluorescence data to be appropriately fitted by a standard sigmoidal function. In amyloid fibril formation in homogenous solutions, *i.e.,* in absence of co- factors such as GAGs, the lag-phase is ascribed to primary nucleation, which involves the assembly of oligomers capable of initiating protofilament growth. Primary nucleation is commonly considered as the rate-limiting step of the amyloidogenic process and can be overcome by providing the reaction with pre-formed nucleation sites in the form of "seeds", *i.e.,* small amounts of mature amyloid fibrils. The reduced ability of dd-PACAP27 to fold into α-helix drastically abridged the time necessary for primary nucleation. Thus, we compared the kinetics of dd-PACAP27 self-assembly with seeded fibril growth of WT peptide (**Error! Reference source not found.**). A small amount of pre-formed PACAP27 amyloid fibrils (2.5% (mol/mol)) obtained after a 24h incubation period was added to the aggregation mixture, providing a nucleation site at the onset of the reaction, overcoming the rate-limiting step. The seeded fibril kinetics was closely similar to the one of dd-PACAP27, indicating that inhibiting GAG-induced helical folding dramatically reduces the time required for primary nucleation. When the seeded assembly reaction was performed in absence of LMWH, no seeding effect was observed (figure s2.8). This result further emphasizes the low aggregation propensity of PACAP27 and the necessary role of sulfated GAGs for amyloid formation.

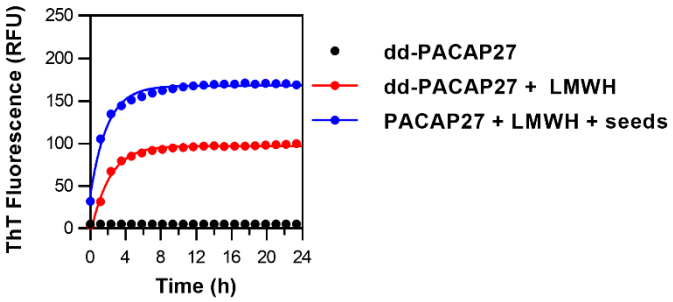

Figure 2.7 Preventing the formation of helical intermediates hastens GAG-induced amyloid formation. ThT-fluorescence kinetics of dd-PACAP27 with LMWH and seeded kinetics of WT PACAP27 (seeded with pre-formed amyloid fibrils 2.5% (mol/mol)). Data from at least three separate experiments performed in triplicate were averaged and fitted to a sigmoidal curve, when possible ($R^2 \geq 0.95$), indicated by a solid line.

2.4.6 Mechanisms of GAG-mediated amyloid formation of non-amyloidogenic peptides.

Previous studies have demonstrated that GAGs are incorporated into the mature fibrils as structural components along the longitudinal axis (Dharmadana *et al.*, 2018; Madine *et al.*, 2012; Malmos *et al.*, 2016; Nespovitaya *et al.*, 2017; Stewart *et al.*, 2016). Taking into consideration the results of the present study, we proposed a mechanism describing GAG-mediated self-assembly (figure 2.8). PACAP27 forms amyloid fibrils in presence of sulfated GAGs by means of a concerted (supra)molecular conformational conversion process, as demonstrated by the concurrent transitions in secondary structure (helix-to-β-sheet) and quaternary structure (fibril growth and increased hydrophobicity). After the initial particulate formation, both secondary and quaternary rearrangements are necessary to form amyloid nuclei. Although it is unclear how many distinct steps are required, it is likely that there is some dynamic exchange between the LMWH-bound α-helix form and the LMWH-bound β-sheet, which occurs during the lag phase. We propose that this could occur at the interface between the globular

particulate and the surrounding water, allowing the formation of amyloid-favouring hydrophobic regions inside the particulate. The rate-limiting step in the self-assembly of PACAP27 in the presence of sulfated GAGs is therefore the conformational rearrangements necessary to convert the spherical aggregates into amyloid fibrils. Among such possible rearrangements is the adoption of the α-helix motif, which appears to be an off-pathway intermediate capable of slowing the fibril formation process. This stands in contrast to the formation pre-fibrillar nuclei in solution, as is the case of strongly amyloidogenic peptides such as IAPP, Aβ and α-synuclein.

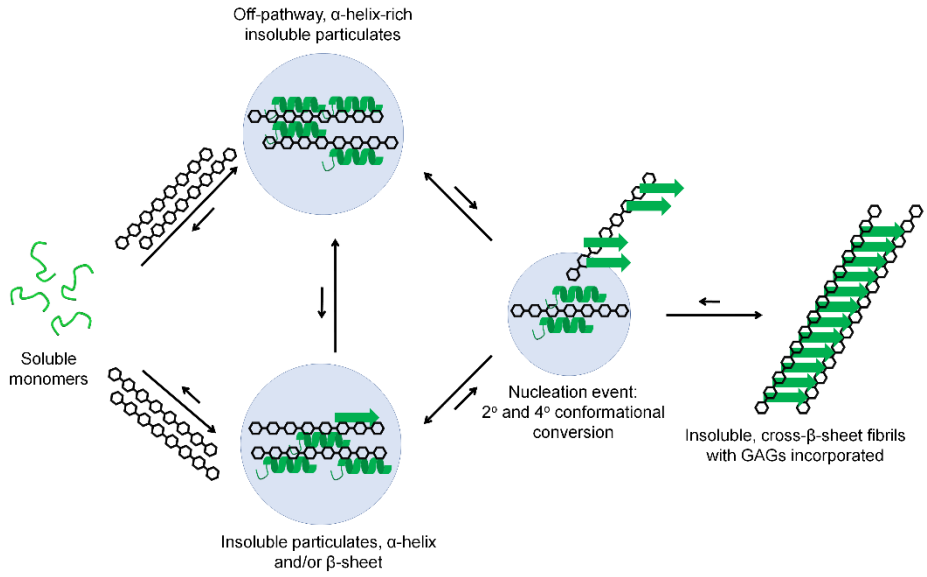

Figure 2.8 Schematic representation of GAGs-induced amyloid formation of PACAP27. Upon addition of sulfated GAGs (black hexagons) to the monomeric random coil peptide solution, particulates rich in α-helical secondary structure are rapidly formed. The peptide must undergo conformational changes within these insoluble particulates into increasingly β-sheet-rich structures for nuclei formation, allowing amyloid elongation. This involves concerted secondary and quaternary conformational conversions. When

helical folding is inhibited, with d,d-substitution, the formation of α-helix rich particulate (*top pathway*) is hindered and amyloid formation is dramatically accelerated.

2.5 Conclusion

The mechanisms by which intrinsically disordered peptide hormones form amyloid fibrils in presence of GAGs appear to be fundamentally different from the frequently described nucleated polymerisation of natively amyloidogenic proteins. Where typical models of amyloid self-assembly describe the dynamic states of soluble pre-fibrillar species, such as oligomers, this event was not observed in the case of PACAP27 with LMWH. Rather, the rapid formation of large spherical particulates sequestered the vast majority of PACAP27 as an off-pathway, somewhat stable intermediate, and no appreciable amount of the monomeric peptide in the bulk solution was detected. This initial binding event is largely driven by electrostatic interactions between the LMWH and the peptide. When considered together with the decrease in particulate size observed during the early phases of the assembly process, it appears that the initial stages of fibril formation occur in a dense and somewhat hydrophobic environment. Furthermore, the α-helical intermediates observed during GAG-mediated amyloid self-assembly delay primary nucleation, thereby stabilising off-pathway intermediates. Overall, these findings are important for our understanding of the interplay between biological linear polyanions (GAGs, RNA) and intrinsically disordered proteins/peptides in the context of amyloid formation. Recent discoveries, such as the storage of peptide hormones as amyloid in secretory granules (Maji *et al.*, 2009) as well as the formation of nuclear amyloid bodies in response to cellular stressors (Audas *et al.*, 2016), are potentially described by the process highlighted in this work. In both cases, a mainly disordered polypeptide sequence binds to a linear polyanion, and under physiological conditions, this binding event leads to the formation of amyloid, or amyloid-like, assemblies. Notably, these functional amyloids depend on a significant degree of reversibility, or disassembly, which may be ultimately studied in more

details, as the mechanistic details of the polyanion-induced amyloid self-assembly processes are being uncovered.

ASSOCIATED CONTENT

Supporting Information. Figures showing aggregation predictions of PACAP27 and peptides, extended incubation of PACAP27 with or without LMWH, cellular viability assays, data of ThT kinetic assays of amyloid fibril formation, binding to sulfated GAGs, and the formation of heterogeneous and insoluble particles in presence of LMWH are available free of charge via http//pubs.acs.org.

2.6 Supporting information

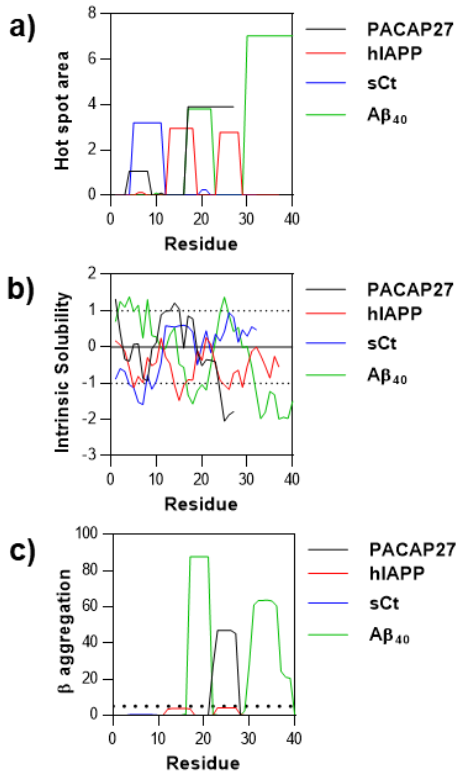

Figure S2.1 Aggregation predictions of PACAP27 and various peptides. Computational predictions for PACAP27 (black), hIAPP (red), salmon calcitonin (sCt; blue), and $A\beta_{40}$ (green) aggregation-prone regions by AGGRESCAN (a), CamSol (b), and Tango (c). Predictions were carried out at pH 6 when applicable and selecting for amidated C-termini when possible/necessary.

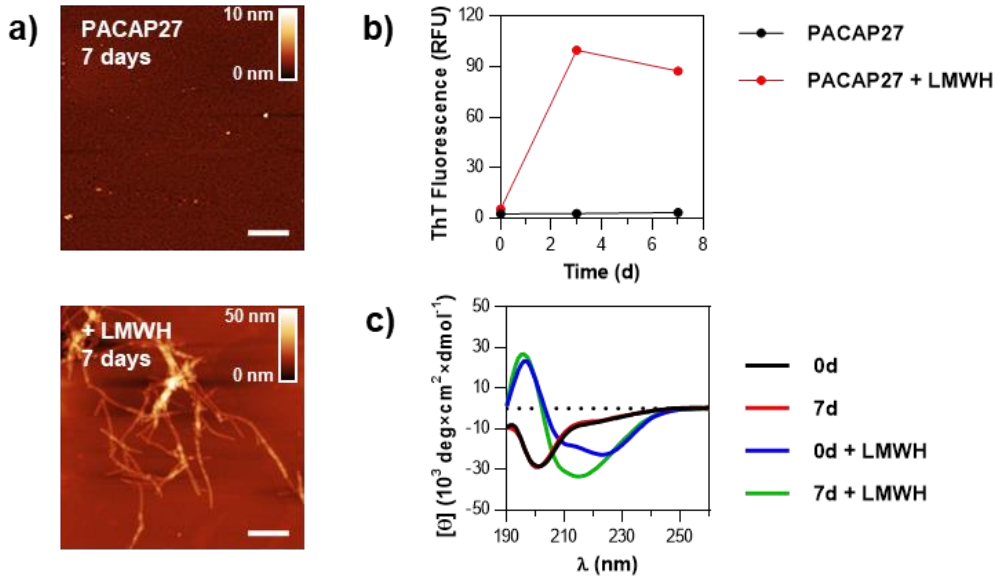

Figure S2.2 Extended incubation of PACAP27 with or without LMWH. PACAP27 (635 µM) was incubated alone or with LMWH (400 µM) under standard aggregation conditions (37 °C, 50 rpm). (a) AFM images of PACAP27 alone (top) and with LMWH (bottom) showing no fibril formation in the absence of LMWH. (b) ThT fluorescence of PACAP27 indicated no amyloid formation in the absence of LMWH. (c) No change in the secondary structure of PACAP27 was observed when the peptide was incubated in absence of LMWH.

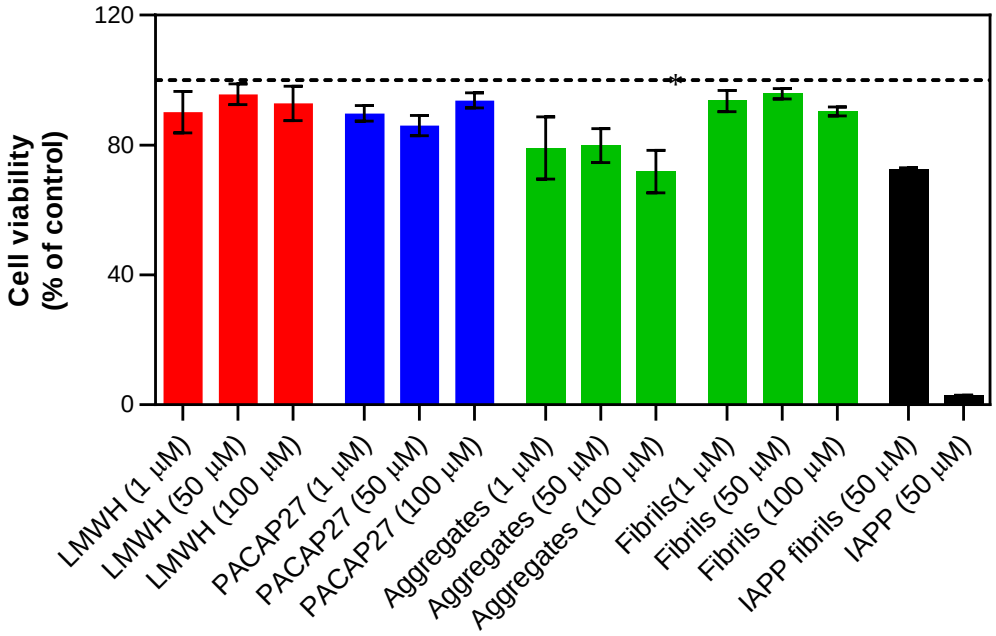

Figure S2. 3 Cellular viability assays. PACAP27 (625 µM) was incubated with LMWH (400 µM) to form amyloid fibrils under standard sefl-assembly conditions (37 °C, 50 rpm) for 0h (aggregates) and 24h (fibrils) in 5% D-mannitol, without the addition of sodium azide. Samples were then diluted to the appropriate corresponding monomeric peptide concentrations directed applied to H9C2 cardiomyocytes. Monomeric PACAP27 and LMWH were also evaluated. IAPP fibrils and monomers (50 µM) were used as positive control of proteotoxicity. Results were analysed using the Student's t-test and the statistical difference (between buffer and sample) was established at $P < 0.01$.

Table S2. 1 Data of ThT kinetic assays of amyloid fibril formation. Sigmoidal curve fittings were selected based on $R^2 \geq 0.95$, and time to half-max (t_{50}), lag time (t_{lag}), elongation rate (k), and maximum fluorescence intensity (F_{max}) were extracted.

		t_{50} (h)	k (h^{-1})	t_{lag} (h)	F_{max} (AU)
PACAP27		Fit not possible			
+HEP		8.68	0.92	6.8	12 154
+LMWH		11.70	1.30	9.1	7321
[LMWH] (µM)	100	Fit not possible			
	200	9.40	1.95	5.50	7790
	400	11.17	1.28	8.61	7705
	600	13.34	1.21	10.92	7605
	800	16.38	1.43	13.52	7239
[NaCl] (mM)	0	12.56	0.97	10.62	8407
	50	27.70	4.12	19.46	5297
	150	26.90	10.67	5.56	5267
	500	36.19	6.83	22.53	3778
pH	2.0	Fit not possible			
	6.0	13.72	1.26	11.20	9401
	7.4	12.65	0.95	10.75	6454
	8.5	10.30	1.49	7.32	7290
	12.0	11.10	0.59	9.92	7054

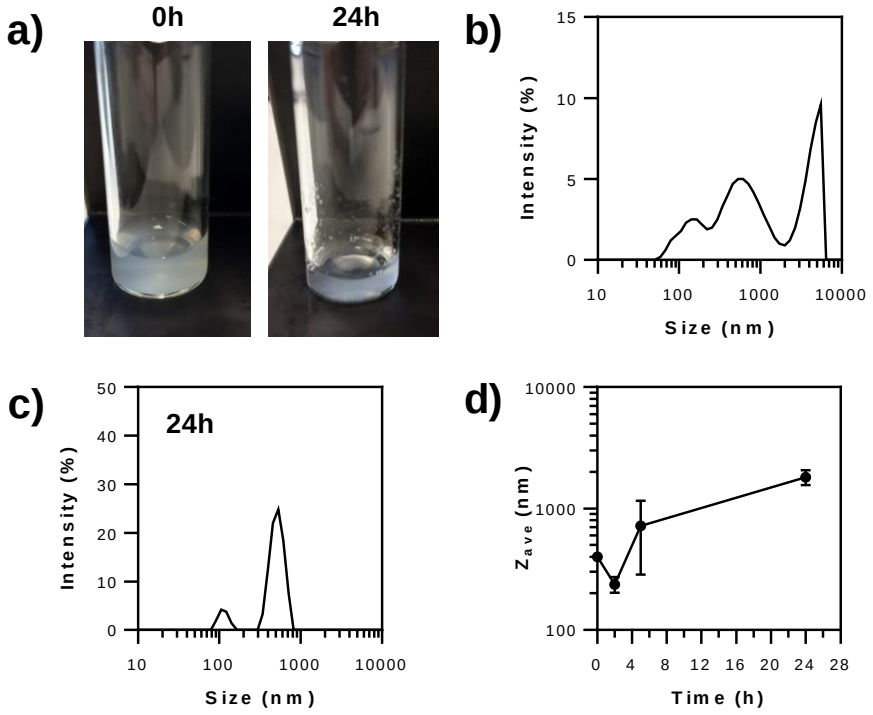

Figure S2.4 PACAP27 rapidly forms heterogeneous and insoluble particles in presence of LMWH. PACAP27 (635 µM) was incubated with LMWH (400 µM) under standard aggregation conditions (37 °C, 50 rpm). (a) At 0 h and after 24 h incubation, the solution remained turbid. (b,c) DLS analysis of the solutions at 0 h (b) and 24 h (c), respectively. (d) Average particle sizes inferred from DLS analysis. (e) CD and ThT fluorescence spectra showing amyloid formation in the presence of 150 mM NaCl.

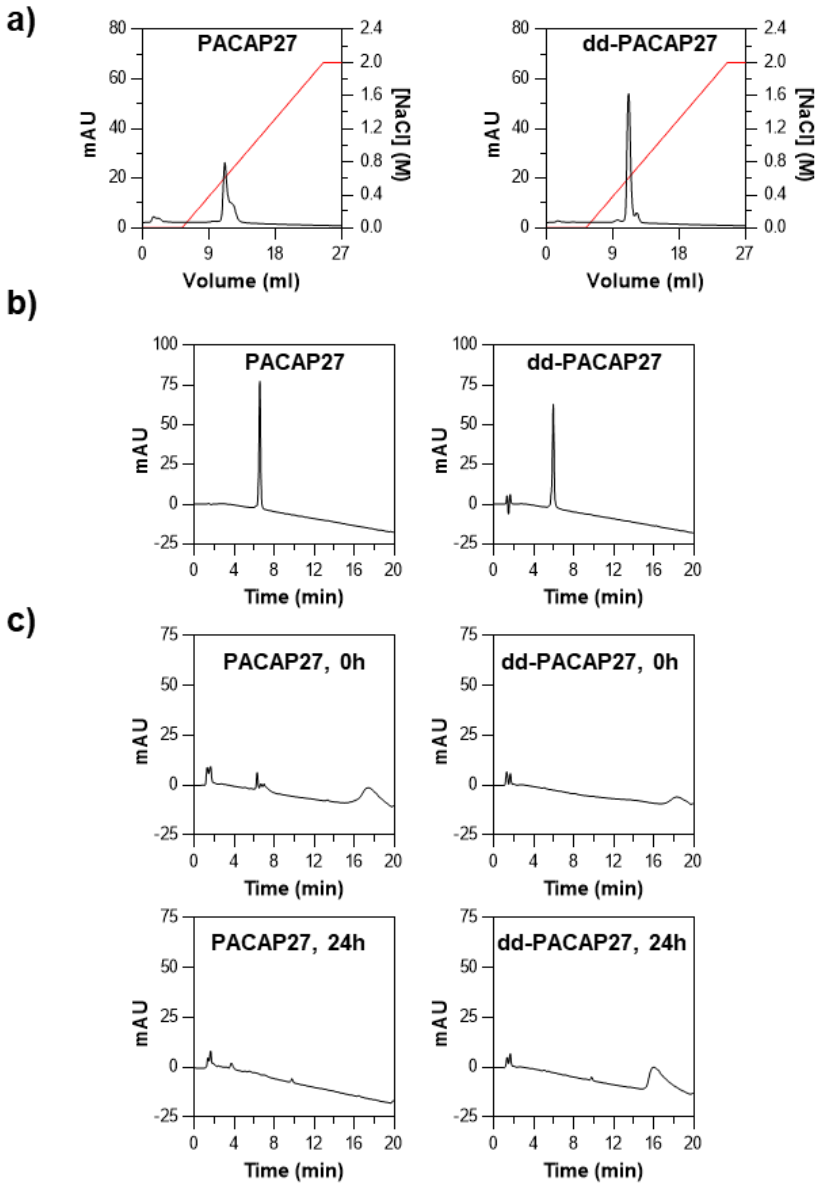

Figure S2.5 WT PACAP27 and dd-PACAP27 bind to sulfated GAGs with a similar affinity. (a) Heparin-affinity chromatography of WT and dd-PACAP27 (0.5 mg). The NaCl gradient (0-2 M) is represented in red. (b) RP-HPLC of peptides demonstrating purity ≥ 95%. (c) RP-HPLC of supernatants from peptides (635 µM) incubated with LMWH (400 µM) under standard aggregation conditions (37 °C, 50 rpm) and centrifuged (16 000g, 20 min) at 0h and 24h.

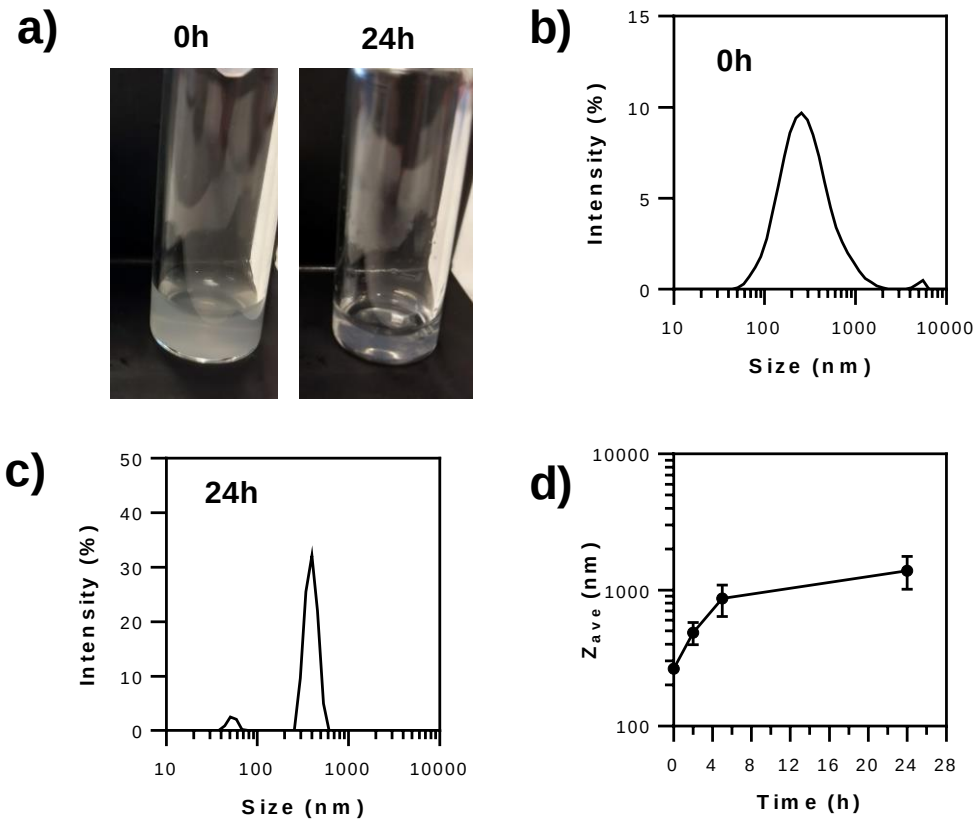

Figure S2.6 dd-PACAP27 rapidly forms insoluble particles in presence of LMWH. dd-PACAP27 (635 µM) was incubated with LMWH (400 µM) under standard aggregation conditions (37 °C, 50 rpm). (a) At 0h the solution became turbid, though turned mostly clear after 24h. (b,c) DLS analysis of the solutions at 0h and 24h. (d) Average particle sizes inferred from DLS analysis.

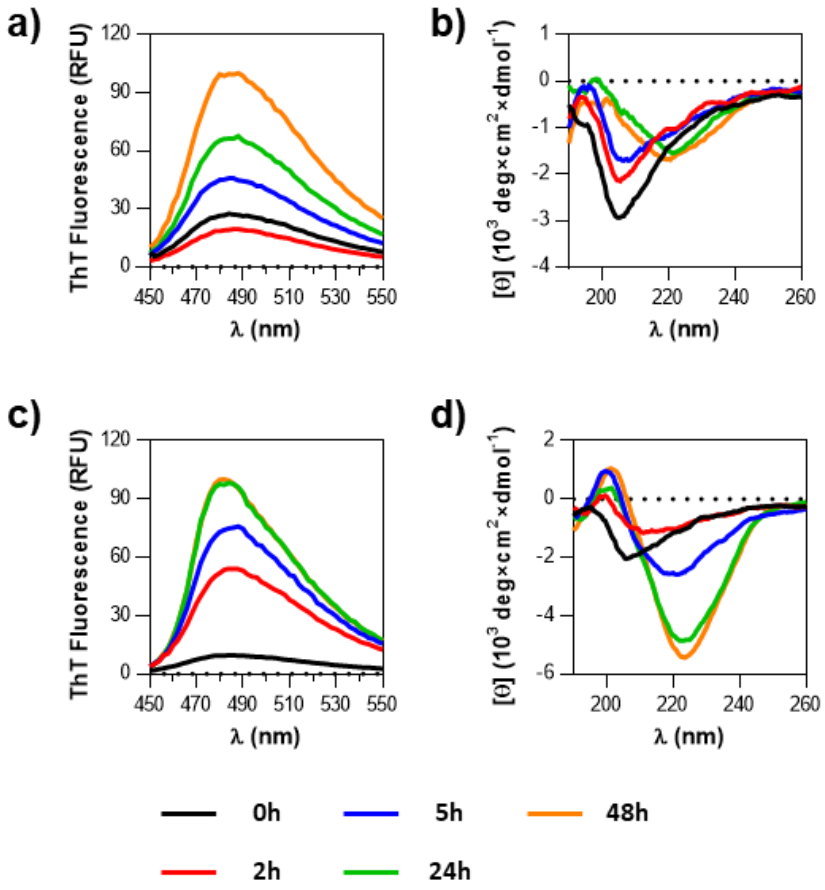

Figure S2.7 The presence of 150 mM NaCl prevents the formation of helical intermediates. WT PACAP27 and dd-PACAP27 (635 μM) were incubated with LMWH (400 μM) in D-mannitol (5% w/v, 0.01% NaN_3, 150 mM NaCl) under standard aggregation conditions over 48 hours. a) ThT fluorescence spectrum of WT PACAP27. b) Far-UV CD of WT PACAP27. c) ThT fluorescence spectrum of dd-PACAP27. d) Far-UV CD of dd-PACAP27.

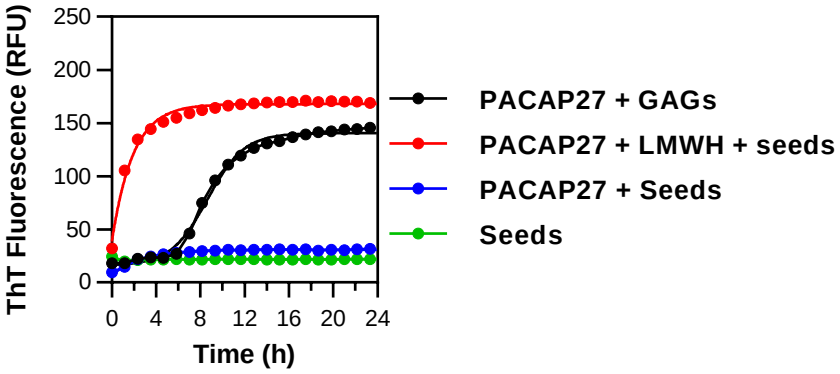

Figure S2.8 ThT-fluorescence kinetics of WT PACAP27 + LMWH and seeded kinetics of WT PACAP27 ± LMWH (seeded with pre-formed amyloid fibrils 2.5% (mol/mol)). Data were averaged from three separate experiments (n = 3) and fitted to a sigmoidal curve when possible ($R^2 \geq 0.95$), indicated by a solid line.

CHAPTER III:

ARTICLE 2

DEVELOPMENT OF A NOVEL FLUORESCENCE ASSAY FOR STUDYING LIPID BILAYER PERTURBATION INDUCED BY AMYLOIDOGENIC PEPTIDES USING CELL PLASMA MEMBRANE VESICLES

Mathew Sebastiao, Margaryta Babych, Noé Quittot, Kiran Kumar, Alexandre A. Arnold, Isabelle Marcotte, Steve Bourgault

Manuscript published in the journal BBA Biomembranes, (2023), 1865 (3):184118.

Keywords: Cell plasma membrane; lipid vesicles; amyloid; islet amyloid polypeptide; membrane perturbation; giant plasma membrane vesicles

Author contributions:

Mathew Sebastiao was responsible for the experimental design, data collection (microscopy, NMR, kinetics), data processing, interpretation of the results, wrote the manuscript, and revised the manuscript. Margaryta Babych was responsible for data collection (kinetics), preparation of GPMVs, and revised the manuscript. Noe Quittot was responsible for data collection (microscopy, kinetics), and revised the manuscript. Kiran Kumar assisted in the preparation of ghosts and revised the manuscript.

Alexandre Arnold assisted in sample preparation for NMR, experimental design (NMR), interpretation of the results, and revised the manuscript. Isabelle Marcotte was responsible for the conceptualization of the project, experimental design, and revised the manuscript. Steve Bourgault was responsible for the conceptualization of the project, experimental design, and revision of the manuscript.

3.1 Highlights

- IAPP induces the clustering of lipid vesicles derived from mammalian cell plasma membranes.
- Membrane clusters exhibit colocalization between lipid bilayer vesicles.
- Perturbation of cell-derived vesicles induced by IAPP can be detected by FRET.
- FRET signal obtained from damaged cell-derived lipid vesicles can be kinetically followed using a microplate format.
- A new assay is reported to investigate cell plasma membrane perturbation under biologically relevant conditions.

3.2 Abstract

Numerous pathophysiological conditions are associated with the misfolding and aggregation of proteins into insoluble amyloid fibrils. The mechanisms by which this process leads to cellular dysfunction remain elusive, though several hypotheses point toward the perturbation of the cell plasma membrane by pre-fibrillar intermediates and/or amyloid growth. However, current models to study membrane perturbations are largely limited to synthetic lipid vesicles and most of experimental approaches cannot be transposed to complex cell-derived plasma membrane systems. Herein, vesicles originating from the plasma membrane of erythrocytes and β-pancreatic cells were used to study the perturbations induced by an amyloidogenic peptide, the islet amyloid polypeptide (IAPP). These biologically relevant lipid vesicles displayed a characteristic clustering in the presence of the amyloidogenic peptide, which was able to rupture membranes. By exploiting Förster resonance energy transfer (FRET), a rapid, simple, and potentially high-throughput assay to detect membrane perturbations of intact mammalian cell plasma membrane vesicles was implemented. The FRET kinetics of membrane perturbations closely correlated with the kinetics of thioflavin-T fluorescence associated with amyloid formation. This novel kinetics assay expands the toolbox available to study amyloid-associated membrane damage, bridging the gap between synthetic lipid vesicles and living cells.

3.3 Introduction

Amyloid-associated pathophysiologies constitute an important class of degenerative disorders, which involve the accumulation of extracellular fibrillar deposits composed primarily of proteinaceous materials (Chiti and Dobson, 2017). These amyloid fibrils are found in a wide variety of disorders; including systemic amyloidosis, Parkinson's disease, Alzheimer's disease, and type II diabetes (Iadanza *et al.*, 2018). Although these fibrils were historically recognised as the causative agent in diseases, increasing biochemical and pharmacological evidence has shown the low cytotoxicity of well-defined fibrils, and the high cytotoxicity of pre-fibrillar oligomeric species and/or of the process of fibrillization (Abedini *et al.*, 2016b; Birol *et al.*, 2018; Ludtmann *et al.*, 2018; Serra-Batiste *et al.*, 2016; Weise *et al.*, 2010; Yasumoto *et al.*, 2019). Several cellular mechanisms have been proposed to contribute to the cytotoxic pathways of amyloidogenic polypeptides, including the generation of reactive oxygen species (Uttara *et al.*, 2009), autophagy (Salminen *et al.*, 2013), defects in proteasomal degradation (Jackson and Hewitt, 2016), sequestration of essential proteins (Olzscha *et al.*, 2011), and disruption of cell membranes (e.g. mitochondrial, endoplasmic reticulum, and plasma membranes) (Birol *et al.*, 2018; Lu *et al.*, 2018; Quittot *et al.*, 2021; Sciacca *et al.*, 2018; Yasumoto *et al.*, 2019). Over the last two decades, numerous studies have investigated the relationship between the process of amyloid formation and the plasma membrane disruption. Several reports have suggested the formation of transmembrane pore by oligomeric intermediates, which allows for the unregulated passive diffusion of solutes through the cell membrane (Birol *et al.*, 2018; Ludtmann *et al.*, 2018; Sciacca *et al.*, 2012; Serra-Batiste *et al.*, 2016). Alternatively, another mechanism often described is the detergent-like model, wherein the growing oligomers and other pre-fibrillar species pull phospholipids out of the plasma membrane (Walsh *et al.*, 2014). Fibril elongation at the cell surface has also been proposed to induce plasma membrane disruption via a carpet-like mechanism, whereby monomeric/oligomeric peptides adhere to the outer leaflet and fibril growth pulls out

lipids from the bilayer causing large scale damage (Christensen and Schiott, 2019; Evangelisti *et al.*, 2016; Kotler *et al.*, 2014; Sciacca *et al.*, 2012; Terakawa *et al.*, 2018; Wakabayashi and Matsuzaki, 2009).

The mechanistic and kinetics of plasma membrane disruption by amyloid-related assemblies have been mainly investigated using synthetic lipid bilayer models. For example, multilamellar and unilamellar vesicles composed of lipids such as phosphatidylcholines, phosphatidylglycerols, phosphatidylserines, phosphatidylethanolamines, and/or cholesterol in a variety of combinations and molar ratios, have been abundantly employed (Sciacca *et al.*, 2018). These lipid bilayers are advantageous owing to their straightforward preparation, uniformity, compatibility with multiple biophysical analyses, including atomic force microscopy (Quist *et al.*, 2005) and nuclear magnetic resonance (NMR) spectroscopy (Rajput *et al.*, 2021), and the ability to readily modulate the lipid composition and corresponding physicochemical properties (Sciacca *et al.*, 2020; Sciacca *et al.*, 2018; Terakawa *et al.*, 2018). However, synthetic lipid vesicles are deficient in key biological components present in, or on, cellular plasma membranes, such as transmembrane and membrane-anchored cytoskeletal proteins, proteoglycans, and complex glycolipids. Some studies have used more representative lipid bilayers, such as liposomes incorporating gangliosides (Amaro *et al.*, 2016; Bucciantini *et al.*, 2020; Christensen and Schiott, 2019; Matsubara *et al.*, 2018), or lipid mixtures extracted from living cells (Lee *et al.*, 2017; Mrdenovic *et al.*, 2019). Lipids extracted from plasma membranes and ganglioside-containing vesicles more accurately reflect the complexity and heterogeneity of eukaryotic cell membranes than conventional synthetic models and can be prepared in sufficient quantities for mechanistic investigations. Still, these bilayers are free of any proteins and are deficient of the cytoskeleton, ultimately altering their response to stressors, such as those associated with amyloid formation. Moreover, they lack the asymmetry of mammalian cell membranes, where the outer and inner leaflets are composed of different lipid mixtures and surface architectures.

To address these limitations, recent works have utilised giant plasma membrane vesicles (GPMVs), which fully maintain the complex composition of cell plasma membranes (Birol *et al.*, 2018; Birol *et al.*, 2019; Quittot *et al.*, 2021). However, there are still no available assays with sufficient throughput capacity to readily interrogate the kinetics of membrane perturbation of cell-derived vesicles, compared to the prototypical dye-leakage assays performed with synthetic liposomes (Cao *et al.*, 2013a; Godin *et al.*, 2019; Hoffmann *et al.*, 2018; Khemtemourian *et al.*, 2021). Thus, there is an urgent need for the development of novel experimental strategies and approaches to study the membrane disruption induced by amyloidogenic peptides using biologically relevant model systems.

In this study, we investigated the usage of physiologically relevant lipid model systems to implement a novel assay that aims at kinetically evaluating plasma membrane perturbations induced by amyloidogenic peptides, *i.e.* erythrocytes, hemolyzed red blood cells (RBCs), known as ghosts, and GPMVs. The islet amyloid polypeptide (IAPP), a 37-residue polypeptide whose extracellular deposition is associated with type II diabetes mellitus, was used as a model of amyloidogenic peptide (Nguyen *et al.*, 2015; Westermark *et al.*, 2011). Ghosts and GPMVs allowed for the study of cell membrane perturbations through confocal microscopy, fluorescence spectroscopy, and solid-state (SS) NMR spectroscopy. Furthermore, using two independently labelled preparations of vesicles, a rapid, sensitive, and simple assay was developed to efficiently probe the kinetics of membrane disruption under various conditions. This versatile and potentially high-throughput assay offers key advantages over the commonly used dye-release assay based on synthetic lipid bilayer systems: biologically representative lipid compositions, and presence of structural and non-lipid components.

3.4 Materials and methods

3.4.1 Peptide synthesis, purification and monomerization

IAPP (KCNTATCATQRLANFLVHSSNNFGAILSSTNVGSNTY) and rat IAPP (rIAPP; KCNTATCATQRLANFLVRSSNNLGPVLPPTNVGSNTY) were synthesized on rink amide resin by standard Fmoc chemistry, as previously described (De Carufel *et al.*, 2015). For fluorescein labeling, an additional residue (Fmoc-Lys-(Alloc)-OH) was first coupled at the N-terminus of the peptidyl-resin. The Alloc protecting group was orthogonally removed using palladium $(Pd(PPh_3))_4$ in the presence of 24 eq. PhSiH3 in DCM under an argon. After washed, a solution of DMF containing 3 eq fluorescein isothiocyanate (FITC) and 6 eq triethylamine (TEA) was added before the mixture was left to react overnight. After cleavage from the solid support (TFA/EDT/PhOH/H_2O), crude peptides were precipitated and washed with diethyl ether, recovered by vacuum filtration, and dissolved in distilled water before being lyophilized. Peptides were purified by reverse-phase high performance liquid chromatography (RP-HPLC) on a preparative C18 column with a linear gradient of acetonitrile (ACN) in H_2O/TFA (0.06% v/v). Collected fractions were analyzed by analytical RP-HPLC and mass-verified by electrospray ionization time-of-flight mass spectrometry (ESI-TOF MS). Fractions containing the peptide of interest at 95% purity or higher were pooled and lyophilized. The disulfide bridge between Cys2 and Cys7 was formed by dissolving the peptides in DMSO (1 mg/mL) and agitating the solution overnight, at room temperature. The resulting solution was re-purified using the conditions described above and lyophilized. The resulting peptide powder was first dissolved in HFIP at 1 mg/mL and sonicated for 30 min. The solution was filtered through a 0.22 μm PVDF filter and lyophilized. Peptides were subsequently dissolved in HFIP (1.5 mg/mL), sonicated for 30 min and the solution was aliquoted and lyophilized. Peptides were stored dry at -20 °C and used within the next 4 weeks.

3.4.2 Hemolysis assay of red blood cells

Horse RBCs (100% packed, Cedarlane) were suspended in 20 mM HEPES, 150 mM NaCl, pH 7.4 buffer and centrifuged at 500×g for 3 min to pellet intact cells. This was repeated 4 times to remove all cell debris and extracellular hemoglobin, until the supernatant was clear. Volumes of the viscous, fluid-like RBC pellet were then collected by micropipette (pipette tips were cut 0.5 cm shorter to increase the diameter of the opening and accommodate the viscosity of the pellet) and resuspended at 5% v/v in isotonic buffer. The resulting suspension of RBCs was then combined with peptide solutions to obtain a final concentration of 2.5% v/v for RBCs with the desired concentration of peptide. These mixtures were incubated at 37°C and recovered at the indicated times. Of each mixture, 200 μL was centrifuged to remove intact cells (500×g, 3 min) and the optical density of the supernatant was measured at 576 nm to estimate the presence of hemoglobin. This was normalized against a positive control of 100% membrane disruption, where 50 μL of the incubation mixture was diluted with 50 μL of 0.2% v/v triton-X100.

3.4.3 Quantification of phospholipids

Samples of each preparation were added to glass vials, along with 450 μL H_2SO_4 (8.9 N) and boiled for 25 min at 220 °C. A standard curve was also prepared (0 – 162.5 nmol P_i). The samples were then cooled,150 μL of 30% H_2O_2 was added, and the samples were boiled again for 30 min at 220 °C. Solutions were transferred to a larger vial with 3.9 mL H_2O, 500 μL ascorbic acid (10% w/v) and 500 μL ammonium molybdate hexahydrate (2.5% w/v). This final solution was incubated at 100 °C for 7 min. Samples were then cooled and transferred to a 96-well microplate (200 μL per well) to measure the optical density at 820 nm. Concentrations were determined for each membrane preparation using a linear regression (Chen *et al.*, 1956).

3.4.4 Preparation of ghosts and fluorescent labelling

In 40 mL round bottom centrifuge tubes, 2.5 mL of horse RBCs were suspended in 25 mL of isotonic buffer (20 mM HEPES, 150 mM NaCl, pH 7.4). This suspension was mixed before being centrifuged (1000×g, 5 min, 4 °C). The supernatant was removed, the pellet resuspended in 25 mL of isotonic buffer, and the process repeated until the supernatant was clear, *i.e.,* between 3 to 5 times). Once the clear supernatant was removed, the RBCs were resuspended in 25 mL of hypotonic buffer (20 mM HEPES, pH 7.4) and vortexed. Solutions were centrifuged to pellet the ghosts (25,000×g, 45 min, 4 °C). The supernatant was carefully removed, and the resulting viscous, pink pellet transferred to a new tube, leaving behind a protease-rich deposit known as the "red button." This process was repeated as needed, until no visible tint of pink remained, *i.e.* between 3 to 5 times. The final white pellet was resuspended in 25 mL isotonic buffer to seal the membranes and centrifuged (25,000×g, 20 min, 4 °C). The supernatant was removed, and the pellet was resuspended in 2 mL of isotonic buffer before being stored at 4 °C and used within the next 3 days. The phospholipid concentration of the resulting ghost suspension was determined using the colorimetric assay, based on the assumption that all phosphorus arise from the phospholipids. This is apparent from the subsequent ^{31}P NMR experiments (figure s3.1).

Ghosts (100 µL) were diluted 10 times in isotonic buffer (20 mM HEPES, 150 mM NaCl, pH 7.4) from the concentrated suspension prepared above to reach a final volume of 1 mL. This suspension was incubated with either FAST-DiO (10 µg/mL) or FAST-DiI (2 µg/mL) for 1 h at 37°C. The suspension of labelled ghosts was centrifuged (16,000×g, 15 min) and the supernatant removed to eliminate excess fluorophore. The pellet was resuspended with 500 µL isotonic buffer and the phospholipid concentration was measured.

3.4.5 Preparation of giant plasma membrane vesicles and labelling

INS-1E cells were cultured in RPMI-1640 media supplemented with 10% FBS, 2 mM L-glutamine, 100 U/mL penicillin, 100 mg/mL streptomycin, 10 mM HEPES, 1 mM sodium pyruvate, and 50 mM β-mercaptoethanol at 37°C and 5% CO_2. Cultures were allowed to reach confluency in 150 mm tissue culture petri dishes before being washed twice with Hank's buffered saline solution (HBSS). Cells were then washed twice with GPMV buffer (10 mM HEPES, 150 mM NaCl, 2 mM $CaCl_2$, pH 7.4). After washing, the cells were incubated in GPMV buffer supplemented with 2 mM N-ethylmaleimide (NEM) for 2 h at 37 °C. After incubation, the solution was collected and centrifuged to remove cell debris (5 min, 500×g). The supernatants were either concentrated directly using 100K amicon centrifugal filter units or labelled with lipophilic tracers (2 μg/mL FAST-DiI or 10 μg/mL FAST-DiO) in separate batches for 45 min. Labelled GPMVs were then concentrated, and the concentration of phospholipids was determined. GPMV suspensions were kept at 4 °C for up to 48 h.

3.4.6 Confocal microscopy

For colocalization experiments, suspensions of ghosts and GPMVs were respectively prepared to reach a total phospholipid concentration of 25 μM, using equal parts of FAST-DiO and FAST-DiI labelled lipid vesicles. To this suspension, peptide solutions were added to reach the desired molar ratio (phospholipid:peptide). The samples (500 μL final volume) were left to incubate at room temperature under quiescent conditions. After incubation, 300 μL of each sample were transferred to an 8-well chambered microscopy slide and images were acquired using a Nikon confocal microscope equipped with a 60x oil-immersion lens. For samples where particle diffusion was slow enough to not impede the resolution, images were acquired as a vertical stack and represented using a Z-projection to better demonstrate the three-dimensional layering of the structures formed. To detect ThT or FITC-labelled peptides, FAST-DiI

membranes were used in combination with either FITC-labelled peptides, or unlabelled peptides for ThT staining after incubation. Samples were stained with 40 μM ThT prior to loading the slides. Images were processed, and the Pearson's correlation coefficients were calculated using ImageJ.

3.4.7 Transmission electron microscopy

Samples were prepared using ghosts at 12.5 μM phospholipid concentrations in buffer (20 mM HEPES, 150 mM NaCl, pH 7.4), in presence of 12.5 μM peptide. The samples were left to incubate for 24 h and were then applied to glow-discharged carbon films on 300-mesh copper grids. Samples were stained with 1.5 % w/v uranyl formate and images acquired using an FEI Tecnai G2 Spirit Twin microscope at 120 kV with a Gatan Ultrascan 4k × 4k CCD system.

3.4.8 Solid-state nuclear magnetic resonance spectroscopy

To dried peptide aliquots, a suspension of ghosts prepared with a phospholipid concentration of 125 μM in isotonic buffer (20 mM HEPES, 150 mM NaCl, pH 7.4) was added and the suspension vortexed. Final peptide concentrations were 125 μM to obtain a peptide:phospholipid (P/L) ratio of 1:1. Final incubation volumes were 4 mL, mixed by vortex, and incubated at room temperature for 24 h. After incubation, samples were centrifuged (16,000×g, 20 min) and the resulting pellet was recovered and loaded into a 4-mm zirconium oxide rotor for SS-NMR spectroscopy. All SS-NMR experiments were recorded at 298 K with a 400 MHz wide-bore Bruker Avance III-HD spectrometer (Milton, Canada) operating at 400.03 and 161.9 MHz for ^{1}H and ^{31}P respectively. Spectra were externally referenced using the single peak of 85% phosphoric acid, set at 0 ppm. MAS spectra were recorded using a spinning frequency of 6 kHz and 2k scans were accumulated using a single 90^{o} pulse. Static spectra were obtained using 26k scans and recorded with a Hahn echo pulse sequence with an

interpulse delay of 30 μs. All spectra were recorded using high-power ^{1}H decoupling (continuous wave or TPPM decoupling for static or MAS spectra, respectively). The radiofrequency fields applied were 83.33 and 50 kHz for ^{31}P and ^{1}H respectively. For quantitative analyses of the relative phosphorus content in ghosts and RBCs (figure S1), the recycling delay was adjusted to 10 s to ensure complete signal relaxation. Data were collected and processed using Bruker TopSpin software.

3.4.9 Kinetics of fibril formation and lipid vesicle perturbation

For thioflavin-T (ThT) and fluorescence resonance energy transfer (FRET) kinetics, lipid vesicles were prepared as described above without labelling (for ThT assays) or with labelling (for FRET-based assays). In each case, the corresponding vesicles were prepared at various concentrations ranging from 3.125 to 50 μM phospholipids and incubated with either IAPP, or rIAPP, at 12.5 μM to reach the desired P/L ratios (1:0.25, 1:1, 1:4). The peptide concentration was kept constant in kinetic assays to facilitate comparisons between different conditions. Microplates were sealed with silicone covers and measurements were made every 10 min, without any programmed agitation, at room temperature. ThT assays used 440 nm/485 nm as the excitation/emission wavelengths, respectively. For FRET assays, samples were excited using the FAST-DiO wavelength of 485 nm and detected at the emission maximum of FAST-DiI of 570 nm. ThT and FRET kinetics were processed by first normalizing the intensity relative to the corresponding blank and data were averaged, normalized, and fit with a sigmoidal curve to extract maximum fluorescence values, slopes (k), and half-times (t_{50}). All data processing and statistical analysis (ANOVA, t-test) was done using GraphPad Prism.

3.5 Results

3.5.1 The erythrocyte hemolysis assay can be used to monitor the kinetics of membrane perturbation induced by IAPP

To expand the usage of lipid vesicles derived from mammalian cells to readily interrogate the perturbation nature of amyloidogenic polypeptides under physiologically relevant conditions, we initially targeted RBCs. Erythrocytes can be obtained in large quantities, are easy to manipulate owing to their robustness, and are a good model of eukaryotic cell plasma membranes while having virtually no cellular machinery. Particularly, RBCs contain high concentration (22 mM) of intracellular hemoglobin (Hb) (Papasouliotis *et al.*, 1999), which can be exploited as a pre-encapsulated chromophore to perform hemolysis assays. While hemolysis assays have been abundantly used to study antimicrobial peptides (Chen *et al.*, 2021) and therapeutic compounds (Gavriilaki *et al.*, 2019), they have been less utilized to evaluate the kinetics of membrane perturbation associated with amyloid formation (Dubey *et al.*, 2017; Huang *et al.*, 2009; Kakinen *et al.*, 2018). Accordingly, we first evaluated if the RBC hemolysis assay can be conveniently implemented to study the kinetics of membrane perturbation induced by the amyloidogenic peptide IAPP. Isolated RBCs were treated with IAPP, or the non-amyloidogenic rat analog (rIAPP) as a control, for 24 h before measuring the release of Hb using standard hemolysis protocol that involved the separation of intact cells and Hb by centrifugation. In comparison to human IAPP, rIAPP contains six substitutions that prevent the peptide from aggregating into fibrils (Middleton *et al.*, 2012). Although rIAPP has been shown to readily form oligomers, it is poorly cytotoxic and does not induce significant membrane leakage (Cao *et al.*, 2013a). Results revealed that an IAPP concentration of 50 μM is required to significantly detect hemolysis ($p > 0.05$) after 24 h incubation (figure 1A). The release of Hb was not observed in the presence of rIAPP, indicating that membrane leakage is likely associated with the aggregation propensity of the peptide. The effect

of IAPP on RBC membrane integrity was corroborated using confocal microscopy by labelling the RBCs with the lipophilic tracer FAST-DiO. RBCs treated for 24 h with rIAPP remained well dispersed and with defined round shape, whereas treatment with IAPP resulted in the aggregation of erythrocytes into large amorphous lipid clusters (figure 1B). Additionally, changes to the morphology of the RBCs were noticeable, such as regions of high curvature, intense bright spots, and diffusion of the fluorophore throughout the clusters. Next, the possibility to follow the kinetics of membrane perturbation induced by IAPP was evaluated by measuring Hb leakage from erythrocytes after different incubation period with 50 and 100 μM peptide. A sharp increase of hemolysis was observed for erythrocytes treated with 100 μM IAPP (figure 1C), during the first 4 h of the experiment, followed by a more gradual increase of Hb release before a plateau was reached after 16 h. In the presence of 50 μM IAPP, a significant increase of hemolysis was detectable only after 8 h incubation (figure 1D). In sharp contrast, hemolysis was undetectable for RBCs treated with rIAPP. While the kinetics of lipid membrane perturbation could be inferred from the Hb release of erythrocytes, this approach requires demanding experimental manipulation, including centrifugation steps, which is not suitable for evaluating multiple conditions and/or for screening a library of membrane-active compounds. Moreover, the discontinuous measurement of Hb release introduces high experimental variability, and the point-to-point type measurement can hide irregular, or multiphasic, kinetics. Besides, the presence of a high concentration of Hb in RBCs could preclude the usage of the amyloid sensitive dye ThT, as observed here (figure 1E) and as previously reported (Jayawardena *et al.*, 2017), as well as potentially interfering with number of biophysical approaches, including SS-NMR (figure s1). Thus, considering that the isolation of plasma membranes from erythrocytes is straightforward and has been employed for decades as a way to study membrane proteins (Schwoch and Passow, 1973), we shifted our assay development towards RBC ‘ghosts’.

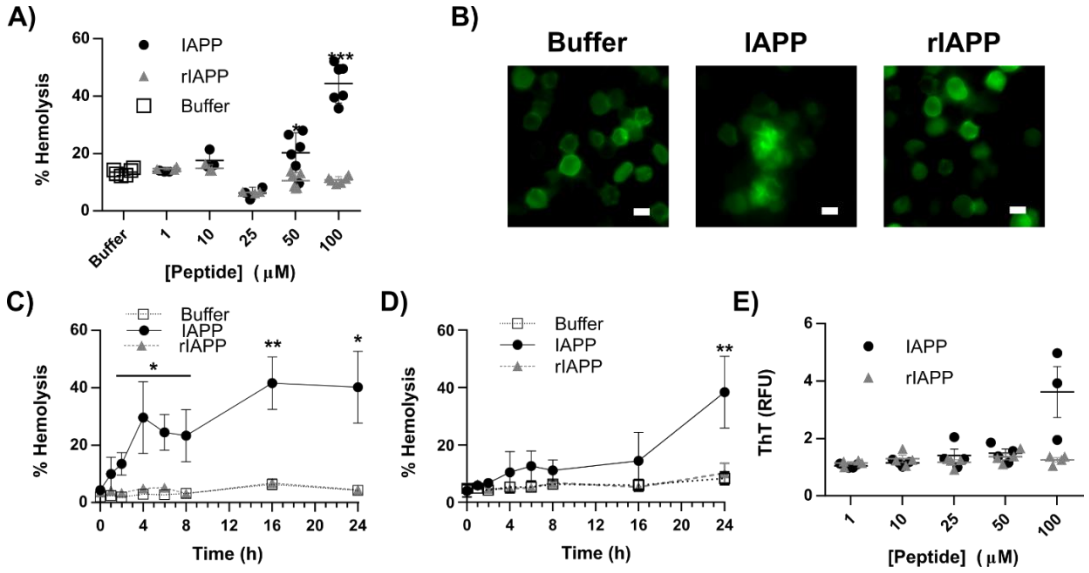

Figure 3.1 Hemolysis of erythrocytes induced by IAPP. (A) RBCs were incubated with increasing concentrations of monomerized peptides for 24 h and extracellular hemoglobin was measured. (B) RBCs were labelled with FAST-DiO and images were acquired after 24 h incubation in the presence, or not, of 50 μM rIAPP or 50 μM IAPP. Scale bars = 5 μm. (C-D) Timepoints during hemolysis were recovered for RBCs incubated with (C)100 μM and (D) 50 μM peptide. (E) ThT fluorescence of IAPP and rIAPP after 24 h incubation with RBCs.

3.5.2 IAPP amyloid formation is associated with the clustering of erythrocyte ghosts

RBCs "ghosts", which are lacking Hb and other intracellular (macro)molecules, were prepared by rupturing erythrocytes via an osmotic shock. The resulting ghosts have comparable size, surface, membrane composition and physical properties to erythrocytes (Kumar *et al.*, 2022; Schwoch and Passow, 1973), and the membrane asymmetry is preserved. Moreover, they are readily prepared and constitute highly biologically relevant lipid vesicles. Particularly, the removal of Hb and other cytosolic compounds, such as phosphorylated metabolites, eliminates potential sources of interference with biophysical analyses that are common to study amyloid formation,

such as SS-NMR (figure s1) and ThT fluorescence (figure 1E) (Kumar *et al.*, 2022). Isolated ghosts were treated for 24h at RT with 12.5 μM of peptide at a 1:1 peptide:lipid (P/L) molar ratio and amyloid formation and effect on vesicle morphology were respectively evaluated by ThT fluorescence and electron microscopy. After 24 h incubation, a ThT positive fluorescence signal was measured for IAPP whereas rIAPP did not respond any more than the ghost treated with the buffer vehicle (figure 2A). By TEM, prototypical IAPP amyloid fibrils could be observed around RBC ghosts, which were significantly smaller in diameter than controls and were grouped together in tight clusters (figure 1B). Some extracellular vesicles were detected in the buffer-treated samples, which is consistent with the response of erythrocytes to storage conditions lacking glucose and ATP (Lauren *et al.*, 2018). Similarly, spherical oligomers were

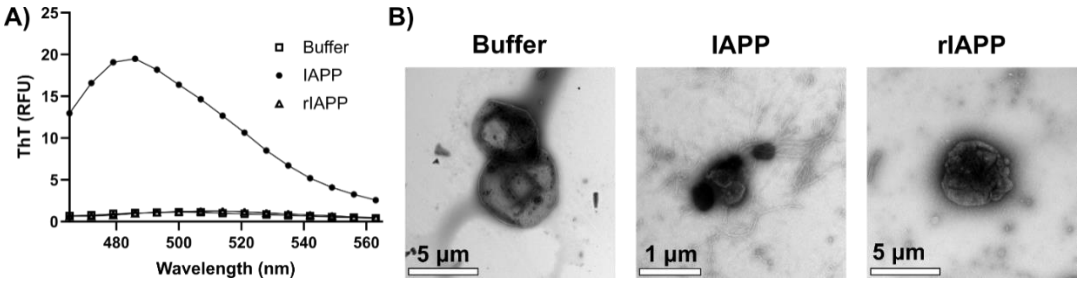

Figure 3.2 IAPP amyloid formation is associated with the clustering of erythrocyte ghosts. (A,B) Ghosts were incubated for 24h at room temperature with either buffer or peptides at 12.5 μM (1:1 molar ratio of peptide:phospholipid (P/L)). After incubation, (A) ThT fluorescence was measured using 20 μM ThT and (B) samples were imaged by TEM. (B) Scale bar for buffer and rIAPP samples is 5 μm, whereas for IAPP the scale bar is 1 μm.

detected in the ghost samples treated with rIAPP, yet membrane vesicles remained dispersed and of similar size and morphology to those treated with buffer. These observations indicate that IAPP self-assembles into fibrils in the presence of RBC vesicles, which is associated with their clustering and perturbation, encouraging further development of a kinetics assay using ghosts.

3.5.3 Clustering and damage of RBC ghosts induce by IAPP can be visualized by fluorescence microscopy

The observed clustering and morphological perturbation of RBCs associated with IAPP amyloid formation could be exploited to develop a continuous and high-throughput fluorescence-based assay to follow lipid membrane perturbation using labelled vesicles. To do so, ghosts were labelled with either red (FAST-DiI) or green (FAST-DiO) lipophilic tracers, then combined to generate a suspension of red and green vesicles, and this mixture was incubated at room temperature in the presence of IAPP, or rIAPP, at a 1:1 P/L molar ratio (12.5 μM). When the red- and green-labelled ghosts were incubated together in the absence of peptide, they remained well dispersed, and their round shape persisted over the 24 h incubation period (figure 3A). After incubation with IAPP, the ghosts clustered and a clear colocalization of the two fluorophores was observed. These effects are absent when the ghosts were treated with rIAPP, indicating that peptide aggregation is associated with colocalization, vesicle clustering and loss of shape. After 1 h treatment with IAPP, the ghosts formed large clusters that persisted throughout the experiment and no significant differences in aggregate sizes were observed. Colocalization of the fluorophores was detected at each timepoint analyzed, though qualitatively appeared to increase with incubation time. Conversely, rIAPP-treated ghosts displayed no appreciable changes over incubation time.

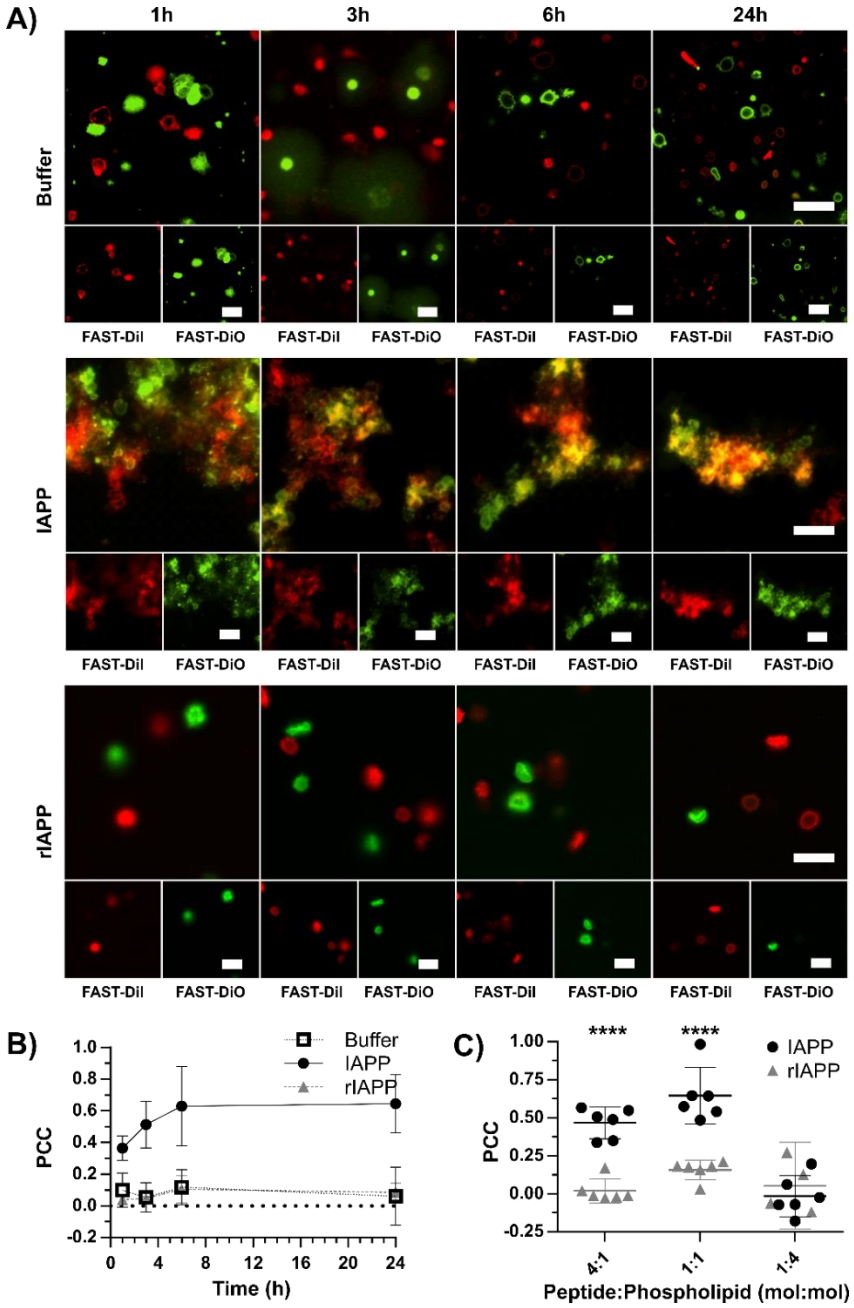

Figure 3.3 IAPP induces lipid bilayer perturbation and clustering of erythrocyte ghosts. A) Confocal microscopy images of a mixture of red labelled (FAST-DiI) and green labelled (FAST-DiO) RBC ghosts, in the presence, or absence, of peptide. Samples were incubated with a molar ratio of 1:1 (P/L) at room temperature. Scale bars = 5 μm. B) Colocalization values for membrane mixtures obtained using the Pearson's correlation

test throughout the incubation time. C) Final colocalization values for the membrane mixtures incubated with various concentration of peptides.

The colocalization of FAST-DiO and FAST-DiI was quantified using the Pearson correlation coefficient (PCC) (figure 3B). The PCC lies between -1 for a perfectly inverse correlation and +1 for a perfectly direct correlation, while a value of 0 indicates the absence of any correlation (Taylor, 1990). Data were extracted from triplicate experiments using P/L molar ratios of 1:1. For IAPP, the PCC at 0 h incubation was ~ 0.4. After 3 to 6 h, the colocalization further increased to a PCC of ~0.6, which persisted over 24 h. In sharp contrast, treatment with rIAPP induced no significant changes to either the ghost morphology, spatial distribution, or colocalization measurements, demonstrating that the effects produced were specific to the amyloidogenic IAPP. Other P/L molar ratios were studied (figures 3C and S2), and the PCC results obtained with a 4:1 P/L molar ratio were equivalent to those obtained with a 1:1 ratio. When reducing the peptide proportion (1:4 P/L molar ratio), the colocalization level was equivalent to that measured with ghosts treated with rIAPP or the buffer control. However, at 1:4 molar ratio, IAPP was able to induce membrane clustering, which was not present for ghosts treated with rIAPP or the buffer (figure S2).

3.5.4 ThT-positive aggregates colocalize with membrane clusters

Clusters of erythrocyte ghosts observed by fluorescence microscopy upon IAPP treatment appeared as large, immobile aggregates and the lipid bilayers were less defined, with more diffuse fluorescent labelling compared to control samples; rIAPP and buffer (figure 3A). Therefore, to verify if IAPP could be located within these lipid clusters, FAST-DiI labelled ghosts were incubated in presence of FITC-labelled peptides at a 1:1 P/L molar ratio. The membrane clusters were enriched in IAPP, while membrane-bound rIAPP was not detected (figure 4A). PCC values of 0.7 and 0.1 were respectively determined for ghosts treated with IAPP and rIAPP. The lipid-peptide clusters obtained with unlabelled IAPP stained positive for ThT (figure 4B), indicating

that the aggregates are rich in peptides likely gathered as amyloid assemblies, as observed by TEM (figure 2B). These microscopy images revealed that the lipophilic tracers are highly diffuse after IAPP exposure, raising questions as to the organization of the lipid bilayer upon treatment with the amyloidogenic peptide.

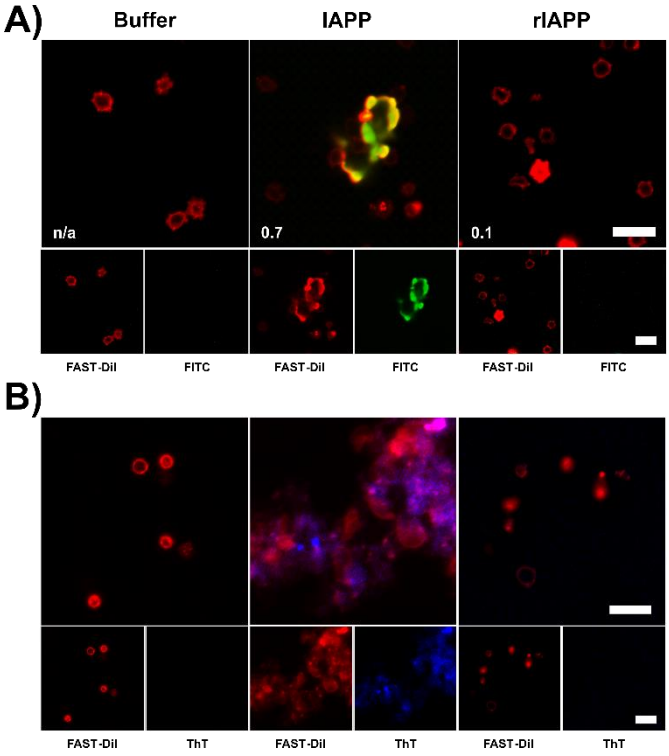

Figure 3.4 Clusters of RBC-derived lipid vesicles colocolize with IAPP and are ThT-positive. A) RBC ghosts labelled with FAST-DiI were incubated with FITC-labelled peptides for 24 h at room temperature at 1:1 molar ratio of P/L. Numbers in lower left corners indicate PCC values B) Labelled RBC ghosts were incubated with unlabelled peptides for 24 h at room temperature, at 1:1 molar ratio of P/L and subsequentially stained with 40 μM of ThT. A,B) Scale bars = 5 μm.

3.5.5 SS-NMR reveals the perturbation of the ghost lipid vesicles induced by IAPP

^{31}P SS-NMR was used to investigate the lipid bilayer organization of erythrocyte ghosts in the presence of IAPP and rIAPP. Phospholipids contain a ^{31}P nucleus that has a high gyromagnetic ratio, a 100% natural abundance, and is an excellent reporter of

both phospholipid headgroup dynamics and lipid phases by SS-NMR (Seelig, 1978). Due to the lower sensitivity of NMR compared to fluorescence microscopy, ghosts were incubated at higher phospholipid concentrations (125 μM) with equimolar peptides (125 μM) for 24 h. The spectra were then recorded under either static or magic angle spinning (MAS) conditions. As shown in figure 5A, the ghost membranes in buffer displayed a characteristic powder spectrum for phospholipids in the lamellar fluid phase under static conditions (Traïkia *et al.*, 2000). Spectral simulation allowed determining the chemical shift anisotropy (CSA) values, corresponding to the spectrum width. There was an inverse relationship between lipid dynamics and CSA, such that smaller CSA measurements are indicative of higher lipid dynamics. The CSA values of ghosts in the presence of buffer or rIAPP were identical (26 ppm); however, a decrease was observed when the ghosts were treated with IAPP (24 ppm), suggesting a slight increase in the dynamics of the phospholipid headgroup. This central peak, which corresponds to approximately 12% of the lipids, could possibly be an indication of high-curvature regions of the membrane, bound to IAPP. Moreover, the spectrum showed the appearance of a small peak at approximately 3 ppm. Typically, a central isotropic peak indicates the presence of small, highly mobile lipid species (*e.g.*, micelles). However, this is unlikely to be the case since phospholipids were not detectable in the supernatant after centrifugation of the ghost-peptide suspensions (data not shown), moreover, the observed chemical shift (3 ppm) differs from the isotropic value measured under MAS conditions (figure 5B). This narrow peak could possibly be an indication of high-curvature regions of the membrane, bound to IAPP (Yang *et al.*, 2015). A more detailed analysis of this effect is however outside the scope of this study.

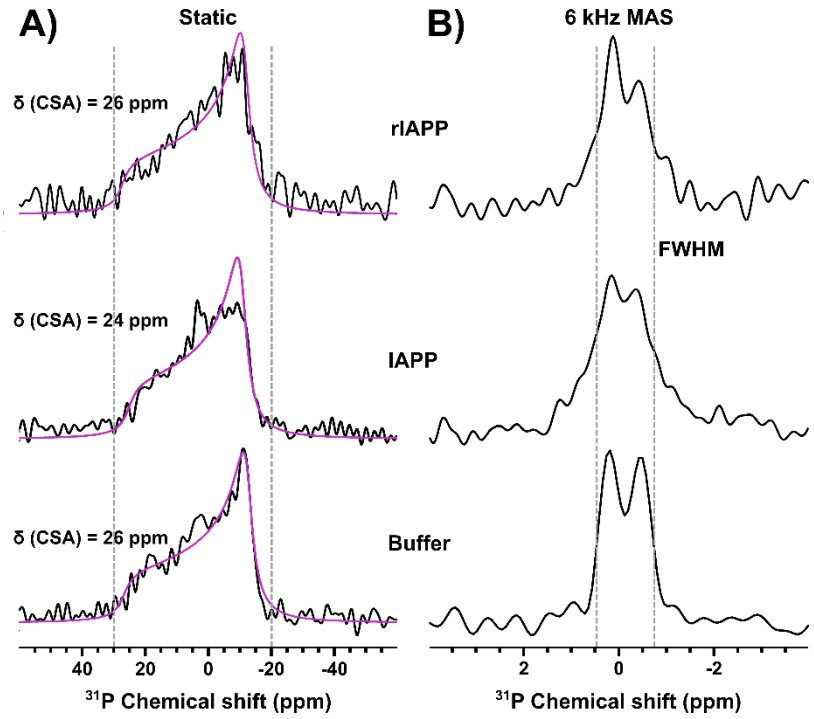

Figure 3.5 Effect of IAPP on RBC ghost membranes studied by solid-state NMR. A) Static spectra of ghosts treated with buffer, IAPP, or rIAPP, for 24 h. Line fitting was performed using the Bruker Topspin software in SOLA to measure the CSA. Vertical dashed lines indicate full width of spectra. B) 6 kHz MAS spectra of the same samples. Dotted lines represent the full width at half max (FWHM) of the control sample to facilitate comparison. All spectra were recorded at 25 °C.

MAS of the samples allowed for the resolution of two peaks at 0.20 ppm and -0.46 ppm, respectively ascribed to sphingomyelin and phosphatidylcholine head groups (Kumar *et al.*, 2022). The addition of both peptides broadened the linewidths, with a more pronounced effect observed for IAPP (figure 5B). Taken with the results from the static spectra, this suggests that despite being largely intact, there is a noticeable change in the membrane phospholipids local environment. This could be attributed to a reduced axial motion of the phospholipids interacting with IAPP aggregates. Similarly, non-amyloidogenic rIAPP bound to the membrane may slightly interfere with the axial motion, albeit to a lesser degree than large IAPP aggregates. This agrees with previous studies reporting the interactions of rIAPP with lipid micelles and

synthetic liposomes (Nanga *et al.*, 2011; Nanga *et al.*, 2008). According to the literature using synthetic vesicles at a 1:1 P/L molar ratio (Delgado *et al.*, 2016; Haya *et al.*, 2020; Korshavn *et al.*, 2017; Lu *et al.*, 2018; Walsh *et al.*, 2014), a more pronounced effect of IAPP on the bilayer was expected in the SS-NMR experiments. This discrepancy could be explained by the known resilience of erythrocyte membranes and their self-healing ability (McNeil and Steinhardt, 2003), reinforcing the importance of studying lipid membrane perturbation using biologically relevant systems.

3.5.6 The kinetics of ghost lipid membrane perturbation can be measured by Förster resonance energy transfer

The fluorescence microscopy experiments shown in figure 3 revealed that the colocalization observed within the lipid membrane clusters increased over incubation time with the amyloidogenic peptide. Accordingly, we hypothesized that the membrane clustering, which correlates with the perturbation of lipid bilayer, induced by IAPP would translate to a Förster resonance energy transfer (FRET) between FAST-DiO and FAST-Dil dyes that could be easily measured over time, and adaptable to a microplate-based kinetics assay. Preparations of ghosts respectively labelled with FAST-DiO (green) and FAST-DiI (red) were mixed, and the FRET signal was measured after incubation in the presence, or absence, of IAPP. Samples were excited at 460 nm and the resulting emission spectra, from 490 nm to 660 nm, were collected immediately after peptide addition (0 h) and after 24 h incubation at room temperature (figure 6A). The emission signal at 570 nm corresponds to the emission maximum of FAST-DiI, which remained low in all cases except for the ghosts treated with IAPP. The emission spectra were normalized relative to the corresponding buffer-treated sample, and the relative FRET emission spectra are displayed in figure 6B. These results showed that the fluorescence intensity increases throughout the entire spectrum after 24 h of incubation, relative to the control. The largest increase, however, is observed at the FAST-DiI emission maximum of 570 nm, suggesting that the signal does arise from a

fluorescence energy transfer. The stability of the FRET signal was verified by adding the detergent triton-X100 to solubilize lipid membranes. Each sample containing triton-X100 was normalized against the corresponding sample without triton-X100. Ghosts treated with IAPP for 24 h display relatively similar FRET intensity at 570 nm (0.8-fold) compared to sample without detergent, while the change in the buffer-treated sample (1.9-fold) was significantly larger (figure 6C). This suggests that the presence of IAPP largely prevents the solubilization of the ghost membranes. The emission peak at ~ 508 nm, which corresponds to the signal from FAST-DiO, increased slightly in the presence of IAPP. Control experiments showing that ghost suspensions labelled with only one of the two fluorophores did not lead to an equivalent fluorescence response are included in the supporting information (figure S3). Altogether, these results indicate that the mixture of FAST-DiO- and FAST-Dil-labelled ghosts was stable over 24 h and suitable for FRET experiments.

Kinetics of the FRET signal were obtained by incubating the mixture of FAST-DiO- and FAST-DiI-labelled ghosts with 12.5 μM IAPP at three different P/L molar ratios (4:1, 1:1, and 1:4), keeping the peptide concentration constant. These same conditions were maintained when measuring the ThT response using unlabelled ghosts (figure 6A). Regardless of the P/L molar ratio used, there was a clear FRET signal at 570 nm, which followed a sigmoidal growth for IAPP, similar to ThT-fluorescence curves. The maximum fluorescence intensity obtained from the blank-corrected, non-normalized data showed a decrease in ThT and FRET intensity with increasing phospholipid concentration (figure 6B), suggesting that peptide aggregation and membrane disruption processes are less pronounced. The slopes (k) and half-times (t_{50}) were extracted using the Boltzman sigmoidal equation obtained by fitting the normalized data, though only differed substantially at the 1:4 ratio where there was a molar excess of phospholipid relative to the peptide (figure 6C-D). The corresponding experiments were also carried out using rIAPP as a negative control, and no appreciable response to ThT and no FRET response were observed (figure S4A). Additionally, control

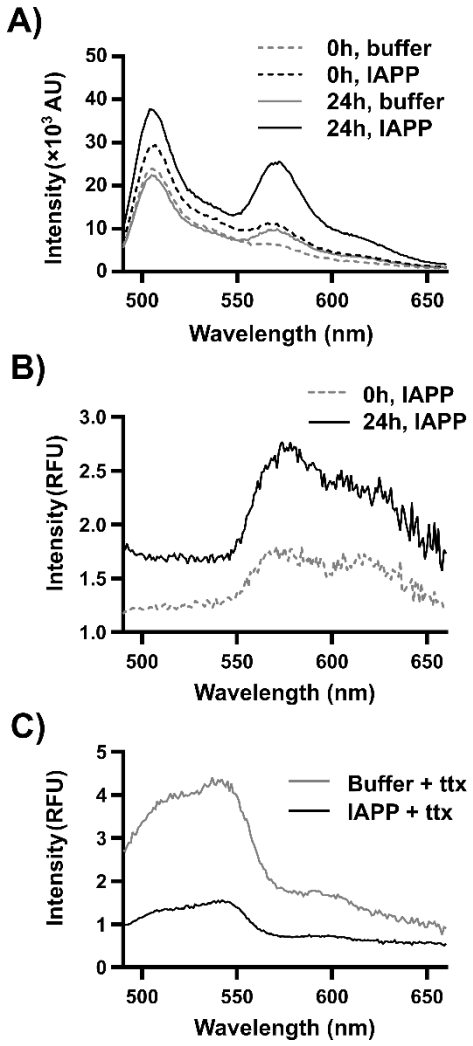

Figure 3.6 FRET response induced by IAPP upon co-incubation of green- and red-labelled erythrocyte ghosts. A) Fluorescence emission spectra of mixed FAST-DiO and FAST-DiI labelled ghosts incubated at room temperature with buffer or IAPP, excited at 460 nm for FAST-DiO. B) Normalized fluorescence spectra of ghosts treated with IAPP relative to buffer-treated ghosts in (A). C) Fluorescence spectra of both buffer and IAPP-treated ghosts after 24 h incubation, excited at 460 nm for FAST-DiO. The addition of 0.5%v/v triton-X100 was done after incubation and prior to recording the spectra, then normalized against the corresponding spectra in the absence of triton-X100.

experiments were carried out to address any potential confounding FRET or ThT signals. Samples of ghosts were freshly prepared and labelled, and the detergent triton X-100 (1% v/v) was added to the microplate assay in the absence of any peptide (figure

S4B). No noticeable changes to the ThT fluorescence or the FRET response were observed when the membranes were solubilized by the detergent, confirming that the positive responses observed for the IAPP treated sample are associated with the process of amyloid formation. Unlike usual leakage assays based on dye-encapsulated synthetic liposomes, this microplate-based kinetics assay uses cell-derived plasma membrane that perfectly mimics biological environments.

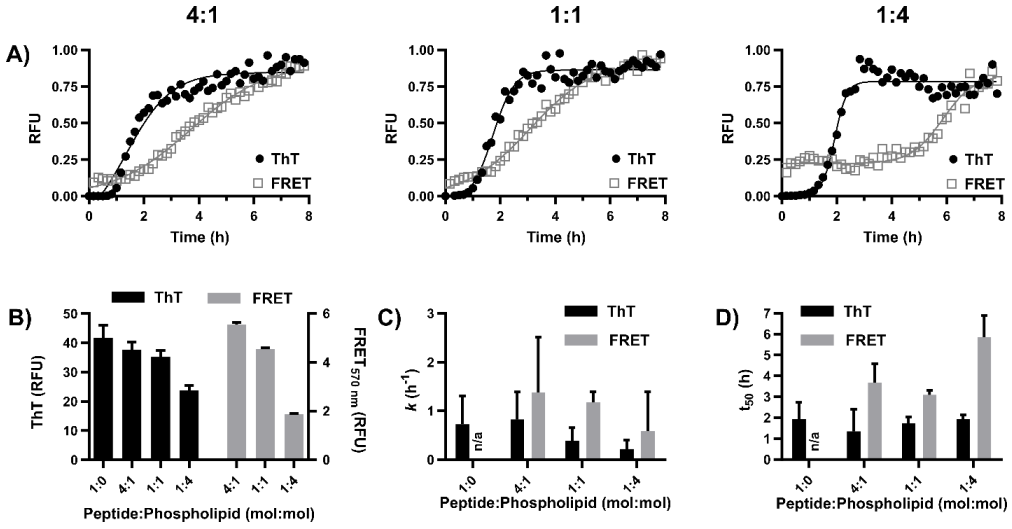

Figure 3.7 Monitoring the kinetics of lipid bilayer disruption of erythrocyte ghosts by FRET. A) ThT and FRET responses of mixtures of labelled RBC ghosts incubated in the presence of 12.5 μM IAPP and at different P/L molar ratios measured over time. B) Values for the final fluorescence of each condition relative to the corresponding blank obtained from the fitting of a sigmoidal curve. C) Values corresponding to the slope (*k*) of the normalized data fitted with sigmoidal curves. D) Half-times (t_{50}) obtained from the normalized data fitted with sigmoidal curves. (B-D) Error bars shown represent the 95% confidence interval. The ratio of 1:0 indicates IAPP incubated in absence of lipid membranes.

3.5.7 Perturbation and clustering of GPMVs derived from pancreatic cells can be observed by fluorescent microscopy

The use of erythrocyte ghosts as a model to study plasma membrane perturbation appears very promising owing to key advantages that include close mimicking of

mammalian cells, relative low cost, convenience, homogeneous size and morphology, long shelf life, and potential high throughput. Despite these advantages and owing to recent studies using GPMVs (Birol *et al.*, 2018; Birol *et al.*, 2019; Quittot *et al.*, 2021), there was a definitive interest in evaluating whether this FRET-based kinetic assay can be transposed to the GPMV model. In this context, we evaluated the use of GPMVs generated from pancreatic β-cells to assess the plasma membrane perturbation induced by IAPP. INS-1E cells were used to prepare GPMVs, as IAPP amyloid deposits are found in the islets of Langerhans and correlate closely with the loss of pancreatic β-cells (Milardi *et al.*, 2021). GPMVs were prepared using our recently reported protocol (Quittot *et al.*, 2021), and were labelled with either FAST-DiO or FAST-DiI. As described above with ghosts, green and red labelled GPMVs were mixed and incubated in the presence, or absence, of peptides. After different times of incubation at room temperature, images were acquired by confocal microscopy. The size distributions of the GPMVs were noticeably more heterogeneous than what was observed with erythrocyte ghosts (figure 8 *vs* figure 3). After 1 h incubation in presence of IAPP, no appreciable clusters of INS-1E GPMVs were observed (figure 8A). After 3 h of incubation with IAPP, a clustering of the GPMVs was observed. After 6 and 24 h, the lipid membrane aggregates were reminiscent of those observed with IAPP-treated RBC ghosts. There was a noticeable colocalization of the fluorophores in these preparations, which was quantified using the PCC. In contrast, no clustering, or colocalization, was detected for GPMVs treated with rIAPP throughout the entire incubation time (figure 8B). There was a rapid increase in the colocalization score for IAPP-treated GPMVs, which reached a plateau after 6 h incubation. In contrast to erythrocyte ghosts, the perturbations of GPMVs as a function of P/L molar ratio did not change significantly (figure 8C). Between 3.125 and 50 μM of IAPP, comparable extents of membrane perturbations were detected (figure S5). Overall, these data demonstrate that the labelling and analyses established with ghosts are transferrable to GPMVs assembled from pancreatic cells.

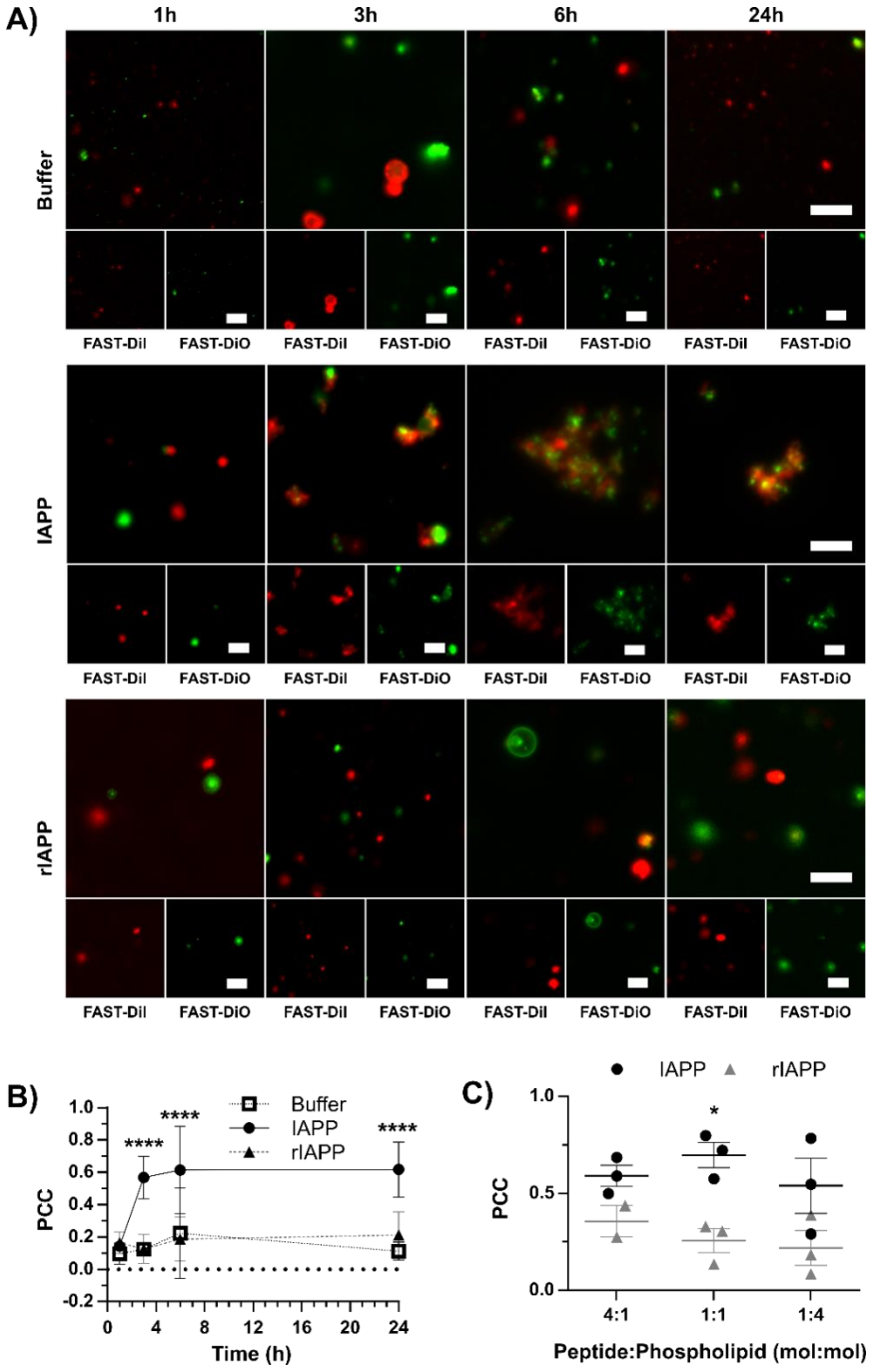

Figure 3.8 IAPP induces the clustering of GPMVs derived from pancreatic cells and the perturbation of their lipid bilayer. A) Confocal microscopy images of mixtures of INS-1E-derived GPMVs respectively labelled with FAST-DiO and FAST-DiI incubated in the presence or absence of 12.5 μM peptide. B) Colocalization values for GPMV

mixtures obtained from the Pearson's correlation test throughout the incubation time. C) Final colocalization values for the GPMV mixtures incubated with various ratios of P/L (1:4, 1:1, 4:1).

Next, GPMVs labelled with FAST-DiI were incubated with FITC-labelled peptides at a 1:1 molar ratio to locate IAPP and rIAPP relative to the lipid membranes. Confocal images of the different preparations showed that there was a significant positive correlation between the labelled GPMVs and FITC-IAPP, with a PCC of 0.52 (figure 9A). In sharp contrast, no significant colocalization could be observed for the non-amyloidogenic rIAPP. This is likely explained by the fact that rIAPP forms primarily small oligomers, not large fibrils (Lu *et al.*, 2018), which did not lead to the formation of large detectable bright spots around the GPMV surface. Subsequently, FAST-DiI labelled GPMVs were incubated in the presence of unlabelled peptides (1:1 P/L molar ratio), to determine if these clusters were enriched in aggregates with a cross-β-sheet quaternary structure, as observed for RBC ghosts. For IAPP, large ThT-positive areas were observed around the membrane clusters, whereas no ThT-positive response was detected for rIAPP (figure 9B), in agreement with the data obtained using erythrocyte ghosts. Additionally, both FITC-IAPP and ThT signals were virtually undetectable outside of the lipid membrane clusters. These data indicate that IAPP is interacting with the β-cell-derived plasma membrane and likely folds into an amyloid quaternary organization, as observed for erythrocyte ghosts.

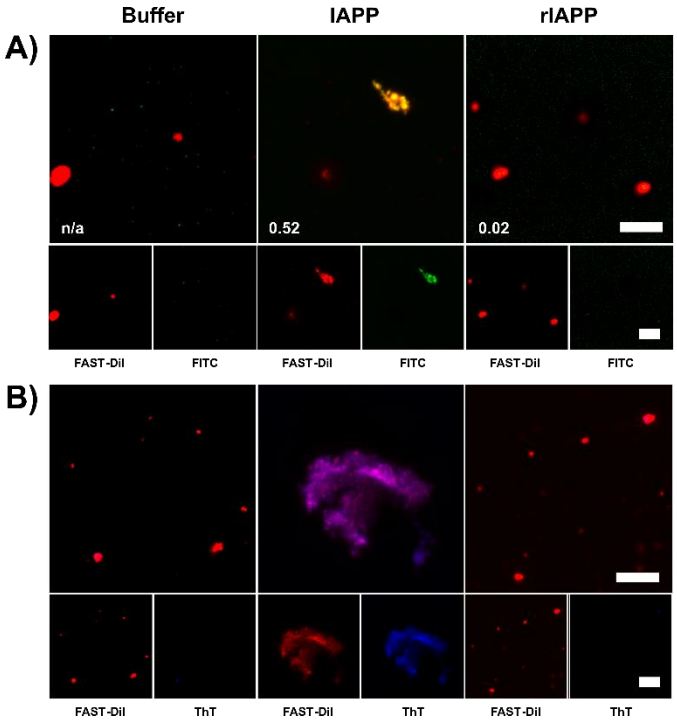

Figure 3.9 IAPP deposits within lipid GPMV clusters. A) GPMVs labelled with FAST-DiI (red) were incubated at 12.5 μM phospholipid concentration with 12.5 μM FITC-labelled peptides, or buffer, for 24 h at room temperature. Numbers in the lower left corner indicate PCC values between FAST-DiI and FITC. B) GPMVs at 12.5 μM phospholipid concentration, labelled with FAST-DiI were incubated in the presence or absence of 12.5 μM unlabelled peptides at room temperature for 24 h before being stained with 40 μM ThT. A,B) Scale bars = 5 μm.

3.5.8 Kinetics of lipid membrane perturbation of GPMVs derived from pancreatic β-cells

Considering that the labelling of GPMVs allowed the observation of the formation of lipid clusters induced by IAPP (figure 8), FRET-based kinetic assays were performed. Mixtures of FAST-DiO and FAST-DiI fluorescently labelled GPMVs were treated with 12.5 μM IAPP under different P/L molar ratios and the FRET kinetics were compared with the kinetics obtained from a ThT assay using unlabelled GPMVs. The kinetics of the FRET response correlated closely with the ThT signal (figure 9), indicative of an aggregation-associated disruption of the plasma membrane by IAPP.

In contrast to RBC ghosts, a significant FRET response was observed at lower P/L molar ratio (1:4), and the overlap of the ThT and FRET curves was particularly noticeable. The extracted kinetic parameters show that despite some minor changes in the ThT curves, the FRET curves remained relatively stable with slight, yet statistically non-significant, changes in k or t_{50}, indicating that the elongation rate and nucleation of the aggregation process remained the same. No positive ThT or FRET response was detected for GPMVs treated with the non-amyloidogenic rIAPP (figure S6). The FRET kinetics of lipid membrane clustering induced by IAPP were closely similar in RBC

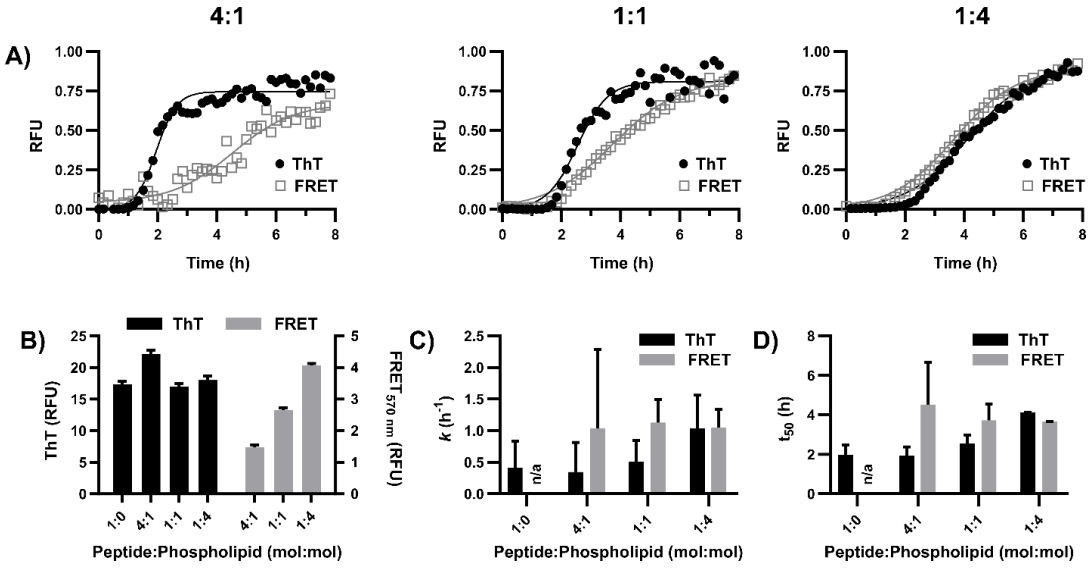

Figure 3.10 FRET signal can be followed in a microplate assay to correlate loss of GPMV membrane integrity with amyloid formation. A) Kinetics by FRET and ThT using 12.5 μM IAPP with GPMVs at 3.125, 12.5, and 50 μM phospholipid concentrations (P/L ratios of 4:1, 1:1, and 1:4). B) Maximum fluorescence values obtained from the fitting of a sigmoidal curve to kinetic data, relative to the blank. Normalized data were used to fit sigmoidal curves and to obtain C) the slopes (k) and D) the half times (t_{50}). The ratio of 1:0 represents IAPP incubated in absence of GPMVs. B-D) Error bars represent the 95% confidence interval.

ghosts and GPMVs, with the only difference observed in the half-times (t_{50}), with statistically significant differences at 1:4 P/L molar ratio ($p < 0.05$). Particularly, for both GPMVs and ghosts, the absence of any positive FRET response in presence of

rIAPP indicates that the FRET signal is due to the membrane-perturbating activity of IAPP.

3.6 Discussion

In this study, we harnessed physiologically relevant model systems to study plasma membrane perturbations induced by IAPP: erythrocytes, RBC ghosts, and GPMVs derived from β-pancreatic cells. Whereas these systems have been employed in recent studies to describe some aspects of amyloid-associated cytotoxicity (Birol *et al.*, 2018; Birol *et al.*, 2019; Huang *et al.*, 2009; Quittot *et al.*, 2021; Schlamadinger and Miranker, 2014; Singer and Dewji, 2006), their usage has been somewhat limited and most research regarding membrane perturbation induced by amyloidogenic polypeptides is still conducted with synthetic lipid vesicles, which lack the complexity of cellular membranes. Consequently, the development of bioanalytical tools and assays remains vital to bridge the gap between entirely synthetic model systems and living organisms. Herein, the combination of two independently labelled preparations of RBC ghosts, or GPMVs, led to the development of a simple microplate-based assay to probe the kinetics of lipid bilayer perturbations induced by membrane-active compounds under biologically relevant conditions.

While RBC ghosts and INS-1E GPMVs constitute advanced lipid bilayer models to study perturbations of the cell plasma membrane, each model presents distinct advantages and limitations. Whereas RBCs are amenable to study membrane disruption using the hemolysis assay, this assay is experimentally demanding and poorly adaptable to high throughput. Moreover, the pores and/or perturbations must be sufficient large to allow the release of Hb, and it is possible that less important perturbations, such as the formation of small-diameter transmembrane pores, remain undetected. To address this potential limitation, smaller fluorophores could be encapsulated into RBC ghosts, as the calcein-based release assay for synthetic vesicles.

Since RBCs can be easily obtained in large quantities, membrane interactions can be investigated at a molecular level by SS-NMR – a powerful approach that is generally limited to model membranes (Warnet *et al.*, 2015). Interestingly, RBC ghosts have been recently labelled with deuterated fatty acids to study changes in membrane dynamics in the presence of antimicrobial peptides (Kumar *et al.*, 2022). This approach could be applied to study the interaction with amyloidogenic peptides, including IAPP. RBC ghosts are representative of the cell plasma membranes found in mammalian organisms and the presence of a glycocalyx is an important aspect to evaluate the impact of the extracellular matrix in peptide-membrane interactions. There was an obvious interest to evaluate if the FRET-based assay implemented with erythrocytes could be transposed to GPMVs derived from cells originating from the tissues where the amyloid deposits are normally found. While the preparation of GPMVs from cultured cells is relatively straightforward, the vesicle populations are less homogeneous, and the final yield of vesicles obtained was substantially lower compared to ghosts. Nonetheless, GPMVs have the advantage of retaining the components of cell plasma membrane, and consequently the surfaces encountered by extracellular amyloid-related proteospecies.

Considering the overall results, two main parameters considerably differed from those previously reported with prototypical synthetic model membrane systems. First, the P/L molar ratios required to observe membrane perturbations, ranging from 4:1 to 1:4 (P/L), were markedly lower than those typically used with model vesicles composed of synthetic lipids, which range from 1:10 to 1:100 (Bera *et al.*, 2020; Divakara *et al.*, 2019; Sciacca *et al.*, 2020). In fact, the P/L molar ratios required to observe a FRET response in the kinetic assays corresponded better with those used in recent works employing vesicles derived from plasma membrane (Birol *et al.*, 2018; Quittot *et al.*, 2021). Secondly, in the microplate-based experiments, the membrane perturbations of RBC ghosts and GPMVs detected by FRET were noticeably delayed compared to most previous works based on dye leakage from synthetic anionic LUVs (De Carufel *et al.*,

2015; Godin *et al.*, 2019; Nguyen *et al.*, 2021). Moreover, the leakage kinetics of synthetic LUVs with encapsulated fluorophores are often lacking a defined lag phase, although the corresponding kinetics of self-assembly measured by ThT display a definite lag phase (Sciacca *et al.*, 2016; Zhang *et al.*, 2018). These differences in the kinetics of perturbation between synthetic LUVs and cell-derived plasma membrane vesicles could be related to the nature of the FRET-based approach being less sensitive to small-scale perturbations compared to dye leakage, including the formation of transmembrane pores by oligomers.

The discrepancies in term of P/L molar ratios and kinetics of perturbation between synthetic LUVs and vesicles from cell plasma membrane are likely associated with differences in lipid composition, in size and curvature of the vesicles, and/or with the presence of non-lipidic components. For instance, it is known that the composition of synthetic liposomes dramatically modulates the effects of membrane-active polypeptides (Sciacca *et al.*, 2018; Scollo *et al.*, 2018; Terakawa *et al.*, 2018). Particularly, it has been shown that liposomes rich in phospholipids with anionic head groups are more prone to IAPP and Aβ-peptide mediated membrane damage than liposomes composed of zwitterionic phospholipids (Sciacca *et al.*, 2018). Plasma membrane of erythrocytes and of rat INS-1 pancreatic cells are mostly composed of zwitterionic phosphatidylcholine (between 45 to 55% of total lipids) and phosphatidylethanolamine (22%), whereas lipids with an anionic head are less abundant, such as 4% for phosphatidylserine (Kumar *et al.*, 2022; MacDonald *et al.*, 2008). In addition, the distribution of charged lipid headgroups in mammalian cells is asymmetrical, with the majority of anionic phospholipid headgroups located in the membrane inner leaflet. It is also important to consider that the presence of sulfated proteoglycans on the cell surface ensures that the outer leaflet of the mammalian plasma membrane is negatively charged. In this view, numerous studies have shown that sulfated glycosaminoglycans promote amyloid formation and are implicated in the tissue deposition of insoluble protein aggregates (Bourgault *et al.*, 2011c; Christensen

et al., 2016; De Carufel *et al.*, 2013; Iannuzzi *et al.*, 2015; Mehra *et al.*, 2018; Quittot *et al.*, 2017b; Sebastiao *et al.*, 2019), further emphasizing the importance of conducting such studies with lipid vesicles derived from living cells. Likewise, phospholipid acyl chain length also plays an important role in determining membrane permeability and leakage, as observed with liposomes composed of longer acyl chain phospholipids being more resistant to leakage than their counterparts composed of shorter chains (Cao *et al.*, 2013a; Sciacca *et al.*, 2020; Scollo *et al.*, 2018).

Although the scope of the present work was principally focused on the development of a novel membrane perturbation assay using biologically relevant lipid vesicles, some mechanistic observations could be inferred. First, IAPP induced the clustering of cell plasma membrane vesicles into large and dense lipidic aggregates, a phenomenon closely related with amyloid formation. Second, lipids originating from different vesicles within these clusters are in proximity, leading to the observed FRET signal. Third, this FRET response induced by IAPP amyloid formation is not entirely lost when a detergent is added into the peptide-membrane mixtures, suggesting that some of the lipids remain tightly bound within, or around, the assembled amyloid fibrils. Fourth, a close correlation was observed between the kinetics of membrane perturbation (FRET signal) and IAPP amyloid formation (ThT signal). Overall, while these observations do not exclude the formation of transmembrane pore by oligomeric intermediates, they suggest that IAPP fibril growth constitutes a major contribution to lipid vesicle perturbation, likely through a carpet-like mechanism.

3.7 Conclusion

Owing to their ease of use, synthetic phospholipid bilayers have been the workhorse to study amyloid-associated membrane perturbations over the last decades, although they do not accurately depict the complexity of the cell plasma membrane. Here, model membrane systems were generated from mammalian cells to obtain lipid bilayer

vesicles, which retain the heterogeneous compositions and properties of living cells. Particularly, a novel binary labelling protocol supported the use of these biologically derived lipid vesicles to study the kinetics of membrane perturbation through fluorophore colocalization and FRET-based assays. In conjunction with ThT-binding assays to monitor peptide self-assembly, this approach has the potential to be applied to mechanistic studies of membrane damage, allowing for the rapid investigation of multiple conditions. Especially, this approach constitutes a novel tool that will support the mechanistic studies of plasma membrane perturbations, not only limited to amyloid disorders, but also regarding antimicrobial and lytic peptides, and membrane-active pharmacological drugs.

Acknowledgements

This work was supported by the Natural Sciences and Engineering Research Council (NSERC) of Canada (RGPIN-2018-06209 to S.B. and RGPIN-2018–06200 to I.M.). M.S. is grateful to the NSERC for the award of a scholarship. We would like to thank Dr. Dror Warschawski (Sorbonne Université, Paris, France) for his expertise and invaluable contributions to the initial stages of the project and to Dr. Phuong Trang Nguyen (Université du Québec à Montréal, Canada) for her time and efforts synthesizing the necessary peptides.

3.8 Supporting information

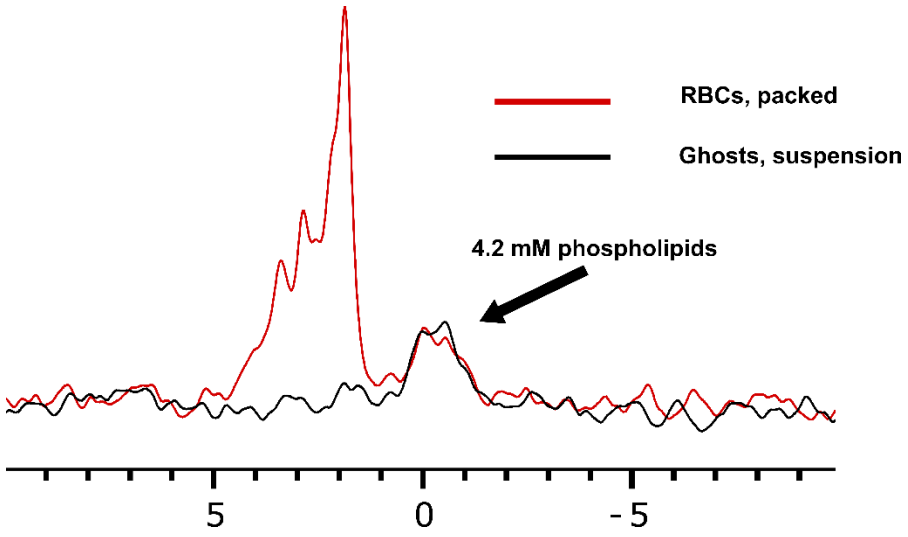

Figure S3.1 ^{31}P MAS NMR to correlate RBC phospholipid concentration with that of ghosts. Samples were acquired under quantitative conditions with sufficient time between acquisitions to allow for complete signal relaxation (10 s), for 512 scans at 298 K with a spinning speed of 6 kHz.

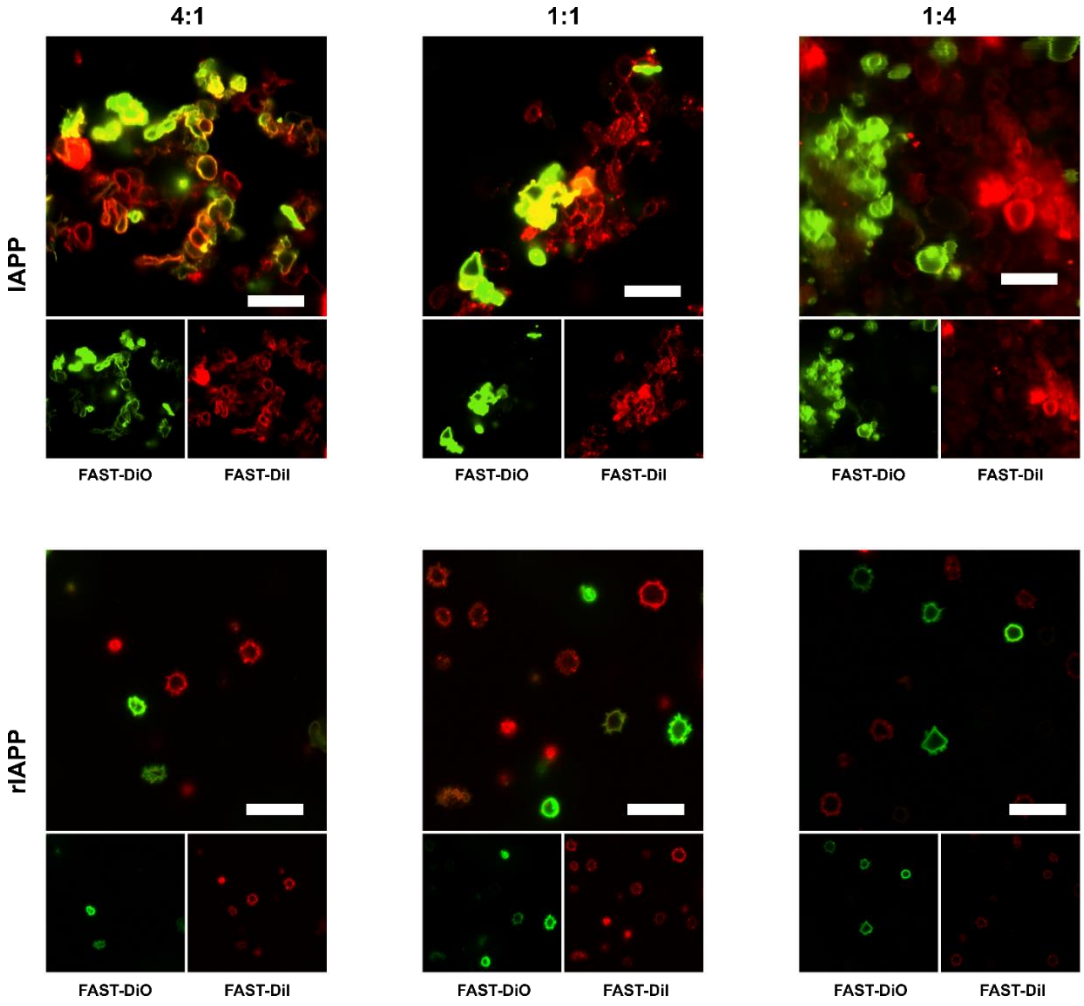

Figure S3.2 Representative images from confocal microscopy of ghost mixtures treated with IAPP or rIAPP at different ratios of peptide:phospholipid. Ghosts were labelled with either FAST-DiO or FAST-DiI and combined to obtain a final phospholipid concentration of 12.5 μM. Samples were incubated at room temperature for 24 h with IAPP or rIAPP at 50, 12.5, or 3.125 μM to obtain the desired molar ratios (4:1, 1:1, and 1:4, respectively). Scale bars = 5 μm.

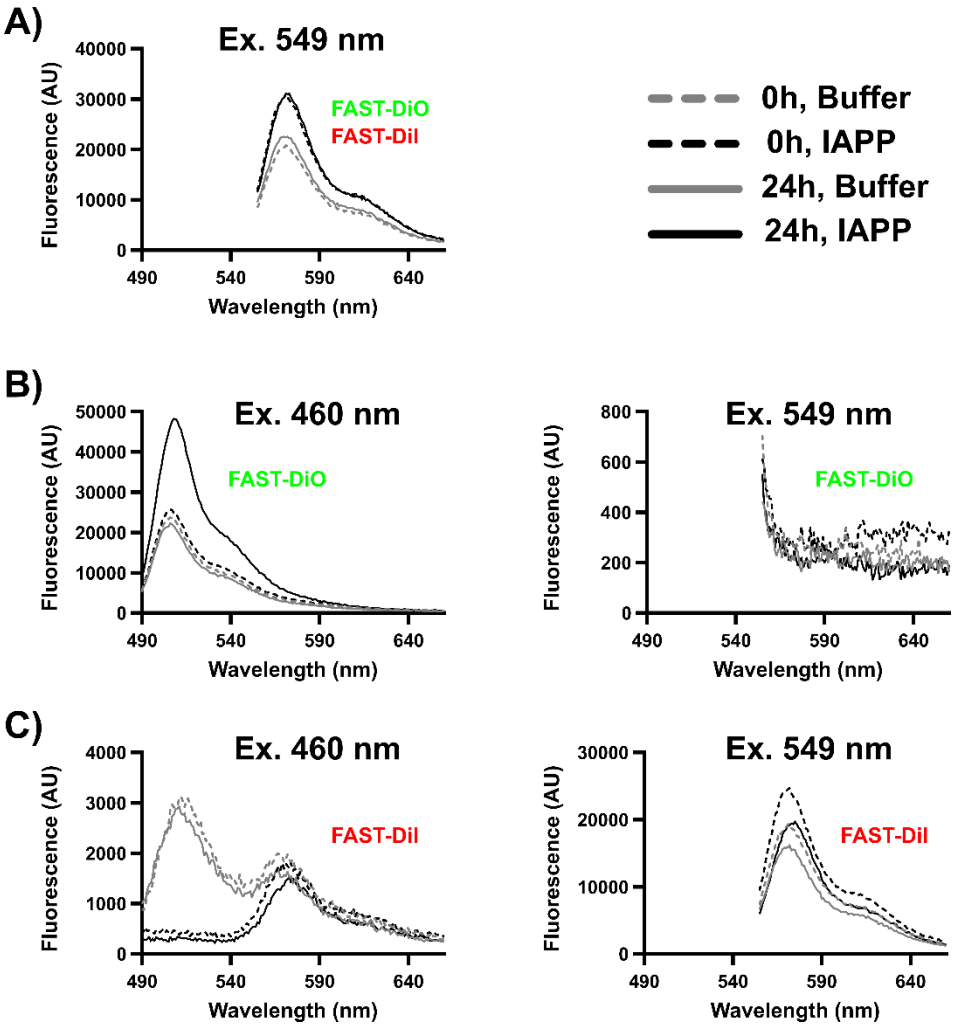

Figure S3.3 Fluorescence spectra of ghosts in control conditions for FRET experiments. Ghosts were prepared and labelled with either FAST-DiO or FAST-DiI. Suspensions of labelled ghosts were incubated with buffer or IAPP for 0 and 24 h, then loaded into a 1 cm quartz cuvette and excited at either the FAST-DiO or the FAST-DiI wavelength (460 and 549 nm, respectively). A) Mixture of FAST-DiO and FAST-DiI labelled ghosts excited at 549 nm. B) FAST-DiO labelled ghosts excited at 460 and 549 nm. C) FAST-DiI labelled ghosts excited at 460 and 549 nm. Note different scales in axes.

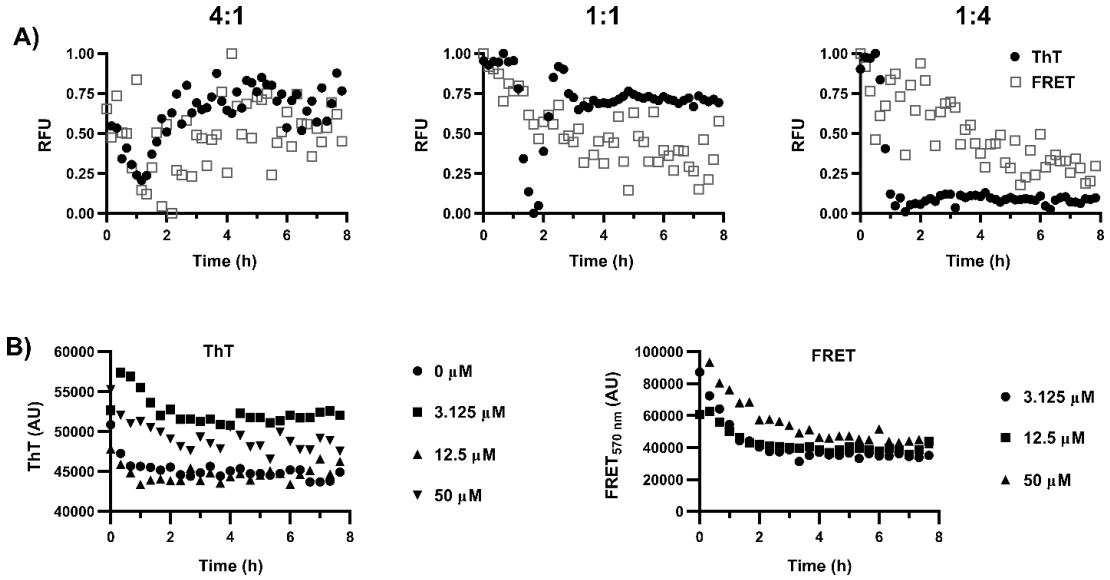

Figure S3.4 Thioflavin-T and FRET kinetics of rIAPP and ghosts. A) Ghosts were prepared and labelled with FAST-DiO or FAST-DiI for FRET measurements. Equal parts FAST-DiO and FAST-DiI labelled ghosts were used, and phospholipid concentrations were adjusted to obtain the desired peptide:lipid ratios while the concentration of rIAPP was held constant at 12.5 μM. For ThT measurements, unlabelled ghost suspensions were used at the same ratios with 12.5 μM rIAPP and 20 μM ThT. B) Baseline measurements for ghosts solubilized with triton-X100 (1% w/v) under the same conditions as A).

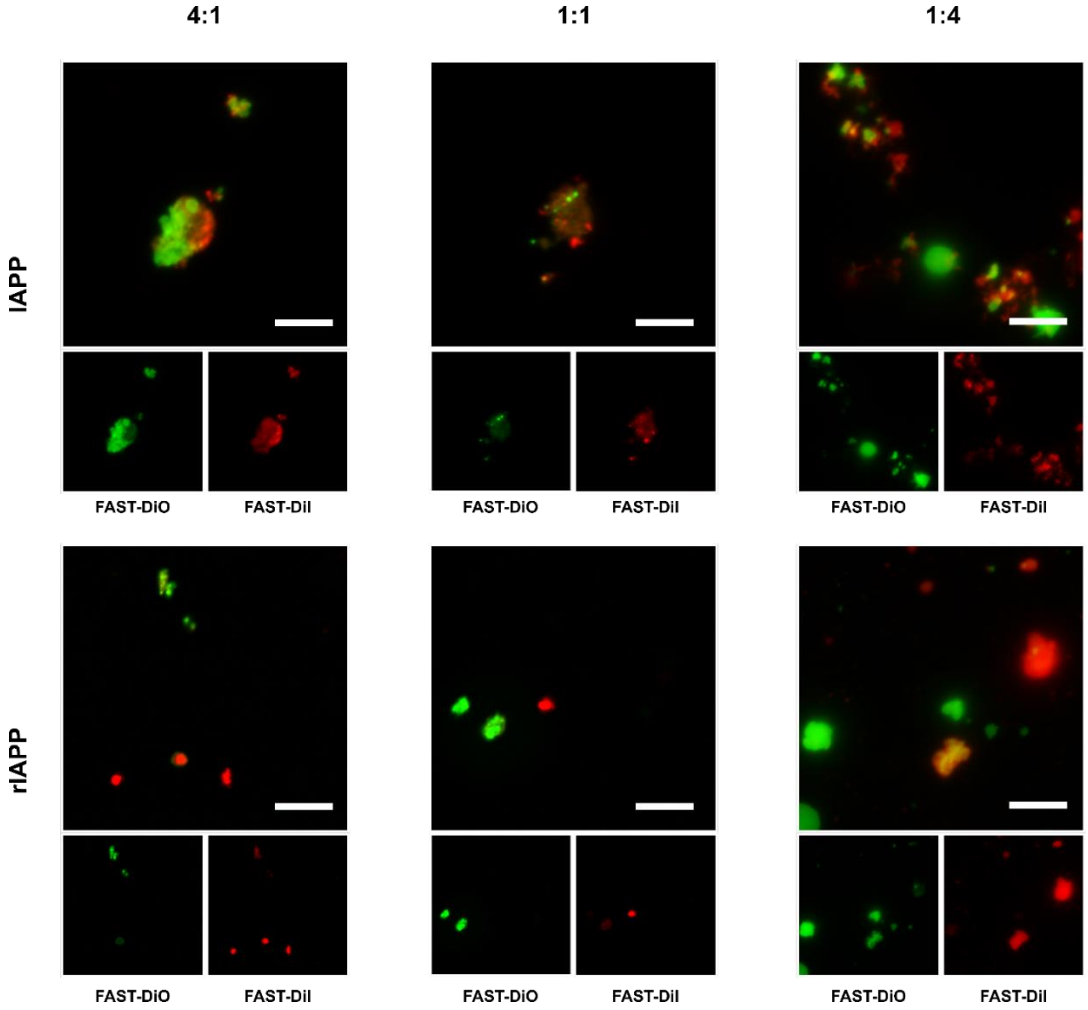

Figure S3.5 Representative confocal images of GPMVs treated with varying concentrations of IAPP or rIAPP. GPMVs were labelled with either FAST-DiO or FAST-DiI and combined to obtain a final phospholipid concentration of 12.5 μM. Samples were incubated at room temperature for 24 h with IAPP or rIAPP at 50, 12.5, or 3.125 μM to obtain the desired molar ratios (4:1, 1:1, and 1:4, respectively). Scale bars = 5 μm.

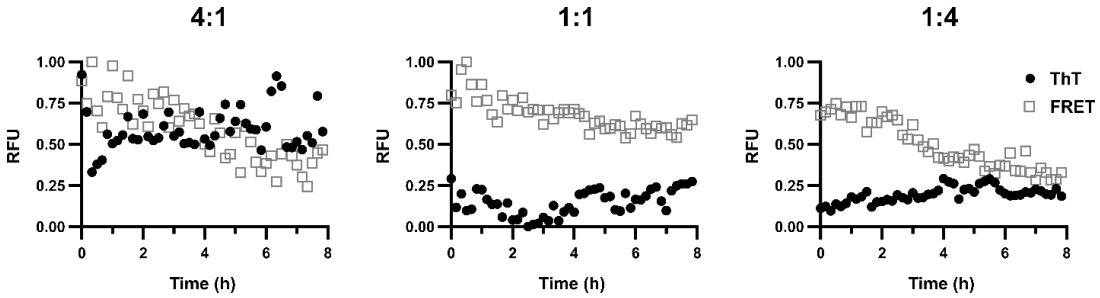

Figure S3.6 Thioflavin-T and FRET kinetics of rIAPP and GPMVs. GPMVs were prepared and labelled with FAST-DiO or FAST-DiI for FRET measurements. Equal parts FAST-DiO and FAST-DiI labelled GPMVs were used, and phospholipid concentrations were adjusted to obtain the desired peptide:lipid ratios while the concentration of rIAPP was held constant at 12.5 μM. For ThT measurements, unlabelled GPMVs were used at the same ratios with 12.5μM rIAPP and 20 μM ThT.

CHAPTER IV:

ARTICLE 3

THIOFLAVIN T FLUORESCENCE TO ANALYSE AMYLOID FORMATION KINETICS: MEASUREMENT FREQUENCY AS A FACTOR EXPLAINING IRREPRODUCIBILITY

Mathew Sebastiao, Noe Quittot and Steve Bourgault

Manuscript published in the journal Analytical Biochemistry 532 (2017) 83 – 86

Mathew Sebastiao participated in the experimental design, performed experimental work and data collection (microscopy, circular dichroism, kinetics), data interpretation, wrote the manuscript, and revised the manuscript. Noé Quittot performed experimental work (kinetics), data interpretation, and revised the manuscript. Steve Bourgault provided the initial conceptualization of the project, experimental design, and revised the manuscript.

4.1 Abstract

The most frequent method to monitor amyloid formation relies on the fluorescence of thioflavin T (ThT). The present study reports a novel factor of irreproducibility in ThT kinetic assays performed in microplate. Discrepancies among kinetics of amyloid assembly, performed under quiescent conditions, were associated with the frequency of fluorescence measurement. Evaluating self-assembly of the islet amyloid polypeptide at short intervals hastened its fibrillization. This observation was confirmed by transmission electron microscopy, circular dichroism spectroscopy and 8-anilino-1-naphthalenesulfonic acid fluorescence. This effect, attributed to agitation during microplate displacements between fluorescence measurements, reinforces the importance of a better standardization in amyloid formation assays.

4.2 Introduction

Aggregation and tissue deposition of proteins into the form of amyloid fibrils are intrinsically associated with pathological states, including Alzheimer's disease, transthyretin amyloidosis and type II diabetes (Chiti and Dobson, 2006). The causative association between amyloid formation and the pathogenesis has been demonstrated by compelling genetic and pharmacological evidences (Chiti and Dobson, 2006). Nonetheless, therapeutic strategies to arrest protein aggregation and cell degeneration are still sparse. Thus, the identification of pharmaceutical inhibitors of amyloid formation is an active area of research. Moreover, understanding the molecular details of amyloid assembly is critical for the rational design of inhibitors. Therefore, evaluation of amyloid formation *in vitro* is important from both a mechanistic and a pharmaceutical perspective. The most commonly used approach to study kinetic of amyloid formation is the time-course measurement of thioflavin T (ThT) fluorescence (Biancalana and Koide, 2010). ThT is a benzothiazole dye that exhibits a strong increase of its fluorescence quantum yield and a shift of its excitation spectrum upon binding to cross-β-sheet quaternary structure of amyloids (LeVine, 1993; Naiki *et al.*, 1989; Wolfe *et al.*, 2010). Since the first study reporting over 50 years ago that ThT detects amyloids in *ex vivo* tissues (Vassar and Culling, 1959), the ThT kinetic assay has become widespread for the mechanistic study of fibrillization (Ban *et al.*, 2003; Naiki *et al.*, 1989). Particularly, this assay can be performed in a microplate, allowing for high-throughput screening of amyloid modulators (Hebda *et al.*, 2014; Nguyen *et al.*, 2016).

While fibrillization kinetic assays are important for the development of pharmaceuticals and mechanistic studies, polypeptide self-assembly is notoriously sensitive to numerous parameters, including concentration (Brender *et al.*, 2015), temperature (Brender *et al.*, 2015), buffer (De Carufel *et al.*, 2013), surfaces (Murray *et al.*, 2013), air-liquid interface (Jean *et al.*, 2012), exogenous compounds

(Alexandrescu, 2005; Hudson *et al.*, 2009; Quittot *et al.*, 2017b) and agitation (Batzli and Love, 2015). Accordingly, comparison of ThT kinetic assays between studies is particularly problematic owing to small differences in experimental conditions. We recently noticed that even when all these parameters are carefully maintained constant, discrepancies among kinetics of amyloid formation monitored by ThT fluorescence in microplates were still observed. These differences were associated with the frequency at which fluorescence is measured. Strikingly, intervals of ThT fluorescence measurement during amyloid assays performed under quiescent conditions vary significantly between studies (Benilova *et al.*, 2014; Bourgault *et al.*, 2011c; De Carufel *et al.*, 2013; Horvath and Wittung-Stafshede, 2016; Ryan *et al.*, 2012) and the effect of this unstandardized, most often unreported, parameter has not been addressed so far. In this study, by using the islet amyloid polypeptide (IAPP), we depicted how amyloid formation is modulated by the measurement frequency in microplate.

4.3 Results and discussion

IAPP is a 37-residue peptide hormone whose deposition into the pancreatic islets is associated with type-II diabetes (Nguyen *et al.*, 2015). Due to its high amyloidogenicity, amyloid assembly of IAPP under quiescent conditions occurs within a few hours, as observed by ThT fluorescence (De Carufel *et al.*, 2015). To specifically probe the effect of the frequency at which ThT fluorescence is measured on the fibrillization kinetic, the fluorescence of ThT was measured using intervals between 30 sec to 1 h (for detailed materials and methods, please consult the supporting information). As shown in figure 4.1A, decreasing the interval between each measurement hastened amyloid assembly; *i.e.* a shorter lag-phase is observed at 0.5-min and 1-min intervals compared to 60 min. The times to reach half the maximum ThT fluorescence (t_{50}) were obtained by fitting the data to a Boltzmann sigmoidal and were used to calculate the lag-time (t_{lag}). Both t_{50} and t_{lag} increased proportionally with the measurement interval (figure 4.1B) . In contrast, ThT fluorescence intensities at the

plateau were not considerably different, except for the 60-min interval (figure 4.1B). We also confirmed this effect with a different microplate spectrophotometer (figure s4.1). Moreover, this effect persisted throughout a wide range of peptide concentrations (figure s4.2).

We next verified whether the differences in the fibrillization kinetics under quiescent conditions as a function of measurement interval correspond to actual IAPP conformational transition. An amyloid assembly experiment in microplate and in presence of ThT was performed and at specific times, samples were analyzed by circular dichroism (CD) spectroscopy and transmission electron microscopy (TEM). When fluorescence was measured every 10 min, the random coil-to-β-sheet secondary conformational conversion associated with amyloid formation occurred after 5h incubation (figure 4.1C). By TEM, no fibrils were observed after 3 h incubation whereas upon 5 h and 24 h incubation, fibrillar aggregates were detected (figure 4.1D). In sharp contrast, when fluorescence was measured every 1 min, the change in secondary structure was noticeable after 3 h (figure 4.1E) and the presence of fibrillar assemblies was confirmed by TEM (figure 4.1F). Interestingly, the morphology of the mature fibrils obtained after 24 h incubation was similar under both paradigms; *i.e.* 1-min and 10-min reading intervals.

According to studies showing that photoirradiation of ThT causes fragmentation of amyloid fibrils (Ozawa *et al.*, 2009; Yagi *et al.*, 2010), we initially suspected that a similar mechanism involving ThT photodegradation could be implicated in these observations. To investigate whether or not ThT was directly involved in this effect, the concentration of ThT was initially varied by five orders of magnitude. By reducing the amount of ThT present in solution, any potential reactive intermediates generated

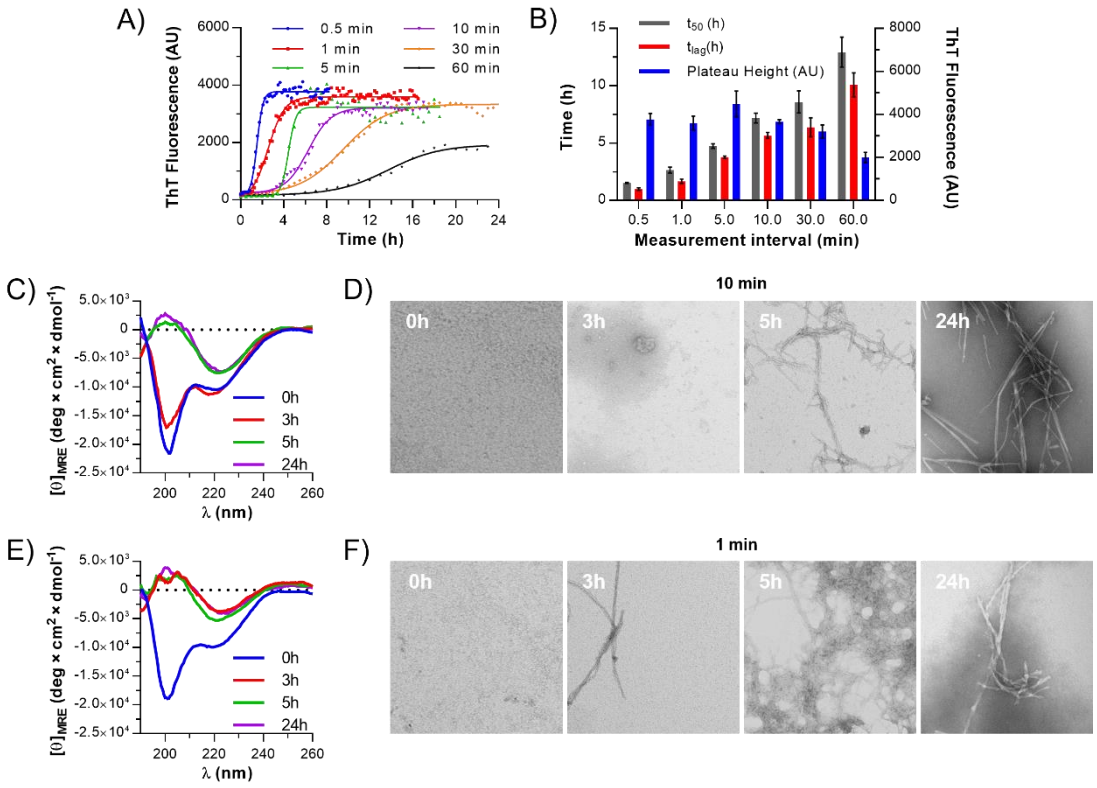

Figure 4.1 Frequent ThT fluorescence measurements accelerate amyloid formation. A) Kinetics of amyloid formation of IAPP (25 μM) measured by ThT fluorescence, with measurements taken every 0.5, 1, 5, 10, 30 and 60 mins. B) Kinetic parameters obtained from Boltzmann sigmoidal fit**.** C,E) Circular dichroism spectra of samples taken from microplate assays showing changes in secondary structure for measurements taken at 10-min (C) and 1-min (E) intervals. D,F) TEM images of samples taken from the microplate assays (in presence of 20 μM ThT) with 10-min (D) and 1-min (F) measurement intervals. Scale bar: 200 nm.

by fluorescence measurement would have also been reduced. No differences were observed (figure 4.2A, figure 4.2B and figure s4.3). We then investigated if this effect could be related to an increase of local temperature around the ThT-fibril interface. Thus, assays were performed at 24°C and 30°C and variations between temperatures were negligible (figure 4.2C). To confirm that ThT excitation played no role in the

alteration of fibrillization kinetics, the ThT was replaced by the hydrophobic-probe 8-anilino-1-naphthalenesulfonic acid (ANS). Strikingly, changing measurement intervals also altered the fibrillization measured by ANS fluorescence (figure 4.2D).

An additional variable that had to be considered was the movement of the microplate between the measurements of each well. Indeed, although the present assay was performed under quiescent conditions (no agitation before each read), plate readers move the microplate between each well-measurement. To evaluate this parameter, we compared the kinetics of amyloid assembly (10-min interval) under two paradigms; 3 wells were read *vs* the entire plate (96 wells). In both cases, samples from the same 3 wells were used for the analysis (wells A10 to A12). Strikingly, there was a clear difference between the kinetics obtained from 3-well and 96-well measurements (figure 4.2E). The same effect was observed with the amyloid-beta peptide $A\beta_{1\text{-}40}$ (figure s4.4).This indicates that the slight displacements of the microplate accelerated fibrillization and that kinetics of assembly is sensitive to the number of samples read. This hypothesis was confirmed by comparing the fibrillization kinetics using 10-min and 1-min measurement intervals in a cuvette instead of a microplate, with the cuvette holder fixed in the spectrofluorimeter. The results showed no difference between both paradigms in the cuvette (figure 4.2F). Although agitation has been abundantly shown to be a critical factor in amyloid formation (Batzli and Love, 2015), it was always used intentionally. The present data demonstrate a level of sensitivity not previously discussed and have implications on research relying on ThT assays to monitor fibrillization kinetics. The process of amyloid formation *in* vitro appears to be remarkably sensitive to agitation and the slight displacement of a microplate inside of a spectrophotometer is sufficient to significantly alter the kinetics of fibrillization. This finding offers a novel perspective regarding the reproducibility issues in amyloid formation assay. In

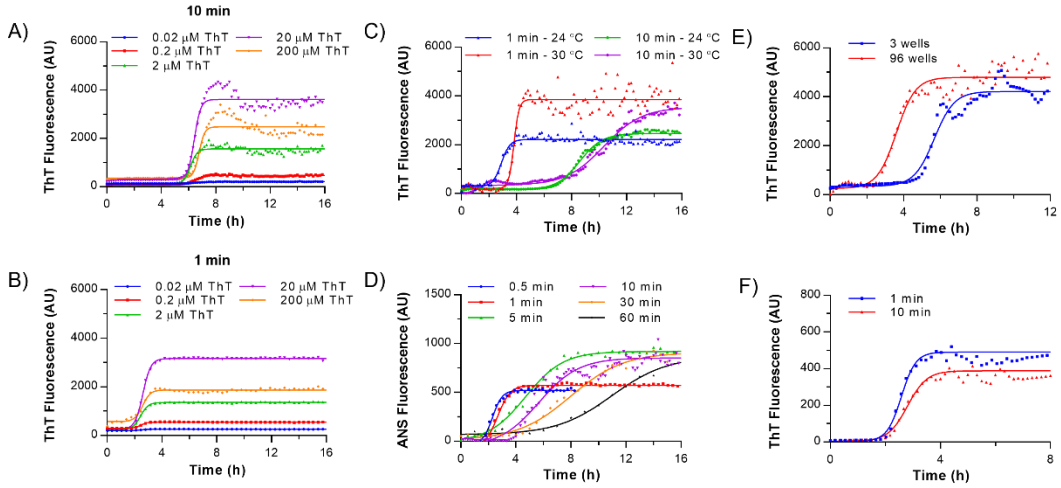

Figure 4.2 Increasing the number of microplate wells measured hastens amyloid formation. A,B) Fibrillization kinetics of hIAPP (25μM) with different ThT concentrations with measurements taken at 10-min (A) and 1-min (B) intervals. C) Effect of temperature on the kinetics of IAPP self-assembly. D) Kinetics of amyloid formation of IAPP (12.5 μM) measured by ANS fluorescence, with measurements taken every 0.5, 1, 5, 10, 30 and 60 mins. E) Fibrillization kinetics comparing measurements taken from 3 wells and 96 wells. F) Kinetics of IAPP (100 μM) self-assembly measured by ThT fluorescence in a cuvette with measurements taken at 10-min and 1-min intervals.

particular, care should be taken when comparing results obtained from quiescent fibril formation on the benchtop with what may not actually be quiescent measurements in a microplate reader. This study emphasizes that amyloid assembly is very sensitive to environmental factors and reinforces the importance of a better standardization in experimental procedures, including measurement intervals and the number of samples per microplate.

Appendix A. Supplementary data

Materials and Methods as well as supplementary data related to this article can be found at: http://dx.doi.org/10.1016/j.ab.2017.01.001

Acknowledgements

This work was supported by grants from the Natural Sciences and Engineering Research Council of Canada (NSERC) and the Fonds de Recherche du Québec-Nature et technologies (FRQNT) to S.B.

4.4 Supporting information

4.4.1 Materials and methods

Peptide synthesis and sample preparation

IAPP was synthesized on a Tribute peptide synthesizer (Protein Technologies) using Fmoc chemistry and a 2-(6-chloro-1-H-benzotriazole-1-yl)-1,1,3,3-tetramethylaminium hexafluorophosphate (HCTU) coupling strategy, as previously described (De Carufel *et al.*, 2015). Oxazolidine pseudoproline dipeptide derivatives were incorporated to facilitate the synthesis (Abedini and Raleigh, 2005). After cleavage, crude peptides were purified by reverse-phase high performance liquid chromatography (RP-HPLC). Collected fractions were analyzed by analytical RP-HPLC using an Aeris peptide XB C18 column (Phenomenex) and by 'time of flight' mass spectrometry using a LC/MS-TOF (Agilent). Fractions corresponding to the desired peptide with purity higher than 95% were pooled and lyophilized. Disulfide bond formation between Cys-2 and Cys-7 was achieved by dimethyl sulfoxide (DMSO) oxidation under mild agitation overnight. Peptides were repurified by RP-HPLC as described above. $A\beta_{1\text{-}40}$ was purchased from DG Peptides and purety and identity was assessed by LC-MS-TOF. Aliquots of monomerized IAPP and $A\beta_{1\text{-}40}$ were prepared by dissolving the pure peptide in hexafluoro-2-propanol (HFIP) to a concentration of 1 mg/mL. The solution was sonicated for 30 min and filtered through

a 0.22 μm hydrophilic PVDF filter before being lyophilized. The lyophilized peptide was solubilized for a second time in HFIP, sonicated for 30 min and the solution was aliquoted and IAPP was lyophilized while $A\beta_{1\text{-}40}$ aliquots were evaporated under N_2 gas. Monomerized IAPP and $A\beta_{1\text{-}40}$ samples were kept dried at -80°C until used, but not for longer than 4 weeks.

Kinetics of amyloid assembly

Monomerized IAPP was solubilized at 50 μM in tris-HCl (20 mM, pH 7.4) and sonicated for 3 minutes. The peptide solution was then diluted to 25, 12.5, and 6.25 μM with tris-HCl and ThT was added for a final concentration of 20 μM. Monomerized Aβ1-40 was solubilized in DMSO, then diluted to 50 μM with a final concentration of 1% DMSO. This stock solution was then diluted to 25, 12.5, and 6.25 μM with phosphate buffer (20 mM, pH 7.4). For Aβ1-40, assays were carried out with 100 μL volumes in triplicate in sealed 96-well microplates (Corning, black walled, clear bottomed, non-treated surface). Using an M1000 Pro Tecan plate reader, the microplate was incubated at 37 ºC with 5 seconds of agitation (linear shaking, 2 mm amplitude, 654 rpm) immediately prior to each measurement. For IAPP, assays were carried out with 100 μL volumes in triplicate in sealed 96-well microplate under quiescent conditions (Corning, black walled, clear bottomed, non-binding surface). Using an M1000 Pro plate reader (Tecan), the microplate was agitated for 5 seconds (linear shaking, 2 mm amplitude, 654 rpm) and the fibrillisation kinetics were performed at 24 °C, unless specified. Amyloid formation was monitored by thioflavin T fluorescence ($\lambda_{excitation}$ = 440 nm, $\lambda_{emission}$ = 485 nm) with measurements taken from the bottom of the plate every 0.5, 1, 5, 10, 30, or 60 minutes under quiescent conditions. ThT kinetics assays were also conducted on a Molecular Devices Spectramax i3 plate reader under the same conditions. Kinetic data from triplicates were averaged and fitted with a Boltzmann sigmoidal curve where t_{50} is the time to half-maximum intensity, *k* is the

apparent first-order rate constant and F_0 and F_{max} are the minimum and maximum fluorescence intensities, respectively.

$$F = \frac{F_0 + (F_{max} - F_0)}{1 + e^{\frac{-(t - t_{50})}{k}}}$$

The lag time (t_{lag}) was defined as the time before the any detectable amyloid forms, and was calculated from the sigmoidal model as: $t_{lag} = t_{50} - 2k$.

Circular dichroism spectroscopy

Far-ultraviolet circular dichroism (CD) spectra were recorded at room temperature using a Jasco J-810 CD spectrometer (Jasco, Easton, MD, USA). All spectra were measured from 260 to 190 nm and were corrected by subtracting the appropriate blank solution (buffer with ThT). All data was collected in 2 mm path length quartz cuvettes and converted to mean residue ellipticity (MRE):

$$MRE\ (deg \cdot cm^2 \cdot dmol^{-1}) = \frac{Mean\ residue\ weight\ (g \cdot mol^{-1})\ \times\ CD\ signal\ (deg)}{10 \times path\ length\ (cm) \times peptide\ concentration\ (g \cdot mL^{-1})}$$

Transmission electron microscopy

Samples, taken from microplate wells (25 μM IAPP; 20 mM tris-HCl and 20 μM ThT), were applied to a glow-discharged carbon film on a 400-mesh copper grid and left to stand for 1 minute. The grid was then blotted with filter paper and the sample immediately negatively stained with uranyl-formate (1.5% w/v). The stain was left to stand for 1 minute before being blotted dry and the grid set aside to dry completely

(24h) before analysis. Sample grids were analyzed on a FEI Tecnai 12 BioTwin system at 120 kV, and images were captured with a AMT XR80C CCD camera system.

4.4.2 Supplementary figures

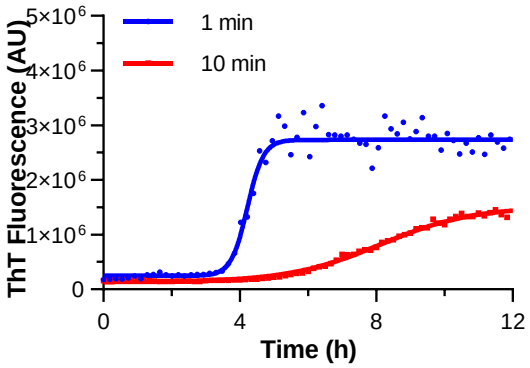

Figure S4.1 Reducing measurement interval during fibrillisation kinetics accelerates the response in ThT fluorescence regardless of plate reader model. Using a different microplate reader (Molecular Devices, Spectramax M2) yielded the same shortening of lag phase as the time between measurements was reduced from 10-min to 1-min intervals.

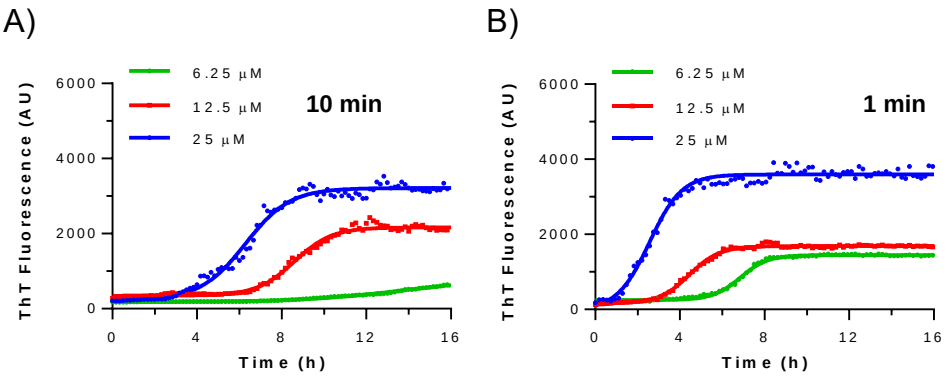

Figure S4.2 Reducing measurement interval during fibrillization kinetics accelerates the response in ThT fluorescence across a range of peptide concentrations. IAPP was tested at different concentrations (6.25, 12.5, 25 µM) with fluorescence measured at A) 10-min and B) 1-min intervals in non-binding microplate. The same shortening of lag-phase during the fibrillization kinetics was observed for all three concentrations.

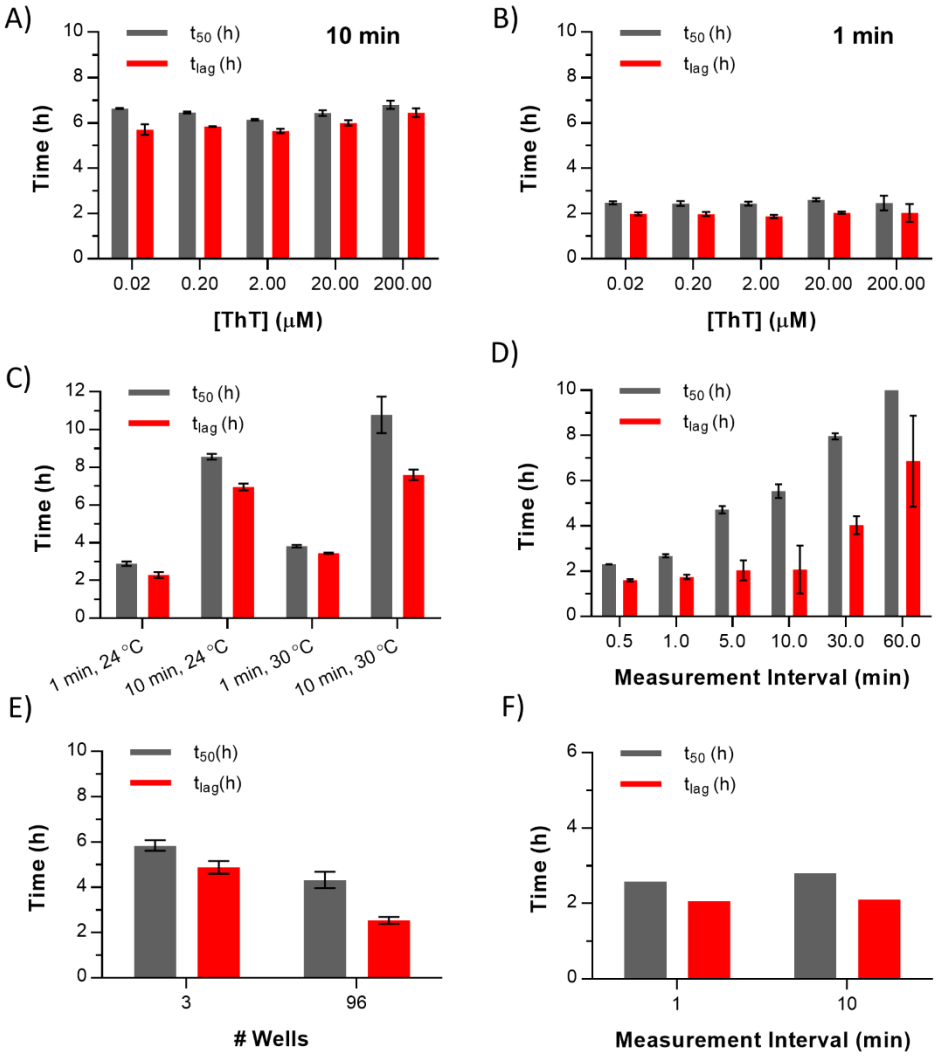

Figure S4.3 Lag time and t_{50} from fibrillization kinetics (obtained from Figure 2). A,B) Fibrillization kinetics of IAPP (25μM) with different ThT concentrations with measurements taken at 10-min (A) and 1-min (B) intervals. C) Effect of temperature on the kinetics of IAPP self-assembly. D) Kinetics of amyloid formation of IAPP (12.5 μM) measured by ANS fluorescence, with measurements taken every 0.5, 1, 5, 10, 30 and 60 mins. E) Fibrillization kinetics comparing measurements taken from 3 wells and 96 wells. F) Kinetics of IAPP (100 μM) self-assembly measured by ThT fluorescence in a cuvette with measurements taken at 10-min and 1-min intervals.

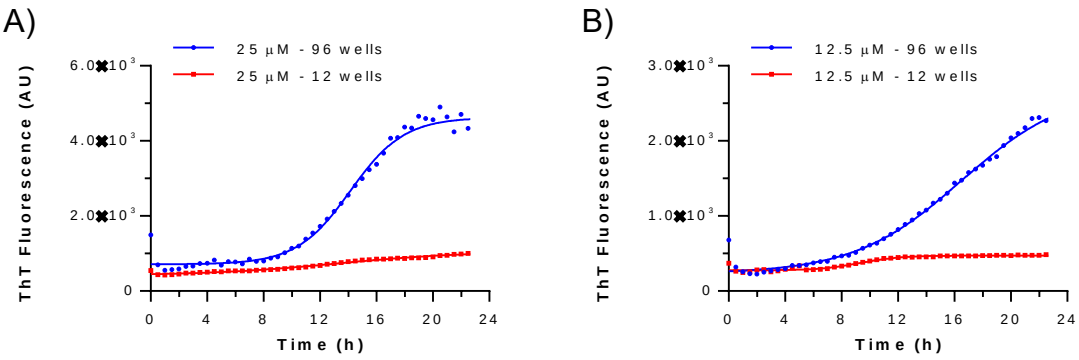

Figure S4.4 Increasing the number of wells measured accelerates the formation of amyloid fibrils of $A\beta_{1\text{-}40}$. $A\beta_{1\text{-}40}$ amyloid assembly was evaluated at peptide concentrations of A) 25 µM and B) 12.5 µM in the presence of 20 µM ThT with measurements taken every 10 minutes with 5 seconds of agitation (linear shaking) before each read. Similar to IAPP, increasing the number of wells measured noticeably reduced the lag-phase during $A\beta_{1\text{-}40}$ fibrillization.

CHAPTER V:

DISCUSSION

The self-assembly of peptide hormones is a complex process which occurs within a multitude of different contexts, ranging from heterogeneous amyloid deposits *in vivo* to simple amorphous aggregates *in vitro*. Regardless of where such aggregates are forming, there is a dire need to advance the current state of knowledge behind the aggregation process. An improved understanding behind this fundamental property of peptide hormones, and virtually all peptides or proteins for that matter, has broad implications in drug design and formulation, disease progression and treatment, as well as physiological functions. Furthermore, the work done on peptide hormones is likely transferrable to other aggregation-prone peptides, such as amyloid-β and α-synuclein, which aggregate in a similar manner. Throughout this thesis, peptide hormone aggregation was studied in both functional and pathological contexts. Mechanistic aspects of the processes which drive self-assembly were addressed, contributing to the overall scientific understanding of peptide hormone aggregation. Finally, improvements to standard experimental approaches used to study such processes were proposed.

In this context, this thesis aimed to uncover innovative biophysical strategies and approaches to study the process and factors affecting the aggregation of peptide hormones into amyloid fibrils. This overarching goal was attained, as testified by the publication of three separate manuscripts in renowned peer-reviewed journals for the

field. First, a new mechanism was proposed by which amyloid forms due to the interaction of a soluble peptide hormone, PACAP, and a linear polyanion, heparin, and the role of phase separation was demonstrated under conditions closely replicating those found within the physiological environment of secretory granules. Next, plasma membrane vesicles were exploited using a novel fluorescent labelling approach to study changes and damage to membranes by induced by IAPP, typically ascribed to an important source of the associated cytotoxicity of pancreatic cells during T2D in a mid- to high-throughput assay format. Finally, the ubiquitous use of microplate assays to follow amyloid growth result in a wide range of kinetic behaviours of IAPP in the literature. We discovered that the number of measurements, as well as intervals between measurements, may dramatically alter the kinetic profile of self-assembly. It demonstrated to be such that the self-assembly process is remarkably sensitive to even little sources of agitation, and the movements of the sample within the microplate reader are sufficient to accelerate the process. In the following sections, the results obtained during this thesis will be examined in the context of the relevant literature, primarily divided into two axes: 1) the roles of lipid bilayers and GAGs as co-factors during the self-assembly of peptide hormones, and 2) experimental approaches to study the biophysical process associated with amyloid formation.

5.1 Lipid bilayers and GAGs as co-factors during peptide hormone aggregation

5.1.1 Phase transitions during the process of amyloid formation

Despite amyloid being insoluble fibrils, which arise from soluble monomers and oligomers, the phase transition of the process is often not addressed. This is, however, a crucial aspect to consider when discussing the physiological and pathological roles of amyloids. As peptide hormones are stored as densely packed amyloid-like states inside secretory granules, higher concentrations can be attained than if the hormones were required to remain soluble (Maji *et al.*, 2009). Additionally, for high

concentrations of soluble molecules, an osmotic gradient would need to be maintained through ion pumps. This implies, therefore, that the insolubility of amyloid fibrils may act as an evolutionary advantage by lowering the cellular energy requirements (Maji *et al.*, 2009; Nespovitaya *et al.*, 2016). The caveat is that this solid material must be reversible enough to liberate biologically active, soluble monomers on demand. This so far appears to be the case where peptide hormones are stored reversibly as insoluble amyloid-like states inside of secretory granules, yet upon release, the aggregates are disassembled by chaperones and/or environmental changes (e.g., pH) to produce active monomers (Maji *et al.*, 2009).

The findings in Chapter II support the presence of insoluble fibrils formed from PACAP, a soluble peptide hormone, in the presence of GAGs, but an intermediate state was also described. PACAP was able to remain soluble for long durations and at elevated concentrations, mimicking those found in secretory granules. However, a liquid-liquid phase separation immediately occurred upon the addition of the highly anionic biopolymer, heparin. This was observed macroscopically as the formation of demixed white particulates, which rapidly settled in the absence of agitation and were easily pelleted via centrifugation. Microscopically, these particulates were spherical and decreased in size as the amyloid fibrils formed, suggesting that they were composed of the soluble peptide. HPLC analysis of supernatants showed that virtually no soluble peptide remained. A mechanism was proposed, whereby amyloid formation is initiated within the dense particulates in a water-depleted environment, rather than from soluble oligomers as most of the current mechanisms for pathological amyloid suggest.

Additional experiments could be performed to refine the proposed mechanism. For example, the notion of functional amyloid in secretory granules relies on a certain reversibility of the amyloid, which was not addressed in the course of this research thesis. Therefore, experiments could be performed to validate the capacity to release

monomers (Anoop *et al.*, 2014; Maji *et al.*, 2009; Nespovitaya *et al.*, 2016). Although it would be unlikely that any type of structural rearrangement or assembly may occur in a solid state, fluorescence recovery after photobleaching (FRAP) experiments could be done to confirm that these spherical particles were liquid. In FRAP, a powerful laser is used to photobleach an area of the phase-separated liquid droplet. Then, due to fluidity and mixing within the droplet, fluorescence to that area is restored over time, as recently demonstrated (Pytowski *et al.*, 2020). Other spectroscopic approaches could also be employed, such as solution NMR that can detect the presence of fluids but not solids, provided that the quantity of such species is sufficiently elevated. Therefore, as insoluble amyloid is formed, it would be expected to see a decrease in NMR signal from the peptide if it is in a fluid-like state (Hoffmann *et al.*, 2018). If this is not possible due to the peptide being in a gel-like state, then another potential use of NMR would be to measure the signal relaxation of ^{13}C-labelled PACAP in the monomeric, particulate, and fibrillar states. Solids and solid-like materials undergo faster relaxation in NMR environments than liquid-like materials (Hellstrand *et al.*, 2013; Rajput *et al.*, 2021).

5.1.2 Composition and complexity in models of lipid membranes

The interactions between amyloidogenic peptides and lipid membranes have been studied for decades, but the types and composition of model membranes used to study such interactions varies considerably. The majority of the work reported in the literature uses liposomes, prepared from a binary mixture of synthetic phospholipids, which is then extruded to obtain LUVs. It has been repeatedly observed that phospholipids with anionic head groups (e.g., PG, PS) accelerate the amyloidogenic process, whereas zwitterionic head groups (e.g., PC, PE, SM) exert far less of an effect. As a result, many studies prepare LUVs with disproportionate amounts of anionic phospholipids, on the order of 20 to 50 %mol, while mammalian cell membranes typically contain 2 to 10 %mol (Zhang *et al.*, 2017). Furthermore, in mammalian cells,

the anionic phospholipids are primarily localized In the inner leaflet of the bilayer, while in LUVs the distribution is equal between the two leaflets (Harayama and Riezman, 2018). Necessarily, this implies that any peptide in the presence of such anionic LUVs will encounter considerably more anionic phospholipids than would be possible under biological conditions. Cholesterol is abundant in mammalian cell membranes and most often absent in the model systems selected to study amyloidogenic peptide-membrane interactions. Cholesterol rigidifies fluid membranes and even using simple two-lipid model LUVs, the presence of cholesterol has a drastic effect in reducing peptide-induced disruptions (Sciacca *et al.*, 2016; Walsh *et al.*, 2014). The remaining plasma membrane components – extracellular matrix and cytoskeleton – also likely stabilize the membrane. As a result, plasma membranes are more resistant to amyloid-associated damage than liposomes, as demonstrated in Chapter III using both ghosts and GPMVs. Both of these models required significantly higher peptide:phospholipid ratios to detect significant disruption of the bilayer – on the order of 10-fold higher levels of monomeric peptide. Additionally, while ghosts retain the asymmetry of the inner and outer membrane leaflets (Gordesky and Marinetti, 1973), GPMVs have been observed to flip significant amounts of the anionic PS to the outer leaflet (Kelly *et al.*, 2009). This offers one potential explanation as to why the colocalization of the lipophilic tracers occurred at lower peptide:phospholipid ratios for GPMVs than for ghosts.

A significant portion of the literature describes plasma membrane perturbation associated with the process of amyloid formation . The mechanisms by which amyloid disrupts the membrane, however, are still a subject of debate. Typically, such interactions are viewed as either the formation of transmembrane pores by pre-fibrillar oligomers, or a carpeting/detergent-like mechanism by which oligomers/pre-fibrillar species are hydrophobic enough to partially solubilize the lipid bilayer, which results in lipids becoming incorporated into the amyloid fibrils (Gellermann *et al.*, 2005; Hellstrand *et al.*, 2013; Sciacca *et al.*, 2018; Westermark *et al.*, 2011). In reality, it is

possible to conceive that both of these processes occur, something which has been proposed using model membranes (Sasahara, 2018). As addressed in Chapter III, one improvement to the models used would be the encapsulation of a fluorophore to detect small-scale membrane perturbations. Although not the primary purpose of the work, results obtained in Chapter III correspond well with a carpeting mechanism where IAPP covers the membrane surface and the ensuing fibril growth damages the lipid membranes. These mechanisms have been investigated due to the low intrinsic cytotoxicity of most fully formed amyloid fibrils, although in some cases it is likely that the sheer mass of extracellular deposits can result in tissue damage or organ dysfunction as with systemic amyloidosis, where kilograms of amyloid proteinaceous materials are found (Knowles *et al.*, 2014).

A common limitation in the literature is the difficulty in reconciling amyloidogenicity, membrane perturbation in model systems, and cytotoxicity (Cao *et al.*, 2013a). This was one of the primary factors that motivated the work in Chapter III. Potentially, these discrepancies may simply be a result of insufficiently representative model membranes – the lack of polyanions, cytoskeleton, and lipid distribution or composition. Future work could exploit recent ssNMR experiments to further explore the peptide-membrane interactions between amyloidogenic peptide hormones and plasma membranes. One example is the incorporation of deuterated fatty acids to probe the membrane fluidity, which has so far been done with antimicrobial peptides (Kumar *et al.*, 2022). Similarly, to answer the question of which polar headgroups interact more strongly with the peptide, two-dimensional experiments such recoupling of the chemical shift anisotropy would be able to distinguish changes in the ^{31}P headgroup organization (Warschawski *et al.*, 2018). Of course, detecting structural changes of IAPP would also prove useful in understanding its membrane interactions. The possibility must be acknowledged, however, that the disagreements between cytotoxicity and membrane perturbation arise from something else altogether, and in that case, it is important to consider other mechanisms responsible for cell death in the

context of IAPP amyloidogenesis. This concept has been proposed previously, suggesting that multiple mechanisms of cytotoxicity not only exist, but occur simultaneously (Abedini *et al.*, 2018; Abedini and Schmidt, 2013; Cao *et al.*, 2013b). One such example is the perturbation of the plasma and mitochondrial membranes which in turn leads to the accumulation of reactive oxygen species, increased intracellular Ca^{2+}, and stress to the endoplasmic reticulum.

There is also evidence that pre-fibrillar forms of IAPP bind to RAGE, a receptor which recognizes patterns and is involved in various inflammatory conditions, including T2D. It was concluded that soluble, pre-fibrillar species lead to the upregulation of RAGE expression and to β-cell death via apoptosis, whereas fully formed fibrils did not (Abedini *et al.*, 2018). This strongly supports the oligomer hypothesis and may explain, at least in part, the issue with attempting to directly translate membrane perturbation to cytotoxicity. Since IAPP toxicity is increased by inflammation, and IAPP binding to RAGE generates an inflammatory response, it is entirely possible that the initiation of β-cell death occurs as a result from RAGE binding. The loss of β-cells in the pancreas could be further exacerbated through the other commonly described, non-receptor mediated mechanisms, namely perturbation of the plasma membrane.

5.2 Experimental approaches to study amyloid formation

5.2.1 Agitation during the *in vitro* self-assembly process

While a sizeable amount of the literature is centered around describing the pathological nature of amyloid, an abundant body of work describes amyloid formation *in vitro*. It is already well known that various experimental conditions can alter the aggregation and self-assembly of peptides into amyloid fibrils. This has been observed for pH, salt, peptide concentration, temperature, and agitation (Batzli and Love, 2015). In fact, agitation is a primary driver of amyloidogenesis *in vitro* for a variety of peptides,

ranging from canonical disease-related peptides such as linear oscillations for Aβ (Bharadwaj *et al.*, 2020; Sciacca *et al.*, 2012) to the longitudinal rotation more recently described for amyloid fibrils formed by peptide hormones (Anoop *et al.*, 2014; Maji *et al.*, 2009; Mehra *et al.*, 2018).

Agitation can be applied in two general ways: i) turbulent mixing, which increases the contact between air and water interfaces, and ii) shear, which applies horizontal forces upon the solution resulting in mixing (Batzli and Love, 2015). In each case, the number of molecular collisions is increased, thus raising the probability of a nucleation event occurring. Turbulent mixing is likely the primary driving force in the initiation of aggregation, since shear forces alone were not found to accelerate the nucleation process. Shear, however, is capable of accelerating the fibrilization process at low forces, and at higher forces can result in the breakup of larger aggregates, leading to increased secondary nucleation sites while simultaneously resulting in shorter fibril lengths (Hill *et al.*, 2006). It was further observed that in certain cases, sufficient shear forces could also result in increased air-water contact and in turn, accelerate nucleation. Considering the results obtained in Chapter IV, the increased agitation induced by the number of measurements did not decrease the final ThT fluorescence values, suggesting that a comparable number of ThT binding sites were available regardless of the amount of agitation. Furthermore, the shortening of the nucleation phase and increased rate of elongation (i.e., slope) suggest that there are primarily turbulent forces associated with measurements made in typical microplate reader ThT assays.

5.2.2 Addressing the limitations in current methods used to amdyloid self-assembly

In general, studying the behaviour of aggregating peptides is challenging due to the heterogeneous and dynamic nature of the samples. As other co-factors are added, such as GAGs, membranes, crowding agents, and salts, the selection of experimental techniques becomes increasingly limited. The use of co-factors is becoming ever more

important, however, to accurately depict the corresponding biological processes *in vivo*. Ultimately, it is imperative to select a variety of experimental approaches that may overcome potential limitations such as sample quantity, acquisition time, detection of the desired material, and labelling possibilities. For example, AFM and transmission TEM are commonly used to study amyloid fibril morphology (Heerde *et al.*, 2022; Nguyen *et al.*, 2021). These approaches are generally fast and require no labelling, although samples must be dried. Confocal microscopy is a powerful tool to detect large aggregates, and fluorescent labelling permits the detection of only a desired region of the sample. The resolution of confocal microscopy is considerably lower than AFM and TEM, however. This can be overcome to some degree using modern super resolution microscopy, which has been used to acquire images of real-time fibril growth and the incorporation of GAGs into amyloid fibrils using appropriate combinations of fluorescently labelled sampled (Nespovitaya *et al.*, 2017). The use of super-resolution microscopy could potentially also shed light on the inner workings and dynamics of the phase-separated droplets witnessed during the self-assembly of PACAP.

Spectroscopic approaches provide molecular-level information on the supramolecular and atomic structure of peptide hormone aggregates, in addition to their interactions with other biological structures such as GAGs, lipids, and proteins. NMR is a powerful tool in this regard since it does not require adding tags onto the peptide, thus ensuring that a sample will behave as it should *in vivo*. NMR can be used to detect both soluble and insoluble species along the aggregation pathway, to probe membrane damage, and to measure distances and dynamics. Typically, to improve the relatively insensitive nature of NMR, peptides incorporating ^{13}C and ^{15}N isotopes are preferred, though directly measuring the signal from protons has been accomplished (Nguyen *et al.*, 2021; Yamane *et al.*, 2019). One particularly impressive example detected and characterized oligomers of the Aβ polypeptide (Kotler *et al.*, 2015). While Aβ is not a peptide hormone, it is of comparable size and prepared synthetically in a similar fashion

as many of the peptide hormones used in *in vitro* experiments, indicating that such an approach would be feasible for peptide hormones as well. This could equally be probed by ssNMR using ^{13}C and ^{15}N isotopically labelled IAPP and comparing the changes in chemical shifts between the theoretical values for a random coil and those obtained experimentally. While this has been done previously in the literature (Loquet *et al.*, 2018), synthetic models were used and, considering the important differences observed in the experiments on ghosts or GPMVs, it would be a worthwhile endeavor to study those structural changes in the presence of plasma membranes.

Another spectroscopic approach commonly employed is CD, which offers a relatively simple and rapid way to detect changes in secondary structure using circular polarized light. Since amyloid fibrils are formed from cross-β-sheets and most peptide hormones are disordered or α-helical, there is a clear shift in CD signal during self-assembly (Caillon *et al.*, 2013; Hoffmann *et al.*, 2018; Khemtemourian *et al.*, 2021). CD is particularly sensitive to high salt concentrations and a variety of macromolecules; therefore, samples must be relatively simple in composition. In this case, the model membranes proposed in Chapter III prove to be unsuitable and result in excessive background noise due to the presence of membrane proteins and salts.

Fluorescence spectroscopy is a common technique to detect aggregation, using an assortment of chromophores. ThT is typically used, although CR birefringence has historically been the gold standard. CR can also be detected through UV-vis absorbance and fluorescence spectroscopy (Birol *et al.*, 2019), though this occurs less frequently than ThT-binding fluorescence assays. Other approaches use ANS, which responds to hydrophobic domains (Lu *et al.*, 2018), and pyrene can be applied to determine the critical aggregation concentration of a peptide (Zottig *et al.*, 2021). A somewhat more recent approach used the fluorescent biarsenical hairpin (FlAsH) probe to study the aggregation kinetics of IAPP (Quittot *et al.*, 2018). It has been shown that this method can be applied to several peptides, by adding a double cysteine motif which, during

aggregation binds to FlAsH with a second double cysteine motif and renders it fluorescent. Interestingly, IAPP has an intrinsic double cysteine motif (Cys2, Cys7) and responds to FlAsH without the need for an external tag. This could potentially be exploited for other peptides containing such double cysteine motifs, for example, calcitonin. In many cases, the fluorescence is monitored in a microplate over time as a kinetic experiment (Chiti and Dobson, 2017; Korshavn *et al.*, 2017; Kumar *et al.*, 2017), after which important properties such as the nucleation time, elongation rate, and even the overall mechanism can be determined from the fitting of a sigmoidal curve to the data (Meisl *et al.*, 2016). The principal findings from Chapter IV are therefore essential to ensure an accurate representation of the aggregation kinetics, particularly since the results were shown to be transferrable between different amyloidogenic peptides.

5.3 Conclusions and perspectives

Amyloid remains to this day a complex and challenging biomaterial to accurately study, due to the highly dynamic and sensitive process by which it forms, and the morphological heterogeneity of the mature fibrils. The work performed throughout this thesis has resulted in several key findings that could ultimately contribute to the body of scientific literature describing peptide hormone aggregation, and amyloid-associated pathophysiology. Specifically, this thesis describes commonly overlooked variables to improve the reliability of *in vitro* experiments, presents a simple and efficient assay to detect time-resolved membrane perturbations during peptide aggregation using intact plasma membranes, and defines a novel mechanism behind the biological process of peptide hormone storage as amyloid. The impacts of this work are wide reaching and potentially provide an avenue to reconcile the differences observed during amyloidogenesis in laboratory and in biological/clinical settings.

The notion that peptide hormones self-assemble inside secretory granules in a phase-separated state is entirely new and describes the mechanism behind a newly discovered physiological form of amyloid. The process appears to be fundamentally different from what is generally proposed to occur among pathologically associated amyloid, even for peptide hormones of similar lengths. Important questions should be addressed in future work regarding the nature of pathological and functional amyloids, notably concerning the relationship between self-assembly mechanisms and pathology. It would be particularly interesting to compare other functional forms of amyloid and determine whether the role of phase separation is critical for all functional amyloids. For example, this appears to be an important aspect in nuclear amyloid bodies formed by the Von Hippel Lindau protein in the presence of low-complexity domains of non-coding mRNA (Audas *et al.*, 2016).

The limitations to the current model lipid membrane systems employed in the vast majority of biophysical studies were addressed through the development of a new experimental approach to enable the rapid throughput of samples to test various conditions of amyloid formation using vesicles derived from mammalian plasma membrane. The final FRET assay proposed here and the biologically relevant membranes themselves have important applications, for instance interpreting the effects of and screening for fibrilization inhibitors or comparing the importance of membrane perturbations with expected cytotoxicity.

Finally, the sensitivity of the ubiquitously employed ThT microplate assay was addressed by examining an often-unreported variable: measurement frequency. We demonstrated that the frequency of measurements made during microplate reader experiments provide sufficient agitation to significantly alter the self-assembly kinetics of IAPP, and of the peptide Aβ. These results have aided in improving assay consistency in the Bourgault lab and have the possibility to improve experimental reliability in other labs as well. These results demonstrate that the exact same number

of measurements must be made to accurately compare kinetic data from two datasets. Ultimately, these results also demonstrate how sensitive the amyloidogenic process is to agitation and indicate a dire need for published protocols to provide as much detail as possible to assist in the replication of the work carried out.

BIBLIOGRAPHY

Abedini A, Cao P, Plesner A, Zhang J, He M, Derk J, Patil SA, Rosario R, Lonier J, Song F, et al. (2018) RAGE binds preamyloid IAPP intermediates and mediates pancreatic beta cell proteotoxicity. *J Clin Invest 128*: 682-698.

Abedini A, Cao P and Raleigh DP (2016a) Detection of Helical Intermediates During Amyloid Formation by Intrinsically Disordered Polypeptides and Proteins. *Methods Mol Biol 1345*: 55-66.

Abedini A, Plesner A, Cao P, Ridgway Z, Zhang J, Tu LH, Middleton CT, Chao B, Sartori DJ, Meng F, et al. (2016b) Time-resolved studies define the nature of toxic IAPP intermediates, providing insight for anti-amyloidosis therapeutics. *Elife 5*: e12977.

Abedini A and Raleigh DP (2005) Incorporation of pseudoproline derivatives allows the facile synthesis of human IAPP, a highly amyloidogenic and aggregation-prone polypeptide. *Org Lett 7*: 693-696.

Abedini A and Raleigh DP (2009) A critical assessment of the role of helical intermediates in amyloid formation by natively unfolded proteins and polypeptides. *Protein Eng Des Sel 22*: 453-459.

Abedini A and Schmidt AM (2013) Mechanisms of islet amyloidosis toxicity in type 2 diabetes. *FEBS Lett 587*: 1119-1127.

Aguilera JJ, Zhang F, Beaudet JM, Linhardt RJ and Colon W (2014) Divergent effect of glycosaminoglycans on the in vitro aggregation of serum amyloid A. *Biochimie 104*: 70-80.

Akter R, Cao P, Noor H, Ridgway Z, Tu LH, Wang H, Wong AG, Zhang X, Abedini A, Schmidt AM, et al. (2016) Islet Amyloid Polypeptide: Structure, Function, and Pathophysiology. *J Diabetes Res 2016*: 2798269.

Alexandrescu AT (2005) Amyloid accomplices and enforcers. *Protein Sci 14*: 1-12.

Amaro M, Šachl R, Aydogan G, Mikhalyov II, Vácha R and Hof M (2016) GM1 Ganglioside Inhibits β-Amyloid Oligomerization Induced by Sphingomyelin. *Angewandte Chemie International Edition 55*: 9411-9415.

Ancsin JB (2003) Amyloidogenesis: historical and modern observations point to heparan sulfate proteoglycans as a major culprit. *Amyloid 10*: 67-79.

Anoop A, Ranganathan S, Das Dhaked B, Jha NN, Pratihar S, Ghosh S, Sahay S, Kumar S, Das S, Kombrabail M, et al. (2014) Elucidating the role of disulfide bond on amyloid formation and fibril reversibility of somatostatin-14: relevance to its storage and secretion. *J Biol Chem 289*: 16884-16903.

Arosio P, Knowles TP and Linse S (2015) On the lag phase in amyloid fibril formation. *Phys Chem Chem Phys 17*: 7606-7618.

Arosio P, Michaels TC, Linse S, Mansson C, Emanuelsson C, Presto J, Johansson J, Vendruscolo M, Dobson CM and Knowles TP (2016) Kinetic analysis reveals the diversity of microscopic mechanisms through which molecular chaperones suppress amyloid formation. *Nat Commun 7*: 10948.

Atwood CS, Martins RN, Smith MA and Perry G (2002) Senile plaque composition and posttranslational modification of amyloid-β peptide and associated proteins. *Peptides 23*: 1343-1350.

Audas TE, Audas DE, Jacob MD, Ho JJ, Khacho M, Wang M, Perera JK, Gardiner C, Bennett CA, Head T, et al. (2016) Adaptation to Stressors by Systemic Protein Amyloidogenesis. *Dev Cell 39*: 155-168.

Badtke MP, Hammer ND and Chapman MR (2009) Functional amyloids signal their arrival. *Sci Signal 2*: pe43.

Ban T, Hamada D, Hasegawa K, Naiki H and Goto Y (2003) Direct observation of amyloid fibril growth monitored by thioflavin T fluorescence. *J Biol Chem 278*: 16462-16465.

Batzli KM and Love BJ (2015) Agitation of amyloid proteins to speed aggregation measured by ThT fluorescence: a call for standardization. *Mater Sci Eng C Mater Biol Appl 48*: 359-364.

Bazar E and Jelinek R (2010) Divergent heparin-induced fibrillation pathways of a prion amyloidogenic determinant. *Chembiochem 11*: 1997-2002.

Bechara C, Pallerla M, Zaltsman Y, Burlina F, Alves ID, Lequin O and Sagan S (2013) Tryptophan within basic peptide sequences triggers glycosaminoglycan-dependent endocytosis. *Faseb j 27*: 738-749.

Bellotti V and Chiti F (2008) Amyloidogenesis in its biological environment: challenging a fundamental issue in protein misfolding diseases. *Curr Opin Struct Biol 18*: 771-779.

Benilova I, Gallardo R, Ungureanu AA, Castillo Cano V, Snellinx A, Ramakers M, Bartic C, Rousseau F, Schymkowitz J and De Strooper B (2014) The Alzheimer disease protective mutation A2T modulates kinetic and thermodynamic properties of amyloid-beta (Abeta) aggregation. *J Biol Chem 289*: 30977-30989.

Bera S, Gayen N, Mohid SA, Bhattacharyya D, Krishnamoorthy J, Sarkar D, Choi J, Sahoo N, Mandal AK, Lee D, et al. (2020) Comparison of Synthetic Neuronal Model Membrane Mimics in Amyloid Aggregation at Atomic Resolution. *ACS Chem Neurosci 11*: 1965-1977.

Bharadwaj P, Solomon T, Sahoo BR, Ignasiak K, Gaskin S, Rowles J, Verdile G, Howard MJ, Bond CS, Ramamoorthy A, et al. (2020) Amylin and beta amyloid proteins interact to form amorphous heterocomplexes with enhanced toxicity in neuronal cells. *Sci Rep 10*: 10356.

Biancalana M and Koide S (2010) Molecular mechanism of Thioflavin-T binding to amyloid fibrils. *Biochim Biophys Acta 1804*: 1405-1412.

Birol M, Kumar S, Rhoades E and Miranker AD (2018) Conformational switching within dynamic oligomers underpins toxic gain-of-function by diabetes-associated amyloid. *Nat Commun 9*: 1312.

Birol M, Wojcik SP, Miranker AD and Rhoades E (2019) Identification of N-linked glycans as specific mediators of neuronal uptake of acetylated alpha-Synuclein. *PLoS Biol 17*: e3000318.

Borysik AJ, Morten IJ, Radford SE and Hewitt EW (2007) Specific glycosaminoglycans promote unseeded amyloid formation from beta2-microglobulin under physiological conditions. *Kidney Int 72*: 174-181.

Bourgault S, Chatenet D, Wurtz O, Doan ND, Leprince J, Vaudry H, Fournier A and Vaudry D (2011a) Strategies to convert PACAP from a hypophysiotropic neurohormone into a neuroprotective drug. *Curr Pharm Des 17*: 1002-1024.

Bourgault S, Choi S, Buxbaum JN, Kelly JW, Price JL and Reixach N (2011b) Mechanisms of transthyretin cardiomyocyte toxicity inhibition by resveratrol analogs. *Biochemical and Biophysical Research Communications 410*: 707-713.

Bourgault S, Solomon JP, Reixach N and Kelly JW (2011c) Sulfated glycosaminoglycans accelerate transthyretin amyloidogenesis by quaternary structural conversion. *Biochemistry 50*: 1001-1015.

Bourgault S, Vaudry D, Ségalas-Milazzo I, Guilhaudis L, Couvineau A, Laburthe M, Vaudry H and Fournier A (2009) Molecular and Conformational Determinants of Pituitary Adenylate Cyclase-Activating Polypeptide (PACAP) for Activation of the PAC1 Receptor. *Journal of Medicinal Chemistry 52*: 3308-3316.

Brender JR, Krishnamoorthy J, Sciacca MF, Vivekanandan S, D'Urso L, Chen J, La Rosa C and Ramamoorthy A (2015) Probing the sources of the apparent irreproducibility of amyloid formation: drastic changes in kinetics and a switch in mechanism due to micellelike oligomer formation at critical concentrations of IAPP. *J Phys Chem B 119*: 2886-2896.

Bretscher MS and Raff MC (1975) Mammalian plasma membranes. *Nature 258*: 43-49.

Brunden KR, Richter-Cook NJ, Chaturvedi N and Frederickson RCA (1993) pH-dependent binding of synthetic beta-amyloid peptides to glycosaminoglycans. *Journal of Neurochemistry 61*: 2147-2154.

Bucciantini M, Leri M, Stefani M, Melki R, Zecchi-Orlandini S and Nosi D (2020) The Amphipathic GM1 Molecule Stabilizes Amyloid Aggregates, Preventing their Cytotoxicity. *Biophysical journal 119*: 326-336.

Caillon L, Duma L, Lequin O and Khemtemourian L (2014) Cholesterol modulates the interaction of the islet amyloid polypeptide with membranes. *Mol Membr Biol 31*: 239-249.

Caillon L, Lequin O and Khemtemourian L (2013) Evaluation of membrane models and their composition for islet amyloid polypeptide-membrane aggregation. *Biochim Biophys Acta 1828*: 2091-2098.

Cao P, Abedini A, Wang H, Tu LH, Zhang X, Schmidt AM and Raleigh DP (2013a) Islet amyloid polypeptide toxicity and membrane interactions. *Proc Natl Acad Sci U S A 110*: 19279-19284.

Cao P, Marek P, Noor H, Patsalo V, Tu LH, Wang H, Abedini A and Raleigh DP (2013b) Islet amyloid: from fundamental biophysics to mechanisms of cytotoxicity. *FEBS Lett 587*: 1106-1118.

Cao Q, Boyer DR, Sawaya MR, Abskharon R, Saelices L, Nguyen BA, Lu J, Murray KA, Kandeel F and Eisenberg DS (2021) Cryo-EM structures of hIAPP fibrils seeded by patient-extracted fibrils reveal new polymorphs and conserved fibril cores. *Nat Struct Mol Biol 28*: 724-730.

Cao Q, Boyer DR, Sawaya MR, Ge P and Eisenberg DS (2020) Cryo-EM structure and inhibitor design of human IAPP (amylin) fibrils. *Nat Struct Mol Biol 27*: 653-659.

Cardin AD and Weintraub HJ (1989) Molecular modeling of protein-glycosaminoglycan interactions. *Arteriosclerosis 9*: 21-32.

Castillo GM, Cummings JA, Yang W, Judge ME, Sheardown MJ, Rimvall K, Hansen JB and Snow AD (1998) Sulfate content and specific glycosaminoglycan backbone of perlecan are critical for perlecan's enhancement of islet amyloid polypeptide (amylin) fibril formation. *Diabetes 47*: 612-620.

Chapman MR, Robinson LS, Pinkner JS, Roth R, Heuser J, Hammar M, Normark S and Hultgren SJ (2002) Role of Escherichia coli curli operons in directing amyloid fiber formation. *Science 295*: 851-855.

Chargé SB, Esiri MM, Bethune CA, Hansen BC and Clark A (1996) Apolipoprotein E is associated with islet amyloid and other amyloidoses: implications for Alzheimer's disease. *J Pathol 179*: 443-447.

Chen J, Meng Q, Zhang Y, Dong M, Zhao L, Zhang Y, Chen L, Chai Y, Meng Z, Wang C, et al. (2021) Complexation of an Antimicrobial Peptide by Large-Sized Macrocycles for Decreasing Hemolysis and Improving Stability. *Angewandte Chemie International Edition 60*: 11288-11293.

Chen P, Toribara Tt and Warner H (1956) Microdetermination of phosphorus. *Analytical chemistry 28*: 1756-1758.

Chiti F and Dobson CM (2006) Protein misfolding, functional amyloid, and human disease. *Annu Rev Biochem 75*: 333-366.

Chiti F and Dobson CM (2009) Amyloid formation by globular proteins under native conditions. *Nature Chemical Biology 5*: 15-22.

Chiti F and Dobson CM (2017) Protein Misfolding, Amyloid Formation, and Human Disease: A Summary of Progress Over the Last Decade. *Annu Rev Biochem 86*: 27-68.

Christensen LF, Malmos KG, Christiansen G and Otzen DE (2016) A Complex Dance: The Importance of Glycosaminoglycans and Zinc in the Aggregation of Human Prolactin. *Biochemistry 55*: 3674-3684.

Christensen M and Schiott B (2019) Revealing a Dual Role of Ganglioside Lipids in the Aggregation of Membrane-Associated Islet Amyloid Polypeptide. *J Membr Biol 252*: 343-356.

Christopoulos G, Perry KJ, Morfis M, Tilakaratne N, Gao Y, Fraser NJ, Main MJ, Foord SM and Sexton PM (1999) Multiple amylin receptors arise from receptor activity-modifying protein interaction with the calcitonin receptor gene product. *Mol Pharmacol 56*: 235-242.

Cohlberg JA, Li J, Uversky VN and Fink AL (2002) Heparin and Other Glycosaminoglycans Stimulate the Formation of Amyloid Fibrils from α-Synuclein in Vitro. *Biochemistry 41*: 1502-1511.

Conchillo-Solé O, de Groot NS, Avilés FX, Vendrell J, Daura X and Ventura S (2007) AGGRESCAN: a server for the prediction and evaluation of "hot spots" of aggregation in polypeptides. *BMC Bioinformatics 8*: 65.

Corlin DB, Johnsen CK, Nissen MH and Heegaard NH (2010) Glycosaminoglycans enhance the fibrillation propensity of the beta2-microglobulin cleavage variant--DeltaK58-beta2m. *Biochem Biophys Res Commun 402*: 247-251.

Crooks EJ, Irizarry BA, Ziliox M, Kawakami T, Victor T, Xu F, Hojo H, Chiu K, Simmerling C, Van Nostrand WE, et al. (2020) Copper stabilizes antiparallel β-sheet fibrils of the amyloid β40 (Aβ40)-Iowa variant. *J Biol Chem 295*: 8914-8927.

Davies HA, Phelan MM and Madine J (2016) 1H, 15N and 13C assignment of the amyloidogenic protein medin using fast-pulsing NMR techniques. *Biomol NMR Assign 10*: 75-77.

De Carufel CA, Nguyen PT, Sahnouni S and Bourgault S (2013) New insights into the roles of sulfated glycosaminoglycans in islet amyloid polypeptide amyloidogenesis and cytotoxicity. *Biopolymers 100*: 645-655.

De Carufel CA, Quittot N, Nguyen PT and Bourgault S (2015) Delineating the Role of Helical Intermediates in Natively Unfolded Polypeptide Amyloid Assembly and Cytotoxicity. *Angew Chem Int Ed Engl 54*: 14383-14387.

Delgado DA, Doherty K, Cheng Q, Kim H, Xu D, Dong H, Grewer C and Qiang W (2016) Distinct Membrane Disruption Pathways Are Induced by 40-Residue beta-Amyloid Peptides. *J Biol Chem 291*: 12233-12244.

Dharmadana D, Reynolds NP, Dekiwadia C, Conn CE and Valery C (2018) Heparin assisted assembly of somatostatin amyloid nanofibrils results in disordered precipitates by hindrance of protofilaments interactions. *Nanoscale 10*: 18195-18204.

Diociaiuti M, Giordani C, Kamel GS, Brasili F, Sennato S, Bombelli C, Meneses KY, Giraldo MA and Bordi F (2016) Monosialoganglioside-GM1 triggers binding of the amyloid-protein salmon calcitonin to a Langmuir membrane model mimicking the occurrence of lipid-rafts. *Biochem Biophys Rep 8*: 365-375.

Divakara MB, Martinez D, Ravi A, Bhavana V, Ramana V, Habenstein B, Loquet A and Santosh MS (2019) Molecular mechanisms for the destabilization of model membranes by islet amyloid polypeptide. *Biophys Chem 245*: 34-40.

Doyle L (1988) Lardaceous disease: some early reports by British authors (1722-1879). *J R Soc Med 81*: 729-731.

Dubey K, Anand BG, Shekhawat DS and Kar K (2017) Eugenol prevents amyloid formation of proteins and inhibits amyloid-induced hemolysis. *Sci Rep 7*: 40744.

Egashira M, Takase H, Yamamoto I, Tanaka M and Saito H (2011) Identification of regions responsible for heparin-induced amyloidogenesis of human serum amyloid A using its fragment peptides. *Archives of Biochemistry and Biophysics 511*: 101-106.

Eiden LE (2013) Neuropeptide–Catecholamine Interactions in Stress. *Advances in Pharmacology 68*: 399-404.

Eisenberg DS and Sawaya MR (2017) Structural Studies of Amyloid Proteins at the Molecular Level. *Annu Rev Biochem 86*: 69-95.

Erickson LA, Vrana JA, Theis J, Rivera M, Lloyd RV, McPhail E and Zhang J (2015) Analysis of Amyloid in Medullary Thyroid Carcinoma by Mass Spectrometry-Based Proteomic Analysis. *Endocr Pathol 26*: 291-295.

Evangelisti E, Cascella R, Becatti M, Marrazza G, Dobson CM, Chiti F, Stefani M and Cecchi C (2016) Binding affinity of amyloid oligomers to cellular membranes is a generic indicator of cellular dysfunction in protein misfolding diseases. *Sci Rep 6*: 32721.

Ferguson EV, Roy A, Ciechanski P and Wilson RJA (2013) Stress peptide PACAP stimulates and stabilizes neonatal breathing through distinct mechanisms. *Respiratory Physiology & Neurobiology 187*: 217-223.

Fernandez-Escamilla AM, Rousseau F, Schymkowitz J and Serrano L (2004) Prediction of sequence-dependent and mutational effects on the aggregation of peptides and proteins. *Nat Biotechnol 22*: 1302-1306.

Fitzpatrick AW, Vanacore GM and Zewail AH (2015) Nanomechanics and intermolecular forces of amyloid revealed by four-dimensional electron microscopy. *Proc Natl Acad Sci U S A 112*: 3380-3385.

Fowler DM, Koulov AV, Alory-Jost C, Marks MS, Balch WE and Kelly JW (2006) Functional amyloid formation within mammalian tissue. *PLoS Biol 4*: e6.

Fowler DM, Koulov AV, Balch WE and Kelly JW (2007) Functional amyloid--from bacteria to humans. *Trends Biochem Sci 32*: 217-224.

Fu Z, Aucoin D, Davis J, Van Nostrand WE and Smith SO (2015) Mechanism of Nucleated Conformational Conversion of Abeta42. *Biochemistry 54*: 4197-4207.

Gandhi NS and Mancera RL (2008) The structure of glycosaminoglycans and their interactions with proteins. *Chem Biol Drug Des 72*: 455-482.

Gavriilaki E, Anagnostopoulos A and Mastellos DC (2019) Complement in Thrombotic Microangiopathies: Unraveling Ariadne's Thread Into the Labyrinth of Complement Therapeutics. *Frontiers in Immunology 10*: 1-15.

Gellermann GP, Appel TR, Tannert A, Radestock A, Hortschansky P, Schroeckh V, Leisner C, Lütkepohl T, Shtrasburg S, Röcken C, et al. (2005) Raft lipids as common components of human extracellular amyloid fibrils. *Proceedings of the National Academy of Sciences 102*: 6297-6302.

Geneste A, Andre C, Magy-Bertrand N, Lethier L, Tijani G and Guillaume YC (2015) Thermodynamic study of transthyretin association (wild-type and senile forms) with heparan sulfate proteoglycan: pH effect and implication of the reactive histidine residue. *Biomed Chromatogr 29*: 514-522.

Godin E, Nguyen PT, Zottig X and Bourgault S (2019) Identification of a hinge residue controlling islet amyloid polypeptide self-assembly and cytotoxicity. *J Biol Chem 294*: 8452-8463.

Gordesky SE and Marinetti GV (1973) The asymmetric arrangement of phospholipids in the human erythrocyte membrane. *Biochemical and Biophysical Research Communications 50*: 1027-1031.

Han P, Tang Z, Yin J, Maalouf M, Beach TG, Reiman EM and Shi J (2014) Pituitary adenylate cyclase-activating polypeptide protects against beta-amyloid toxicity. *Neurobiol Aging 35*: 2064-2071.

Harayama T and Riezman H (2018) Understanding the diversity of membrane lipid composition. *Nat Rev Mol Cell Biol 19*: 281-296.

Hay DL, Chen S, Lutz TA, Parkes DG and Roth JD (2015) Amylin: Pharmacology, Physiology, and Clinical Potential. *Pharmacol Rev 67*: 564-600.

Haya K, Makino Y, Kikuchi-Kinoshita A, Kawamura I and Naito A (2020) (31)P and (13)C solid-state NMR analysis of morphological changes of phospholipid bilayers containing glucagon during fibril formation of glucagon under neutral condition. *Biochim Biophys Acta Biomembr 1862*: 183290.

Hebda JA, Magzoub M and Miranker AD (2014) Small molecule screening in context: lipid-catalyzed amyloid formation. *Protein Sci 23*: 1341-1348.

Heerde T, Rennegarbe M, Biedermann A, Savran D, Pfeiffer PB, Hitzenberger M, Baur J, Puscalau-Girtu I, Zacharias M, Schwierz N, et al. (2022) Cryo-EM demonstrates the in vitro proliferation of an ex vivo amyloid fibril morphology by seeding. *Nat Commun 13*: 85.

Hellstrand E, Nowacka A, Topgaard D, Linse S and Sparr E (2013) Membrane lipid co-aggregation with alpha-synuclein fibrils. *PLoS One 8*: e77235.

Hill EK, Krebs B, Goodall DG, Howlett GJ and Dunstan DE (2006) Shear flow induces amyloid fibril formation. *Biomacromolecules 7*: 10-13.

Hirabayashi T, Nakamachi T and Shioda S (2018) Discovery of PACAP and its receptors in the brain. *J Headache Pain 19*: 28.

Hoffmann ARF, Saravanan MS, Lequin O, Killian JA and Khemtemourian L (2018) A single mutation on the human amyloid polypeptide modulates fibril growth and affects the mechanism of amyloid-induced membrane damage. *Biochim Biophys Acta Biomembr 1860*: 1783-1792.

Holmes BB, DeVos SL, Kfoury N, Li M, Jacks R, Yanamandra K, Ouidja MO, Brodsky FM, Marasa J, Bagchi DP, et al. (2013) Heparan sulfate proteoglycans

mediate internalization and propagation of specific proteopathic seeds. *Proceedings of the National Academy of Sciences of the United States of America 110*: E3138-3147.

Horvath I and Wittung-Stafshede P (2016) Cross-talk between amyloidogenic proteins in type-2 diabetes and Parkinson's disease. *Proc Natl Acad Sci U S A 113*: 12473-12477.

Hu G, Jousilahti P, Bidel S, Antikainen R and Tuomilehto J (2007) Type 2 Diabetes and the Risk of Parkinson's Disease. *Diabetes Care 30*: 842-847.

Huang B, He J, Ren J, Yan XY and Zeng CM (2009) Cellular membrane disruption by amyloid fibrils involved intermolecular disulfide cross-linking. *Biochemistry 48*: 5794-5800.

Hudson SA, Ecroyd H, Kee TW and Carver JA (2009) The thioflavin T fluorescence assay for amyloid fibril detection can be biased by the presence of exogenous compounds. *FEBS J 276*: 5960-5972.

Iadanza MG, Jackson MP, Hewitt EW, Ranson NA and Radford SE (2018) A new era for understanding amyloid structures and disease. *Nat Rev Mol Cell Biol 19*: 755-773.

Iannuzzi C, Irace G and Sirangelo I (2015) The effect of glycosaminoglycans (GAGs) on amyloid aggregation and toxicity. *Molecules 20*: 2510-2528.

Iconomidou VA, Vriend G and Hamodrakas SJ (2000) Amyloids protect the silkmoth oocyte and embryo. *FEBS Lett 479*: 141-145.

Inagami T (1989) Atrial Natriuretic Factor. *Journal of Biological Chemistry 264*: 3043-3046.

Itoh-Watanabe H, Kamihira-Ishijima M, Javkhlantugs N, Inoue R, Itoh Y, Endo H, Tuzi S, Saito H, Ueda K and Naito A (2013) Role of aromatic residues in amyloid fibril formation of human calcitonin by solid-state 13C NMR and molecular dynamics simulation. *Phys Chem Chem Phys 15*: 8890-8901.

Jaber T, Dadu R and Hu MI (2021) Medullary thyroid carcinoma. *Curr Opin Endocrinol Diabetes Obes 28*: 540-546.

Jackson MP and Hewitt EW (2016) Cellular proteostasis: degradation of misfolded proteins by lysosomes. *Essays in biochemistry 60*: 173-180.

Jacob RS, Das S, Ghosh S, Anoop A, Jha NN, Khan T, Singru P, Kumar A and Maji SK (2016) Amyloid formation of growth hormone in presence of zinc: Relevance to its storage in secretory granules. *Sci Rep 6*: 23370.

Jayawardena N, Kaur M, Nair S, Malmstrom J, Goldstone D, Negron L, Gerrard JA and Domigan LJ (2017) Amyloid Fibrils from Hemoglobin. *Biomolecules 7*: 1-18.

Jean L, Lee CF and Vaux DJ (2012) Enrichment of amyloidogenesis at an air-water interface. *Biophys J 102*: 1154-1162.

Jekely G, Melzer S, Beets I, Kadow ICG, Koene J, Haddad S and Holden-Dye L (2018) The long and the short of it - a perspective on peptidergic regulation of circuits and behaviour. *J Exp Biol 221*: jeb166710.

Jha NN, Anoop A, Ranganathan S, Mohite GM, Padinhateeri R and Maji SK (2013) Characterization of amyloid formation by glucagon-like peptides: role of basic residues in heparin-mediated aggregation. *Biochemistry 52*: 8800-8810.

Jha S, Patil SM, Gibson J, Nelson CE, Alder NN and Alexandrescu AT (2011) Mechanism of amylin fibrillization enhancement by heparin. *J Biol Chem 286*: 22894-22904.

Jin W, Zhang F and Linhardt RJ (2021) Glycosaminoglycans in Neurodegenerative Diseases. *Adv Exp Med Biol 1325*: 189-204.

Johansson B and Westermark P (1990) The relation of atrial natrluretic factor to isolated atrial amyloid. *Experimental and Molecular Pathology 52*: 266-278.

Kakinen A, Javed I, Faridi A, Davis TP and Ke PC (2018) Serum albumin impedes the amyloid aggregation and hemolysis of human islet amyloid polypeptide and alpha synuclein. *Biochim Biophys Acta Biomembr 1860*: 1803-1809.

Kalappurakkal JM, Sil P and Mayor S (2020) Toward a new picture of the living plasma membrane. *Protein Sci 29*: 1355-1365.

Kawahara M, Kuroda Y, Arispe N and Rojas E (2000) Alzheimer's beta-amyloid, human islet amylin, and prion protein fragment evoke intracellular free calcium elevations by a common mechanism in a hypothalamic GnRH neuronal cell line. *J Biol Chem 275*: 14077-14083.

Kaye GC, Butler MG, Ardenne AJ, Edmondson SJ, Camm AJ and Slavin G (1986) Isolated atrial amyloid contains atrial natriuretic peptide: a report of six cases. *British Heart Journal 56*: 317.

Kelly CV, Kober MM, Kinnunen P, Reis DA, Orr BG and Banaszak Holl MM (2009) Pulsed-laser creation and characterization of giant plasma membrane vesicles from cells. *J Biol Phys 35*: 279-295.

Khemtemourian L, Antoniciello F, Sahoo BR, Decossas M, Lecomte S and Ramamoorthy A (2021) Investigation of the effects of two major secretory

granules components, insulin and zinc, on human-IAPP amyloid aggregation and membrane damage. *Chem Phys Lipids 237*: 105083.

Khurana R, Agarwal A, Bajpai VK, Verma N, Sharma AK, Gupta RP and Madhusudan KP (2004) Unraveling the amyloid associated with human medullary thyroid carcinoma. *Endocrinology 145*: 5465-5470.

Kisilevsky R (2000) The relation of proteoglycans, serum amyloid P and apo E to amyloidosis current status, 2000. *Amyloid 7*: 23-25.

Klaips CL, Jayaraj GG and Hartl FU (2018) Pathways of cellular proteostasis in aging and disease. *J Cell Biol 217*: 51-63.

Klocek G and Seelig J (2008) Melittin interaction with sulfated cell surface sugars. *Biochemistry 47*: 2841-2849.

Knowles TPJ, Vendruscolo M and Dobson CM (2014) The amyloid state and its association with protein misfolding diseases. *Nature Reviews Molecular Cell Biology 15*: 384-396.

Knowles TPJ, Waudby CA, Devlin GL, Cohen SIA, Aguzzi A, Vendruscolo M, Terentjev EM, Welland ME and Dobson CM (2009) An Analytical Solution to the Kinetics of Breakable Filament Assembly. *Science 326*: 1533-1537.

Korshavn KJ, Satriano C, Lin Y, Zhang R, Dulchavsky M, Bhunia A, Ivanova MI, Lee YH, La Rosa C, Lim MH, et al. (2017) Reduced Lipid Bilayer Thickness Regulates the Aggregation and Cytotoxicity of Amyloid-beta. *J Biol Chem 292*: 4638-4650.

Kotler SA, Brender JR, Vivekanandan S, Suzuki Y, Yamamoto K, Monette M, Krishnamoorthy J, Walsh P, Cauble M, Holl MM, et al. (2015) High-resolution

NMR characterization of low abundance oligomers of amyloid-beta without purification. *Sci Rep 5*: 11811.

Kotler SA, Walsh P, Brender JR and Ramamoorthy A (2014) Differences between amyloid-beta aggregation in solution and on the membrane: insights into elucidation of the mechanistic details of Alzheimer's disease. *Chem Soc Rev 43*: 6692-6700.

Krebs MR, Devlin GL and Donald AM (2007) Protein particulates: another generic form of protein aggregation? *Biophys J 92*: 1336-1342.

Kumar EK, Haque N and Prabhu NP (2017) Kinetics of protein fibril formation: Methods and mechanisms. *Int J Biol Macromol 100*: 3-10.

Kumar K, Sebastiao M, Arnold AA, Bourgault S, Warschawski DE and Marcotte I (2022) In situ solid-state NMR study of antimicrobial peptide interactions with erythrocyte membranes. *Biophys J 121*: 1512-1524.

Kumar S and Udgaonkar JB (2009) Structurally Distinct Amyloid Protofibrils Form on Separate Pathways of Aggregation of a Small Protein. *Biochemistry 48*: 6441-6449.

Kusumi A, Fujiwara TK, Chadda R, Xie M, Tsunoyama TA, Kalay Z, Kasai RS and Suzuki KG (2012) Dynamic organizing principles of the plasma membrane that regulate signal transduction: commemorating the fortieth anniversary of Singer and Nicolson's fluid-mosaic model. *Annu Rev Cell Dev Biol 28*: 215-250.

Kusumi A, Suzuki KGN, Kasai RS, Ritchie K and Fujiwara TK (2011) Hierarchical mesoscale domain organization of the plasma membrane. *Trends in Biochemical Sciences 36*: 604-615.

Lasic DD (1988) The mechanism of vesicle formation. *Biochem J 256*: 1-11.

Lauren E, Tigistu-Sahle F, Valkonen S, Westberg M, Valkeajarvi A, Eronen J, Siljander P, Pettila V, Kakela R, Laitinen S, et al. (2018) Phospholipid composition of packed red blood cells and that of extracellular vesicles show a high resemblance and stability during storage. *Biochim Biophys Acta Mol Cell Biol Lipids 1863*: 1-8.

Lee J, Kim YH, F TA, Gillman AL, Jang H, Kagan BL, Nussinov R, Yang J and Lal R (2017) Amyloid β Ion Channels in a Membrane Comprising Brain Total Lipid Extracts. *ACS Chem Neurosci 8*: 1348-1357.

LeVine H, 3rd (1993) Thioflavine T interaction with synthetic Alzheimer's disease beta-amyloid peptides: detection of amyloid aggregation in solution. *Protein Sci 2*: 404-410.

Levine SN, Ishaq S, Nanda A, Wilson JD and Gonzalez-Toledo E (2013) Occurrence of extensive spherical amyloid deposits in a prolactin-secreting pituitary macroadenoma: a radiologic-pathologic correlation. *Ann Diagn Pathol 17*: 361-366.

Li JP and Kusche-Gullberg M (2016) Heparan Sulfate: Biosynthesis, Structure, and Function. *Int Rev Cell Mol Biol 325*: 215-273.

Li S and Leblanc RM (2014) Aggregation of insulin at the interface. *J Phys Chem B 118*: 1181-1188.

Linding R, Schymkowitz J, Rousseau F, Diella F and Serrano L (2004) A comparative study of the relationship between protein structure and beta-aggregation in globular and intrinsically disordered proteins. *J Mol Biol 342*: 345-353.

Loquet A, El Mammeri N, Stanek J, Berbon M, Bardiaux B, Pintacuda G and Habenstein B (2018) 3D structure determination of amyloid fibrils using solid-state NMR spectroscopy. *Methods 138-139*: 26-38.

Louros NN, Iconomidou VA, Tsiolaki PL, Chrysina ED, Baltatzis GE, Patsouris ES and Hamodrakas SJ (2014) An N-terminal pro-atrial natriuretic peptide (NT-proANP) 'aggregation-prone' segment involved in isolated atrial amyloidosis. *FEBS Lett 588*: 52-57.

Lu T, Meng F, Wei Y, Li Y, Wang C and Li F (2018) Exploring the relation between the oligomeric structure and membrane damage by a study on rat islet amyloid polypeptide. *Phys Chem Chem Phys 20*: 8976-8983.

Luca S, Yau WM, Leapman R and Tycko R (2007) Peptide conformation and supramolecular organization in amylin fibrils: constraints from solid-state NMR. *Biochemistry 46*: 13505-13522.

Ludtmann MHR, Angelova PR, Horrocks MH, Choi ML, Rodrigues M, Baev AY, Berezhnov AV, Yao Z, Little D, Banushi B, et al. (2018) alpha-synuclein oligomers interact with ATP synthase and open the permeability transition pore in Parkinson's disease. *Nat Commun 9*: 2293.

Luo Y, Dinkel P, Yu X, Margittai M, Zheng J, Nussinov R, Wei G and Ma B (2013) Molecular insights into the reversible formation of tau protein fibrils. *Chem Commun (Camb) 49*: 3582-3584.

Lutz TA (2010) The role of amylin in the control of energy homeostasis. *American Journal of Physiology-Regulatory, Integrative and Comparative Physiology 298*: R1475-R1484.

Lyons SM and Anderson P (2016) RNA-Seeded Functional Amyloids Balance Growth and Survival. *Dev Cell 39*: 131-132.

MacDonald MJ, Dobrzyn A, Ntambi J and Stoker SW (2008) The role of rapid lipogenesis in insulin secretion: Insulin secretagogues acutely alter lipid composition of INS-1 832/13 cells. *Arch Biochem Biophys 470*: 153-162.

Mackay JP, Matthews JM, Winefield RD, Mackay LG, Haverkamp RG and Templeton MD (2001) The hydrophobin EAS is largely unstructured in solution and functions by forming amyloid-like structures. *Structure 9*: 83-91.

Madine J, Davies HA, Hughes E and Middleton DA (2013) Heparin promotes the rapid fibrillization of a peptide with low intrinsic amyloidogenicity. *Biochemistry 52*: 8984-8992.

Madine J and Middleton DA (2010) Comparison of aggregation enhancement and inhibition as strategies for reducing the cytotoxicity of the aortic amyloid polypeptide medin. *European Biophysics Journal 39*: 1281-1288.

Madine J, Pandya MJ, Hicks MR, Rodger A, Yates EA, Radford SE and Middleton DA (2012) Site-specific identification of an abeta fibril-heparin interaction site by using solid-state NMR spectroscopy. *Angew Chem Int Ed Engl 51*: 13140-13143.

Maiza A, Chantepie S, Vera C, Fifre A, Huynh MB, Stettler O, Ouidja MO and Papy-Garcia D (2018) The role of heparan sulfates in protein aggregation and their potential impact on neurodegeneration. *FEBS Lett 592*: 3806-3818.

Maji SK, Perrin MH, Sawaya MR, Jessberger S, Vadodaria K, Rissman RA, Singru PS, Nilsson KP, Simon R, Schubert D, et al. (2009) Functional amyloids as natural storage of peptide hormones in pituitary secretory granules. *Science 325*: 328-332.

Malmos KG, Bjerring M, Jessen CM, Nielsen EH, Poulsen ET, Christiansen G, Vosegaard T, Skrydstrup T, Enghild JJ, Pedersen JS, et al. (2016) How Glycosaminoglycans Promote Fibrillation of Salmon Calcitonin. *J Biol Chem 291*: 16849-16862.

Marek PJ, Patsalo V, Green DF and Raleigh DP (2012) Ionic strength effects on amyloid formation by amylin are a complicated interplay among Debye screening, ion selectivity, and Hofmeister effects. *Biochemistry 51*: 8478-8490.

Markovics A, Kormos V, Gaszner B, Lashgarara A, Szoke E, Sandor K, Szabadfi K, Tuka B, Tajti J, Szolcsanyi J, et al. (2012) Pituitary adenylate cyclase-activating polypeptide plays a key role in nitroglycerol-induced trigeminovascular activation in mice. *Neurobiology of Disease 45*: 633-644.

Masters SL, Dunne A, Subramanian SL, Hull RL, Tannahill GM, Sharp FA, Becker C, Franchi L, Yoshihara E, Chen Z, et al. (2010) Activation of the NLRP3 inflammasome by islet amyloid polypeptide provides a mechanism for enhanced IL-1beta in type 2 diabetes. *Nat Immunol 11*: 897-904.

Matsubara T, Yasumori H, Ito K, Shimoaka T, Hasegawa T and Sato T (2018) Amyloid-β fibrils assembled on ganglioside-enriched membranes contain both parallel β-sheets and turns. *Journal of Biological Chemistry 293*: 14146-14154.

McLaurin J, Franklin T, Zhang X, Deng J and Fraser PE (1999) Interactions of Alzheimer amyloid-beta peptides with glycosaminoglycans effects on fibril nucleation and growth. *Eur J Biochem 266*: 1101-1110.

McNeil PL and Steinhardt RA (2003) Plasma membrane disruption: repair, prevention, adaptation. *Annu Rev Cell Dev Biol 19*: 697-731.

Mehra S, Ghosh D, Kumar R, Mondal M, Gadhe LG, Das S, Anoop A, Jha NN, Jacob RS, Chatterjee D, et al. (2018) Glycosaminoglycans have variable effects on alpha-synuclein aggregation and differentially affect the activities of the resulting amyloid fibrils. *J Biol Chem 293*: 12975-12991.

Mehra S, Sahay S and Maji SK (2019) α-Synuclein misfolding and aggregation: Implications in Parkinson's disease pathogenesis. *Biochim Biophys Acta Proteins Proteom 1867*: 890-908.

Meisl G, Kirkegaard JB, Arosio P, Michaels TC, Vendruscolo M, Dobson CM, Linse S and Knowles TP (2016) Molecular mechanisms of protein aggregation from global fitting of kinetic models. *Nat Protoc 11*: 252-272.

Middleton CT, Marek P, Cao P, Chiu C-c, Singh S, Woys AM, de Pablo JJ, Raleigh DP and Zanni MT (2012) Two-dimensional infrared spectroscopy reveals the complex behaviour of an amyloid fibril inhibitor. *Nature chemistry 4*: 355-360.

Milardi D, Gazit E, Radford SE, Xu Y, Gallardo RU, Caflisch A, Westermark GT, Westermark P, Rosa C and Ramamoorthy A (2021) Proteostasis of Islet Amyloid Polypeptide: A Molecular Perspective of Risk Factors and Protective Strategies for Type II Diabetes. *Chem Rev 121*: 1845-1893.

Millucci L, Paccagnini E, Ghezzi L, Bernardini G, Braconi D, Laschi M, Consumi M, Spreafico A, Tanganelli P, Lupetti P, et al. (2011) Different factors affecting human ANP amyloid aggregation and their implications in congestive heart failure. *PLoS ONE 6*: 1-12.

Montane J, Klimek-Abercrombie A, Potter KJ, Westwell-Roper C and Bruce Verchere C (2012) Metabolic stress, IAPP and islet amyloid. *Diabetes, Obesity and Metabolism 14*: 68-77.

Morita S, Sakagashira S, Shimajiri Y, Eberhardt NL, Kondo T, Kondo T and Sanke T (2011) Autophagy protects against human islet amyloid polypeptide-associated apoptosis. *J Diabetes Investig 2*: 48-55.

Morton GJ, Cummings DE, Baskin DG, Barsh GS and Schwartz MW (2006) Central nervous system control of food intake and body weight. *Nature 443*: 289-295.

Motamedi-Shad N, Monsellier E and Chiti F (2009) Amyloid formation by the model protein muscle acylphosphatase is accelerated by heparin and heparan sulphate through a scaffolding-based mechanism. *J Biochem 146*: 805-814.

Mrdenovic D, Majewska M, Pieta IS, Bernatowicz P, Nowakowski R, Kutner W, Lipkowski J and Pieta P (2019) Size-Dependent Interaction of Amyloid β Oligomers with Brain Total Lipid Extract Bilayer—Fibrillation Versus Membrane Destruction. *Langmuir 35*: 11940-11949.

Muff R, Bühlmann N, Fischer JA and Born W (1999) An amylin receptor is revealed following co-transfection of a calcitonin receptor with receptor activity modifying proteins-1 or -3. *Endocrinology 140 6*: 2924-2927.

Murray AN, Palhano FL, Bieschke J and Kelly JW (2013) Surface adsorption considerations when working with amyloid fibrils in multiwell plates and Eppendorf tubes. *Protein Sci 22*: 1531-1541.

Mustafa T (2013) Chapter 21: Pituitary Adenylate Cyclase-Activating Polypeptide (PACAP): A Master Regulator in Central and Peripheral Stress Responses. *Advances in Pharmacology 68*: 445-457.

Naiki H, Higuchi K, Hosokawa M and Takeda T (1989) Fluorometric determination of amyloid fibrils in vitro using the fluorescent dye, thioflavin T1. *Anal Biochem 177*: 244-249.

Naito A, Matsumori N and Ramamoorthy A (2018) Dynamic membrane interactions of antibacterial and antifungal biomolecules, and amyloid peptides, revealed by solid-state NMR spectroscopy. *Biochim Biophys Acta Gen Subj 1862*: 307-323.

Nanga RP, Brender JR, Vivekanandan S and Ramamoorthy A (2011) Structure and membrane orientation of IAPP in its natively amidated form at physiological pH in a membrane environment. *Biochim Biophys Acta 1808*: 2337-2342.

Nanga RP, Brender JR, Xu J, Veglia G and Ramamoorthy A (2008) Structures of rat and human islet amyloid polypeptide IAPP(1-19) in micelles by NMR spectroscopy. *Biochemistry 47*: 12689-12697.

Neree AT, Nguyen PT and Bourgault S (2015) Cell-Penetrating Ability of Peptide Hormones: Key Role of Glycosaminoglycans Clustering. *Int J Mol Sci 16*: 27391-27400.

Nespovitaya N, Gath J, Barylyuk K, Seuring C, Meier BH and Riek R (2016) Dynamic Assembly and Disassembly of Functional beta-Endorphin Amyloid Fibrils. *J Am Chem Soc 138*: 846-856.

Nespovitaya N, Mahou P, Laine RF, Schierle GSK and Kaminski CF (2017) Heparin acts as a structural component of beta-endorphin amyloid fibrils rather than a simple aggregation promoter. *Chem Commun (Camb) 53*: 1273-1276.

Nguyen PT, Andraka N, De Carufel CA and Bourgault S (2015) Mechanistic Contributions of Biological Cofactors in Islet Amyloid Polypeptide Amyloidogenesis. *J Diabetes Res 2015*: 515307.

Nguyen PT, Sharma R, Rej R, De Carufel CA, Roy R and Bourgault S (2016) Low generation anionic dendrimers modulate islet amyloid polypeptide self-assembly and inhibit pancreatic β-cell toxicity. *RSC Advances 6*: 76360-76369.

Nguyen PT, Zottig X, Sebastiao M, Arnold AA, Marcotte I and Bourgault S (2021) Identification of transmissible proteotoxic oligomer-like fibrils that expand conformational diversity of amyloid assemblies. *Commun Biol 4*: 939.

Nguyen PT, Zottig X, Sebastiao M and Bourgault S (2017) Role of Site-Specific Asparagine Deamidation in Islet Amyloid Polypeptide Amyloidogenesis: Key Contributions of Residues 14 and 21. *Biochemistry 56*: 3808-3817.

O'Nuallain B, Williams AD, Westermark P and Wetzel R (2004) Seeding Specificity in Amyloid Growth Induced by Heterologous Fibrils *. *Journal of Biological Chemistry 279*: 17490-17499.

Olzscha H, Schermann SM, Woerner AC, Pinkert S, Hecht MH, Tartaglia GG, Vendruscolo M, Hayer-Hartl M, Hartl FU and Vabulas RM (2011) Amyloid-like aggregates sequester numerous metastable proteins with essential cellular functions. *Cell 144*: 67-78.

Opie EL (1901) The relation of diabetes mellitus to lesions of the pancreas. Hyaline degeneration of the islands of langerhans. *J Exp Med 5*: 527-540.

Ott A, Stolk RP, Hofman A, van Harskamp F, Grobbee DE and Breteler MMB (1996) Association of diabetes mellitus and dementia: The Rotterdam Study. *Diabetologia 39*: 1392-1397.

Otzen D and Riek R (2019) Functional Amyloids. *Cold Spring Harb Perspect Biol 11*: a033860.

Ozawa D, Yagi H, Ban T, Kameda A, Kawakami T, Naiki H and Goto Y (2009) Destruction of amyloid fibrils of a beta2-microglobulin fragment by laser beam irradiation. *J Biol Chem 284*: 1009-1017.

Papasouliotis K, Graham SC, Mary, Sparkes AH and Gruffydd-Jones T (1999) Analysis of Feline, Canine and Equine Hemograms Using the QBC VetAutoread. *Veterinary Clinical Pathology 28*: 109-115.

Papy-Garcia D, Christophe M, Huynh MB, Fernando S, Ludmilla S, Sepulveda-Diaz JE and Raisman-Vozari R (2011) Glycosaminoglycans, protein aggregation and neurodegeneration. *Curr Protein Pept Sci 12*: 258-268.

Park YJ, Lee S, Kieffer TJ, Warnock GL, Safikhan N, Speck M, Hao Z, Woo M and Marzban L (2012) Deletion of Fas protects islet beta cells from cytotoxic effects of human islet amyloid polypeptide. *Diabetologia 55*: 1035-1047.

Peila R, Rodriguez BL and Launer LJ (2002) Type 2 Diabetes, APOE Gene, and the Risk for Dementia and Related Pathologies: The Honolulu-Asia Aging Study. *Diabetes 51*: 1256-1262.

Pepys MB and Hirschfield GM (2003) C-reactive protein: a critical update. *Journal of Clinical Investigation 111*: 1805-1812.

Persson A, Ellervik U and Mani K (2018) Fine-tuning the structure of glycosaminoglycans in living cells using xylosides. *Glycobiology 28*: 499-511.

Portela-Gomes GM, Lukinius A, Ljungberg O, Efendic S, Ahrén B and Abdel-Halim SM (2003) PACAP is expressed in secretory granules of insulin and glucagon cells in human and rodent pancreas: Evidence for generation of cAMP compartments uncoupled from hormone release in diabetic islets. *Regulatory Peptides 113*: 31-39.

Pytowski L, Lee CF, Foley AC, Vaux DJ and Jean L (2020) Liquid-liquid phase separation of type II diabetes-associated IAPP initiates hydrogelation and aggregation. *Proc Natl Acad Sci U S A 117*: 12050-12061.

Qiang W, Yau WM, Lu JX, Collinge J and Tycko R (2017) Structural variation in amyloid-β fibrils from Alzheimer's disease clinical subtypes. *Nature 541*: 217-221.

Quist A, Doudevski I, Lin H, Azimova R, Ng D, Frangione B, Kagan B, Ghiso J and Lal R (2005) Amyloid ion channels: A common structural link for protein-misfolding disease. *Proceedings of the National Academy of Sciences 102*: 10427-10432.

Quittot N, Fortier M, Babych M, Nguyen PT, Sebastiao M and Bourgault S (2021) Cell surface glycosaminoglycans exacerbate plasma membrane perturbation induced by the islet amyloid polypeptide. *FASEB J 35*: e21306.

Quittot N, Nguyen PT, Neree AT, Lussier MP and Bourgault S (2017a) Identification of a conformational heparin-recognition motif on the peptide hormone secretin: key role for cell surface binding. *Biochem J 474*: 2249-2260.

Quittot N, Sebastiao M, Al-Halifa S and Bourgault S (2018) Kinetic and Conformational Insights into Islet Amyloid Polypeptide Self-Assembly Using a Biarsenical Fluorogenic Probe. *Bioconjug Chem 29*: 517-527.

Quittot N, Sebastiao M and Bourgault S (2017b) Modulation of amyloid assembly by glycosaminoglycans: from mechanism to biological significance. *Biochemistry and Cell Biology 95*: 329-337.

Raimundo AF, Ferreira S, Martins IC and Menezes R (2020) Islet Amyloid Polypeptide: A Partner in Crime With Abeta in the Pathology of Alzheimer's Disease. *Front Mol Neurosci 13*: 35.

Rajput S, Sani M-A, Keizer DW and Separovic F (2021) Utilizing magnetic resonance techniques to study membrane interactions of amyloid peptides. *Biochemical Society Transactions 49*: 1457-1465.

Ranganathan S, Singh PK, Singh U, Singru PS, Padinhateeri R and Maji SK (2012) Molecular interpretation of ACTH-beta-endorphin coaggregation: relevance to secretory granule biogenesis. *PLoS One 7*: e31924.

Remko M, Broer R and Van Duijnen PT (2013) How acidic are monomeric structural units of heparin? *Chemical Physics Letters 590*: 187-191.

Rivera JF, Gurlo T, Daval M, Huang CJ, Matveyenko AV, Butler PC and Costes S (2011) Human-IAPP disrupts the autophagy/lysosomal pathway in pancreatic beta-cells: protective role of p62-positive cytoplasmic inclusions. *Cell Death Differ 18*: 415-426.

Röder C, Kupreichyk T, Gremer L, Schäfer LU, Pothula KR, Ravelli RBG, Willbold D, Hoyer W and Schröder GF (2020) Cryo-EM structure of islet amyloid polypeptide fibrils reveals similarities with amyloid-β fibrils. *Nat Struct Mol Biol 27*: 660-667.

Rodriguez RA, Chen LY, Plascencia-Villa G and Perry G (2017) Elongation affinity, activation barrier, and stability of Aβ42 oligomers/fibrils in physiological saline. *Biochemical and Biophysical Research Communications 487*: 444-449.

Rousseau F, Schymkowitz J and Serrano L (2006) Protein aggregation and amyloidosis: confusion of the kinds? *Curr Opin Struct Biol 16*: 118-126.

Rouvinski A, Karniely S, Kounin M, Moussa S, Goldberg MD, Warburg G, Lyakhovetsky R, Papy-Garcia D, Kutzsche J, Korth C, et al. (2014) Live imaging of prions reveals nascent PrPSc in cell-surface, raft-associated amyloid strings and webs. *J Cell Biol 204*: 423-441.

Rudecki AP and Gray SL (2016) PACAP in the Defense of Energy Homeostasis. *Trends Endocrinol Metab 27*: 620-632.

Rullo A, Qian J and Nitz M (2011) Peptide-glycosaminoglycan cluster formation involving cell penetrating peptides. *Biopolymers 95*: 722-731.

Ryan TM, Friedhuber A, Lind M, Howlett GJ, Masters C and Roberts BR (2012) Small amphipathic molecules modulate secondary structure and amyloid fibril-forming kinetics of Alzheimer disease peptide Abeta(1-42). *J Biol Chem 287*: 16947-16954.

Sakurai Y, Shintani N, Hayata A, Hashimoto H and Baba A (2011) Trophic Effects of PACAP on Pancreatic Islets: A Mini-Review. *Journal of Molecular Neuroscience 43*: 3-7.

Salamekh S, Brender JR, Hyung SJ, Nanga RP, Vivekanandan S, Ruotolo BT and Ramamoorthy A (2011) A two-site mechanism for the inhibition of IAPP amyloidogenesis by zinc. *J Mol Biol 410*: 294-306.

Salminen A, Kaarniranta K, Kauppinen A, Ojala J, Haapasalo A, Soininen H and Hiltunen M (2013) Impaired autophagy and APP processing in Alzheimer's disease: The potential role of Beclin 1 interactome. *Prog Neurobiol 106-107*: 33-54.

Sasahara K (2018) Membrane-mediated amyloid deposition of human islet amyloid polypeptide. *Biophys Rev 10*: 453-462.

Schlamadinger DE and Miranker AD (2014) Fiber-dependent and -independent toxicity of islet amyloid polypeptide. *Biophys J 107*: 2559-2566.

Schubert D, Behl C, Lesley R, Brack A, Dargusch R, Sagara Y and Kimura H (1995) Amyloid peptides are toxic via a common oxidative mechanism. *Proceedings of the National Academy of Sciences 92*: 1989-1993.

Schultz V, Suflita M, Liu X, Zhang X, Yu Y, Li L, Green DE, Xu Y, Zhang F, DeAngelis PL, et al. (2017) Heparan Sulfate Domains Required for Fibroblast Growth Factor 1 and 2 Signaling through Fibroblast Growth Factor Receptor 1c. *J Biol Chem 292*: 2495-2509.

Schwoch G and Passow H (1973) Preparation and properties of human erythrocyte ghosts. *Molecular and Cellular Biochemistry 2*: 197-218.

Sciacca MF, Kotler SA, Brender JR, Chen J, Lee DK and Ramamoorthy A (2012) Two-step mechanism of membrane disruption by Abeta through membrane fragmentation and pore formation. *Biophys J 103*: 702-710.

Sciacca MF, Lolicato F, Di Mauro G, Milardi D, D'Urso L, Satriano C, Ramamoorthy A and La Rosa C (2016) The Role of Cholesterol in Driving IAPP-Membrane Interactions. *Biophys J 111*: 140-151.

Sciacca MF, Lolicato F, Tempra C, Scollo F, Sahoo BR, Watson MD, Garcia-Vinuales S, Milardi D, Raudino A, Lee JC, et al. (2020) Lipid-Chaperone Hypothesis: A Common Molecular Mechanism of Membrane Disruption by Intrinsically Disordered Proteins. *ACS Chem Neurosci 11*: 4336-4350.

Sciacca MFM, Tempra C, Scollo F, Milardi D and La Rosa C (2018) Amyloid growth and membrane damage: Current themes and emerging perspectives from theory and experiments on Abeta and hIAPP. *Biochim Biophys Acta Biomembr 1860*: 1625-1638.

Scollo F, Tempra C, Lolicato F, Sciacca MFM, Raudino A, Milardi D and La Rosa C (2018) Phospholipids Critical Micellar Concentrations Trigger Different Mechanisms of Intrinsically Disordered Proteins Interaction with Model Membranes. *The Journal of Physical Chemistry Letters 9*: 5125-5129.

Sebastiao M, Quittot N and Bourgault S (2017) Thioflavin T fluorescence to analyse amyloid formation kinetics: Measurement frequency as a factor explaining irreproducibility. *Anal Biochem 532*: 83-86.

Sebastiao M, Quittot N, Marcotte I and Bourgault S (2019) Glycosaminoglycans Induce Amyloid Self-Assembly of a Peptide Hormone by Concerted Secondary and Quaternary Conformational Transitions. *Biochemistry 58*: 1214-1225.

Seelig J (1978) 31P nuclear magnetic resonance and the head group structure of phospholipids in membranes. *Biochim Biophys Acta 515*: 105-140.

Sepulveda-Diaz JE, Alavi Naini SM, Huynh MB, Ouidja MO, Yanicostas C, Chantepie S, Villares J, Lamari F, Jospin E, van Kuppevelt TH, et al. (2015) HS3ST2 expression is critical for the abnormal phosphorylation of tau in Alzheimer's disease-related tau pathology. *Brain 138*: 1339-1354.

Serra-Batiste M, Ninot-Pedrosa M, Bayoumi M, Gairi M, Maglia G and Carulla N (2016) Abeta42 assembles into specific beta-barrel pore-forming oligomers in membrane-mimicking environments. *Proc Natl Acad Sci U S A 113*: 10866-10871.

Shiraki K, Nishikawa K and Goto Y (1995) Trifluoroethanol-induced stabilization of the alpha-helical structure of beta-lactoglobulin: implication for non-hierarchical protein folding. *J Mol Biol 245*: 180-194.

Shriver Z, Capila I, Venkataraman G and Sasisekharan R (2012) Heparin and heparan sulfate: analyzing structure and microheterogeneity. *Handbook of experimental pharmacology* 159-176.

Singer SJ and Dewji NN (2006) Evidence that Perutz's double-β-stranded subunit structure for β-amyloids also applies to their channel-forming structures in membranes. *Proceedings of the National Academy of Sciences 103*: 1546-1550.

Singer SJ and Nicolson GL (1972) The fluid mosaic model of the structure of cell membranes. *Science 175*: 720-731.

Snow AD, Sekiguchi R, Nochlin D, Fraser P, Kimata K, Mizutani A, Arai M, Schreier WA and Morgan DG (1994) An important role of heparan sulfate proteoglycan (perlecan) in a model system for the deposition and persistence of fibrillar aβ-amyloid in rat brain. *Neuron 12*: 219-234.

Solomon JP, Bourgault S, Powers ET and Kelly JW (2011) Heparin binds 8 kDa gelsolin cross-beta-sheet oligomers and accelerates amyloidogenesis by hastening fibril extension. *Biochemistry 50*: 2486-2498.

Sormanni P, Amery L, Ekizoglou S, Vendruscolo M and Popovic B (2017) Rapid and accurate in silico solubility screening of a monoclonal antibody library. *Sci Rep 7*: 8200.

Sormanni P, Aprile FA and Vendruscolo M (2015) The CamSol method of rational design of protein mutants with enhanced solubility. *J Mol Biol 427*: 478-490.

Srinivasan A, Wong FK and Karponis D (2020) Calcitonin: A useful old friend. *J Musculoskelet Neuronal Interact 20*: 600-609.

Stanciu GD, Bild V, Ababei DC, Rusu RN, Cobzaru A, Paduraru L and Bulea D (2020) Link between Diabetes and Alzheimer's Disease Due to the Shared Amyloid Aggregation and Deposition Involving Both Neurodegenerative Changes and Neurovascular Damages. *Journal of Clinical Medicine 9*: 1713.

Stewart KL, Hughes E, Yates EA, Akien GR, Huang TY, Lima MA, Rudd TR, Guerrini M, Hung SC, Radford SE, et al. (2016) Atomic Details of the Interactions of Glycosaminoglycans with Amyloid-beta Fibrils. *J Am Chem Soc 138*: 8328-8331.

Stewart KL, Hughes E, Yates EA, Middleton DA and Radford SE (2017) Molecular Origins of the Compatibility between Glycosaminoglycans and Abeta40 Amyloid Fibrils. *J Mol Biol 429*: 2449-2462.

Stroth N, Holighaus Y, Ait-Ali D and Eiden LE (2011) PACAP: a master regulator of neuroendocrine stress circuits and the cellular stress response. *Annals of the New York Academy of Sciences 1220*: 49-59.

Subramanian SL, Hull RL, Zraika S, Aston-Mourney K, Udayasankar J and Kahn SE (2012) cJUN N-terminal kinase (JNK) activation mediates islet amyloid-induced beta cell apoptosis in cultured human islet amyloid polypeptide transgenic mouse islets. *Diabetologia 55*: 166-174.

Takase H, Tanaka M, Yamamoto A, Watanabe S, Takahashi S, Nadanaka S, Kitagawa H, Yamada T and Mukai T (2016) Structural requirements of glycosaminoglycans for facilitating amyloid fibril formation of human serum amyloid A. *Amyloid 23*: 67-75.

Tan Y-V and Waschek JA (2011) Targeting VIP and PACAP Receptor Signalling: New Therapeutic Strategies in Multiple Sclerosis. *ASN Neuro 3*: AN20110024.

Taylor R (1990) Interpretation of the Correlation Coefficient: A Basic Review. *Journal of Diagnostic Medical Sonography 6*: 35-39.

Tchoumi Neree A, Nguyen PT, Chatenet D, Fournier A and Bourgault S (2014) Secondary conformational conversion is involved in glycosaminoglycans-mediated cellular uptake of the cationic cell-penetrating peptide PACAP. *FEBS Lett 588*: 4590-4596.

Terakawa MS, Lin Y, Kinoshita M, Kanemura S, Itoh D, Sugiki T, Okumura M, Ramamoorthy A and Lee YH (2018) Impact of membrane curvature on amyloid aggregation. *Biochim Biophys Acta Biomembr 1860*: 1741-1764.

Thakur G, Pao C, Micic M, Johnson S and Leblanc RM (2011) Surface chemistry of lipid raft and amyloid Aβ (1-40) Langmuir monolayer. *Colloids Surf B Biointerfaces 87*: 369-377.

Theocharis AD, Skandalis SS, Gialeli C and Karamanos NK (2016) Extracellular matrix structure. *Adv Drug Deliv Rev 97*: 4-27.

Traïkia M, Warschawski DE, Recouvreur M, Cartaud J and Devaux PF (2000) Formation of unilamellar vesicles by repetitive freeze-thaw cycles: characterization by electron microscopy and 31P-nuclear magnetic resonance. *European Biophysics Journal 29*: 184-195.

Tuka B, Helyes Z, Markovics A, Bagoly T, Szolcsányi J, Szabó N, Tóth E, Kincses ZT, Vécsei L and Tajti J (2013) Alterations in PACAP-38-like immunoreactivity in the plasma during ictal and interictal periods of migraine patients. *Cephalalgia 33*: 1085-1095.

Tycko R (2011) Solid-state NMR studies of amyloid fibril structure. *Annu Rev Phys Chem 62*: 279-299.

Tycko R (2014) Physical and structural basis for polymorphism in amyloid fibrils. *Protein Sci 23*: 1528-1539.

Tycko R (2016) Molecular Structure of Aggregated Amyloid-β: Insights from Solid-State Nuclear Magnetic Resonance. *Cold Spring Harb Perspect Med 6*: a024083.

Uttara B, Singh AV, Zamboni P and Mahajan RT (2009) Oxidative stress and neurodegenerative diseases: a review of upstream and downstream antioxidant therapeutic options. *Current neuropharmacology 7*: 65-74.

vandenAkker CC, Engel MF, Velikov KP, Bonn M and Koenderink GH (2011) Morphology and persistence length of amyloid fibrils are correlated to peptide molecular structure. *J Am Chem Soc 133*: 18030-18033.

Vassar PS and Culling CF (1959) Fluorescent stains, with special reference to amyloid and connective tissues. *Arch Pathol 68*: 487-498.

Vaudry D, Falluel-Morel A, Bourgault S, Basille M, Burel D, Wurtz O, Fournier A, Chow BK, Hashimoto H, Galas L, et al. (2009) Pituitary adenylate cyclase-activating polypeptide and its receptors: 20 years after the discovery. *Pharmacol Rev 61*: 283-357.

Vergaro G, Aimo A, Rapezzi C, Castiglione V, Fabiani I, Pucci A, Buda G, Passino C, Lupon J, Bayes-Genis A, et al. (2022) Atrial amyloidosis: mechanisms and clinical manifestations. *Eur J Heart Fail 24*: 2019-2028.

Vilasi S, Sarcina R, Maritato R, De Simone A, Irace G and Sirangelo I (2011) Heparin induces harmless fibril formation in amyloidogenic W7FW14F apomyoglobin and amyloid aggregation in wild-type protein in vitro. *PLoS One 6*: e22076.

Wakabayashi M and Matsuzaki K (2009) Ganglioside-induced amyloid formation by human islet amyloid polypeptide in lipid rafts. *FEBS Lett 583*: 2854-2858.

Walsh P, Vanderlee G, Yau J, Campeau J, Sim VL, Yip CM and Sharpe S (2014) The mechanism of membrane disruption by cytotoxic amyloid oligomers formed by prion protein(106-126) is dependent on bilayer composition. *J Biol Chem 289*: 10419-10430.

Wang H, Abedini A, Ruzsicska B and Raleigh DP (2014) Rationally designed, nontoxic, nonamyloidogenic analogues of human islet amyloid polypeptide with improved solubility. *Biochemistry 53*: 5876-5884.

Wang H and Raleigh DP (2014) The ability of insulin to inhibit the formation of amyloid by pro-islet amyloid polypeptide processing intermediates is significantly reduced in the presence of sulfated glycosaminoglycans. *Biochemistry 53*: 2605-2614.

Warnet XL, Arnold AA, Marcotte I and Warschawski DE (2015) In-Cell Solid-State NMR: An Emerging Technique for the Study of Biological Membranes. *Biophys J 109*: 2461-2466.

Warschawski DE, Arnold AA and Marcotte I (2018) A New Method of Assessing Lipid Mixtures by (31)P Magic-Angle Spinning NMR. *Biophys J 114*: 1368-1376.

Waschek JA (2013) VIP and PACAP: neuropeptide modulators of CNS inflammation, injury, and repair. *Br J Pharmacol 169*: 512-523.

Wechalekar AD, Gillmore JD and Hawkins PN (2016) Systemic amyloidosis. *Lancet 387*: 2641-2654.

Weise K, Radovan D, Gohlke A, Opitz N and Winter R (2010) Interaction of hIAPP with model raft membranes and pancreatic beta-cells: cytotoxicity of hIAPP oligomers. *Chembiochem 11*: 1280-1290.

Wentink A, Nussbaum-Krammer C and Bukau B (2019) Modulation of Amyloid States by Molecular Chaperones. *Cold Spring Harb Perspect Biol 11*: a033969.

Westermark P, Andersson A and Westermark GT (2011) Islet amyloid polypeptide, islet amyloid, and diabetes mellitus. *Physiol Rev 91*: 795-826.

Westermark P, Engström U, Johnson KH, Westermark GT and Betsholtz C (1990) Islet amyloid polypeptide: pinpointing amino acid residues linked to amyloid fibril formation. *Proceedings of the National Academy of Sciences 87*: 5036-5040.

Williamson JA, Loria JP and Miranker AD (2009) Helix Stabilization Precedes Aqueous and Bilayer-Catalyzed Fiber Formation in Islet Amyloid Polypeptide. *Journal of Molecular Biology 393*: 383-396.

Williamson JA and Miranker AD (2007) Direct detection of transient α-helical states in islet amyloid polypeptide. *Protein Science 16*: 110-117.

Wiltzius JJW, Sievers SA, Sawaya MR and Eisenberg D (2009) Atomic structures of IAPP (amylin) fusions suggest a mechanism for fibrillation and the role of insulin in the process. *Protein Science 18*: 1521-1530.

Wolfe LS, Calabrese MF, Nath A, Blaho DV, Miranker AD and Xiong Y (2010) Protein-induced photophysical changes to the amyloid indicator dye thioflavin T. *Proc Natl Acad Sci U S A 107*: 16863-16868.

Xu D and Esko JD (2014) Demystifying Heparan Sulfate–Protein Interactions. *Annual Review of Biochemistry 83*: 129-157.

Yagi H, Ozawa D, Sakurai K, Kawakami T, Kuyama H, Nishimura O, Shimanouchi T, Kuboi R, Naiki H and Goto Y (2010) Laser-induced propagation and destruction of amyloid beta fibrils. *J Biol Chem 285*: 19660-19667.

Yamada H, Watanabe M and Yada T (2004) Cytosolic Ca2+ responses to sub-picomolar and nanomolar PACAP in pancreatic β-cells are mediated by VPAC2 and PAC1 receptors. *Regulatory Peptides 123*: 147-153.

Yamane I, Momose A, Fujita H, Yoshimoto E, Kikuchi-Kinoshita A, Kawamura I and Naito A (2019) Fibrillation mechanism of glucagon in the presence of phospholipid bilayers as revealed by (13)C solid-state NMR spectroscopy. *Chem Phys Lipids 219*: 36-44.

Yang Y, Yao H and Hong M (2015) Distinguishing bicontinuous lipid cubic phases from isotropic membrane morphologies using (31)P solid-state NMR spectroscopy. *J Phys Chem B 119*: 4993-5001.

Yasumoto T, Takamura Y, Tsuji M, Watanabe-Nakayama T, Imamura K, Inoue H, Nakamura S, Inoue T, Kimura A, Yano S, et al. (2019) High molecular weight amyloid beta1-42 oligomers induce neurotoxicity via plasma membrane damage. *FASEB J 33*: 9220-9234.

Young AA, Vine W, Gedulin BR, Pittner R, Janes S, Gaeta LSL, Percy A, Moore CX, Koda JE, Rink TJ, et al. (1996) Preclinical pharmacology of pramlintide in the rat: Comparisons with human and rat amylin. *Drug Development Research 37*: 231-248.

Young ID, Ailles L, Narindrasorasak S, Tan R and Kisilevsky R (1992) Localization of the basement membrane heparan sulfate proteoglycan in islet amyloid deposits in type II diabetes mellitus. *Arch Pathol Lab Med 116*: 951-954.

Zapadka KL, Becher FJ, Gomes Dos Santos AL and Jackson SE (2017) Factors affecting the physical stability (aggregation) of peptide therapeutics. *Interface Focus 7*: 20170030.

Zhang X, London E and Raleigh DP (2018) Sterol Structure Strongly Modulates Membrane-Islet Amyloid Polypeptide Interactions. *Biochemistry 57*: 1868-1879.

Zhang X, St Clair JR, London E and Raleigh DP (2017) Islet Amyloid Polypeptide Membrane Interactions: Effects of Membrane Composition. *Biochemistry 56*: 376-390.

Zottig X, Al-Halifa S, Cote-Cyr M, Calzas C, Le Goffic R, Chevalier C, Archambault D and Bourgault S (2021) Self-assembled peptide nanorod vaccine confers protection against influenza A virus. *Biomaterials 269*: 120672.